Exploring the vacuolin gene family

mRNA production, localization and functional characterization in the *Mycobacterium marinum* - *Dictyostelium discoideum* model system

Dissertation

Submitted in partial fulfillment of the requirements for the award of Doctor of Natural Science *Dr*. *rer*. *nat*.

at the Department of Biology, Faculty of Mathematics, Informatics and Natural Sciences of the University of Hamburg, Germany

by

Frauke Helene Bach

from Berlin

Hamburg, 2014

Genehmigt vom Fachbereich Biologie
der Fakultät für Mathematik, Informatik und Naturwissenschaften
an der Universität Hamburg
auf Antrag von Frau Professor Dr. I. BRUCHHAUS
Weiterer Gutachter der Dissertation:
Professor Dr. E. TANNICH
Tag der Disputation: 11. April 2014

Professor Dr. C. Lohr
Vorsitzender des
Fach-Promotionsausschusses Biologie

Language Certificate I

I am a native speaker, have read the introduction, results and discussion of the present PhD thesis and hereby confirm that it complies with the rules of the English language.

Oxford, January 22, 2013

(Dr. Tim P. Lawrence)

Language Certificate II

I am a native speaker, have read the Materials and Methods of the present PhD thesis and hereby confirm that it complies with the rules of the English language.

Hamburg, January 24, 2013

(Dr. Erin Boyle)

Abstract

Tuberculosis (TB) is the second greatest cause of death due to a single infectious agent worldwide. It caused 8.6 million infections and 1.3 million deaths in 2012. The causative agent of the chronic infection is the bacterium *Mycobacterium tuberculosis.*

The disease is acquired by inhaling contaminated aerosols that most commonly lead to an infection of the human lungs, precisely, the alveolar macrophages. In the case of non-pathogenic bacteria this process leads to the effective killing of the invader in a process named phagosomal maturation. The ability of mycobacteria to circumvent this phagosomal maturation is a critical step towards establishing an infection. However, despite decades of research focused on TB, major gaps of comprehension of the intracellular host - pathogenic interactions remain; but may be a critical component for the identification of new drug targets.

To investigate host - pathogen interactions in this study the *Mycobacterium marinum* - *Dictyostelium discoideum* model system, which was recently established was used. It was shown that, comparable to *M. tuberculosis* in macrophages, *M. marinum* is also able to modulate its phagosome into a replication vacuole and proliferate in *D. discoideum*, an amoeba used as surrogate human macrophages [82].

The first project of this study was performed with the aim to upgrade the methodical spectrum of the *M. marinum – D. discoideum* model system by generating a customized quantitative real time PCR (qPCR) system. The power of the qPCR was demonstrated by a quantitative screening of 34 putative *D. discoideum* innate immunity gene transcripts. In a second objective of this work, the *vacuolin* gene-family, which is strongly up-regulated in infection, was selected for a detailed further analysis. In axenic cultures cells vacuolins localize to organelles of the late endocytic pathway and in a previuos study they were declared as a marker for the *M. marinum* compartment in the late phase of infection. Based on protein domains the human homologues of vacuolins are flotillins. However their function remains largely unknown.

Genetic, cell biological, microscopic and biochemical methods were applied to dissect the role of all vacuolins in several *D. discoideum* life cycle stages: during the uptake of various bacteria as well as during infection with pathogens, in particular *M. marinum.* It was shown that the total vacuolin abundance increased by the factor of 3.4 in response to *M. marinum*. In addition, disproportional vacuolin abundances were uncovered, before and after mycobacterial infection, revealing major changes of vacuolin isoform composition during infection. *VacuolinC* mRNA, usually comprised only 1.5% in axenic cells, increased to 25% under infection conditions. An increase was also measured on protein level and vacuolinC was predominantly targeted to the *M. marinum* containing vacuole. Throughout the main part of the *M. marinum* infection, vacuolinC is recruited to the mycobacterial compartment, constituting the major vacuolin abundance.

Investigations of *D. discoideum* single vacuolin knock out mutants suggested a partial complementation potential of remaining vacuolin isoforms. However, a *D. discoideum* mutant lacking *vacuolinB* and *C* was strongly impaired in its ability to control the

infection, accompanied by significantly increased intracellular *M. marinum* proliferation. This observation suggested a protective role of vacuolin for the host.
Importantly, vacuolin accumulation at the *M. marinum* compartment has been translated into more complex mammalian systems: The accumulation of flotillin1 at the *M. marinum* containing vacuole in human blood derived monocytes [82] provided positive evidence of the *D. discoideum* – *M. marinum* model systems potential to find unknown factors involved in tuberculosis infection.

Keywords: Tuberculosis, *D. discoideum, M. marinum*, model systems, quantitative real time PCR, vacuolin, flotillin, *D. discoideum* knock out, *D. discoideum* knock in

Zusammenfassung

Tuberkulose gehört zu den weltweit am weitetesten verbreiteten Infektionskrankheiten. Im Jahr 2012 waren 8,6 Millionen Menschen mit Tuberkulose infiziert, wobei 1,3 Millionen Krankheitsverläufe tödlich endeten. Der dafür verantwortliche Erreger, *Mykobakterium tuberculosis*, wird durch das Inhalieren von kontaminierten Aerosolen übertragen und in der Lunge von alveolaren Makrophagen phagozytiert. Im Gegensatz zu apathogenen Bakterien verhindert *M. tuberculosis* die phagosomale Reifung und damit ihre Degradation, indem es das es umschließende Kompartiment modifiziert und sich darin vermehrt. Trotz intensiver Forschung sind die involvierten Faktoren sowohl des Pathogens als auch der Wirtszelle noch größtenteils unbekannt. Ein besseres Verständnis dieser Mechanismen könnte allerdings als wichtige Grundlage für die Entwicklung neuer Wirkstoffe und Therapieansätze dienen.
Zur Erforschung der Parasit-Wirt-Interaktionspartnern wurde im Rahmen dieser Arbeit das neu entwickelte *Mykobakterium marinum - Dictyostelium discoideum* Modellsystem verwendet, welches sich durch seine Handhabung unter einfachen Laborbedingungen und seine gute genetische Manipulierbarkeit auszeichnet.
Im ersten Teil der vorliegenden Arbeit diente die Etablierung einer quantitativen *real*-Infektion mit *M. marinum*. Insgesamt wurden 34 Kandidatengene untersucht, wobei insbesondere die unter Infektionsbedingungen erhöhten mRNA-Mengen der drei *vacuolin*-Gene von *D. discoideum* auffielen. Aus diesem Grund wurde diese Genfamilie als Forschungsschwerpunkt für den folgenden Teil der vorliegenden Arbeit ausgewählt. In axenisch kultivierten Zellen lokalisieren Vacuoline an Kompartimenten des späten endozytischen Stoffwechsels. In vorherigen Studien wurden Vacuoline als Marker des späten *M. marinum* – Kompartiment bezeichnet. Auf Grund von Proteindomänen wurden Flotilline als humanes Homolog der Vacuoline bestimmt, wobei ihre Funktion weitestgehend unbekannt ist.
Im *M. marinum - D. discoideum* Modellsystem wiesen alle drei Vacuolin-Isoformen erhöhte mRNA Mengen auf, die Gesamtmenge an *vacuolin* mRNA stieg um den Faktor 3.4. Besonders der Anstieg der *vacuolinC* mRNA-Menge um einen Faktor über 100 war am deutlichsten. Diese erhöhte Quantität an VacuolinC konnte auch auf Proteinebene mit Hilfe einer Zelllinie verifiziert werden, bei der das zelleigene Protein mit einer GFP-Markierung versehen wurde. Diese Zelllinie ermöglichte auch den erstmaligen Nachweis einer Lokalisation des VacuolinC-Proteins in *D. discoideum*, wobei es nach Infektion mit *M. marinum* hauptsächlich am bakteriellen Kompartiment detektiert wurde. Anschließend dienten *D. discoideum knock out*-Zelllinien der Charakterisierung der biologischen Funktion der Vacuolin-Familie, bei denen die einzelnen Vacuolin-Isoformen jeweils fehlten. Mit diesen konnten Hinweise gesammelt werden, dass sich die Vacuolin-Isoformen teilweise funktionell komplementieren können. So konnte die Wirtszelle die bakterielle Infektion nicht mehr kontrollieren, wenn zwei der drei Isoformen, *vacuolinB* und *C,* nicht zur Verfügung standen.

Zusammenfassend kann vermutet werden, dass Vacuoline während der *M. marinum*-Infektion eine protektive Rolle in den Wirtszellen übernehmen. Zudem konnte durch den Vergleichen mit vorherigen Untersuchungen des humanen Flotillins gezeigt werden, dass die Abwehrmechanismen von *D. discoideum* unter Infektionsbedingungen derer humaner Monozyten ähneln. Hierdurch könnten weiterführende Untersuchungen des Modellsystems dazu dienen bisher unbekannte Wirtsfaktoren zu finden, welche auf die humane Tuberkuloseerkrankung übertragbar sind.

Schlagwörter: Tuberkulose, *D. discoideum, M. marinum,* Modelsysteme, quantitative *real-time* PCR, Vacuolin, Flotillin, *D. discoideum knock out*, *D. discoideum knock in*

Table of Contents

LANGUAGE CERTIFICATE I 3
LANGUAGE CERTIFICATE II 4
ABSTRACT 5
ZUSAMMENFASSUNG 7
TABLE OF CONTENTS 9
LIST OF FIGURES 12
LIST OF TABLES 14
ABBREVIATIONS 15

1 INTRODUCTION 18
1.1 TUBERCULOSIS 18
1.1.1 Prevalence, morbidity and mortality 18
1.1.2 Impact on society and economy 19
1.1.3 Pathology, clinical symptoms and diagnosis 19
1.1.4 Prophylaxis, treatment and vaccines 19
1.1.5 The causative agent, *Mycobacterium tuberculosis* 20
1.1.5.1 The *M. tuberculosis* life cycle 20
1.2 NEW MODELS TO STUDY MYCOBACTERIAL PATHOGENICITY 21
1.2.1 *M. marinum* a model to understand *M. tuberculosis* pathogenicity 22
1.2.2 The model organism *D. discoideum* 22
1.2.2.1 The *D. discoideum* life cycle 24
1.2.3 *D. discoideum – M. marinum* infection model 25
1.2.3.1 Mycobacterial intracellular life cycle 25
1.3 THE WELL CONSERVED VACUOLIN / FLOTILLIN FAMILY 27
1.4 PROJECT INTRODUCTION 29

2 MATERIALS AND METHODS 30
2.1 MATERIALS 30
2.1.1 Technical and mechanical devices 30
2.1.2 Labware and disposables 31
2.1.3 Chemicals and biological reagents 32
2.1.4 Kits 34
2.2 METHODS 34
2.2.1 Cell biology 34
2.2.1.1 Culture and seeding of *D. discoideum* 34
2.2.1.2 *D. discoideum* stock preparation 35
2.2.1.2.1 Cell cryopreservation 35
2.2.1.2.2 Spore cryopreservation 35
2.2.1.3 Transfection of *D. discoideum* 35
2.2.1.4 Subcloning of transgenic *D. discoideum* cells 36
2.2.1.5 Control of gene integration into target locus by site-specific PCR 37
2.2.1.6 Lipopolysaccharide exposure of *D. discoideum* 37
2.2.1.7 Cell culture of *Mycobacteria* 37
2.2.1.8 *Mycobacteri*a stock preparation 38
2.2.1.9 Cell culture of *Legionella pneumophila* 38
2.2.1.10 *D. discoideum* phagocytosis assay 38
2.2.1.11 *D. discoideum* development 39
2.2.1.12 Infection of *D. discoideum* 40
2.2.1.12.1 Infection of *D. discoideum* with *Mycobacteria* 40
2.2.1.12.2 Infection of *D. discoideum* with *L. pneumophila* 41
2.2.1.13 Fluorescence activated cell sorting (FACS) 41
2.2.1.14 Quantification of colony forming units (cfu) 41
2.2.2 Molecular biology 42
2.2.2.1 Extraction of genomic DNA from *D. discoideum* 42
2.2.2.2 Extraction of total RNA from *D. discoideum* 42

2.2.2.3 Nucleic acid quantity quality control ... 43
2.2.2.4 Revers transcription of mRNA – cDNA synthesis ... 43
2.2.2.5 Quantitative real time PCR (qPCR) ... 43
2.2.2.5.1 SYBR Green I ... 43
2.2.2.5.2 Multiplex TaqMan qPCR ... 46
2.2.2.6 Cloning of plasmids and preparation for transfection ... 48
2.2.2.6.1 PCR ... 48
2.2.2.6.2 Restriction digestion of DNA ... 49
2.2.2.6.3 Agarose gel electrophoresis ... 49
2.2.2.6.4 Extraction of DNA fragments ... 50
2.2.2.6.5 Ligation of DNA fragments into plasmids ... 50
2.2.2.6.6 Generation of and transformation into electroporation competent *E. coli* bacteria ... 51
2.2.2.6.7 Small-scale extraction of plasmid DNA ... 52
2.2.2.6.8 DNA sequencing ... 52
2.2.2.6.9 Large-scale extraction of plasmid DNA ... 52
2.2.2.6.10 Linearization for transfection ... 52
2.2.2.6.11 DNA precipitation ... 52
2.2.2.7 Specific cloning strategies ... 52
2.2.2.7.1 Overexpression constructs ... 52
2.2.2.7.2 Knock in construct ... 53
2.2.2.7.3 Knock out construct ... 54
2.2.3 Protein biochemistry ... 55
2.2.3.1 Protein extraction from *D. discoideum* ... 55
2.2.3.2 SDS-polyacrylamide gel electrophoresis (SDS-PAGE) ... 55
2.2.3.3 Coomassie staining of protein gels ... 56
2.2.3.4 Silver staining of protein gels ... 56
2.2.3.5 Immunoblot analysis ... 57
2.2.3.6 GFP Trap M co-immunoprecipitation ... 57
2.2.3.7 Indirect immunofluorescence analysis (IFA) ... 59
2.2.3.7.1 Fixation ... 59
2.2.3.7.2 Immunolabeling ... 59
2.2.3.7.3 Antibodies and fixed cell stains ... 59
2.2.4 Microscopy ... 60
2.2.4.1 Confocal point scanning microscope ... 60
2.2.4.1.1 Micrograph processing ... 61
2.2.4.2 Wide-field microscope ... 61
2.2.4.3 Quantification analysis of infected *D. discoideum* strains ... 61
2.2.5 *In silico* biology, databases and software programs ... 62
2.2.5.1 Databases and web-links for sequence retrieval ... 62
2.2.5.2 Generation of oligonucleotides ... 62
2.2.5.3 Sequence analysis ... 62
2.2.5.4 In silico cloning ... 62
2.2.5.5 Software programs ... 62

3 RESULTS ... 63
3.1 EXPRESSION ANALYSIS OF INFECTED *DICTYOSTELIUM DISCOIDEUM* ... 63
3.1.1 Design and evaluation of a quantitative real-time PCR system ... 63
3.1.1.1 Primer design and evaluation ... 63
3.1.1.2 glyceraldehyde 3-phosphate dehydrogenase (gapdh): a reliable internal control ... 65
3.1.1.3 Infection for quantitative real-time PCR analysis ... 66
3.1.2 Screening revealed potential candidate-genes that respond to *M. marinum* infection ... 67
3.1.3 Up-regulation of small RNAs in response to *M. marinum* ... 68
3.1.4 Verification of enhanced *vacuolin* mRNA abundance via TaqMan qPCR ... 69
3.1.5 *Vacuolins* are differentially transcribed in various *D. discoideum* infections ... 70
3.1.6 Elevated vacuolinC protein level in response to *M. marinum* infection ... 71
3.2 LOCALIZATION OF VACUOLIN ISOFORMS ... 72
3.2.1 Localization of overexpressed vacuolin isoforms in axenic cultured *D. discoideum* ... 73
3.2.2 Localization of overexpressed GFP::vacuolin fusion proteins in infected cell lines ... 74
3.2.3 Marker association at the mycobacterial compartment by immune fluorescence analysis ... 75
3.3 FUNCTIONAL STUDIES OF VACUOLIN KNOCK OUT CELL LINES ... 76
3.3.1 Generation of a *D. discoideum vacuolinC* knock out mutant ... 76

3.3.2 Characterizing *vacuolin* knock out mutants 77
3.3.2.1 Residual vacuolin transcription in *D. discoideum* knock out mutants 77
3.3.2.2 Growth: vacB^{KO} cells show an increased proliferation rate 78
3.3.2.3 Phagocytosis 78
3.3.2.4 Development: vacB^{KO} impaired in aggregation 80
3.3.3 Characterizing *vacuolin* knock out mutants in the *M. marinum – D. discoideum* infection model 81
3.3.3.1 Vacuolins potential for functional compensation of other isoforms 81
3.3.3.2 Association of the markers vatA and p80 with the mycobacterial compartment in vacuolin knock out cell lines 83
3.3.3.3 Role of vacuolin in regard to *M. marinum* proliferation in *D. discoideum* 85
3.4 IDENTIFICATION OF INTERACTION PARTNERS 86
3.4.1 Vacuolin isoforms form heterogenic oligomers 86

4 DISCUSSION 88
4.1 TRANSCRIPTIONAL CHANGES OF PUTATIVE *D. DISCOIDEUM* INNATE IMMUNITY GENES IN RESPONSE TO THE *M. MARINUM* INFECTION 88
4.2 THE ROLE OF THE VACUOLIN FAMILY IN THE *D. DISCOIDEUM – M. MARINUM* MODEL SYSTEM 91
4.2.1 The vacuolin isoforms are differentially regultated in *M. marinum* infected *D. discoideum* 91
4.2.2 Protective function of vacuolins in the *D. discoideum – M. marinum* model system 95
4.2.3 Partial complementation of vacuolin isoforms 98
4.2.4 Potential vacuolin organization in membrane microdomains 99
4.3 THE VALUE OF THE *D. DISCOIDEUM – M. MARINUM* MODEL SYSTEM 100

5 REFERENCES 102

6 ACKNOWLEDGEMENTS 116
EIDESSTATTLICHE VERSICHERUNG 118
DECLARATION ON OATH 119

List of Figures

Figure 1-1: Disproportional prevalence of tuberculosis……18
Figure 1-2: The *M. tuberculosis* life cycle……21
Figure 1-3: *M. marinum* is closely related to the *M. tuberculosis* complex……22
Figure 1-4: *D. discoideum* diverged from the animal/fungal lineage after the plant/animal division……23
Figure 1-5: *D. discoideum* has a second life……24
Figure 1-6: Course of infection in the *M. marinum – D. discoideum* model system……27
Figure 1-7: *D. discoideum* vacuolin isoforms and their human homologues flotillins consist of well conserved protein domains and localize to the cytoplasmic leaflet of membranes……28

Figure 2-1: Changing ratio of cells that internalized fluorescent beads versus those that did not……39

Figure 3-1: *Gapdh* primer pair revealed an excellent amplification efficiency of 99%……64
Figure 3-2: Validation of *gapdh's* potential for qPCR normalization……65
Figure 3-3: Dismissal and re-uptake of bacteria led to asynchronous infection……66
Figure 3-4: SYBR Green qPCR screening of 34 candidate-genes revealed a new insight into *D. discoideum* transcriptional response to *M. marinum* infection……67
Figure 3-5: Increase of small RNAs (33 nt) in response to *M. marinum* infection……68
Figure 3-6: Multiplex TaqMan qPCR analysis confirmed previously described enhanced *vacuolin* transcription in response to *M. marinum* infection……69
Figure 3-7: mRNA expression profile of *vacuolinC* specifically increased upon pathogenic *M. marinum* infection……70
Figure 3-8: *M. marinum* infection induced elevated vacuolinC protein level in wild type$^{KI\ vacC::gfp}$……72
Figure 3-9: GFP::vacuolinA, B and C fusion proteins localized to endosomal vacuoles inside of axenic *D. discoideum*……73
Figure 3-10: Isoform specific association behavior of GFP::vacuolinA and B fusion proteins with the *M. marinum* compartment……74
Figure 3-11: VacuolinC localized in close vicinity to *M. marinum* infected *D. discoideum*75
Figure 1-12: GFP::vacuolinC maintained very high association rates with *M. marinum* during the course of infection……
Figure 3-13: The *vacuolinC* knock out construct successfully integrated in the *D. discoideum* genome……77
Figure 3-14: *VacuolinC* mRNA expression almost reached detection limits in axenic *vacB^{KO}*……78
Figure 3-15: Escalated cell division in *vacB^{KO}* compared to *D. discoideum* wild type……79
Figure 3-16: Increased plaque formation of *vacB^{KO}* on *Klebsiella* lawn……80
Figure 3-17: Impaired development of *vacB^{KO}* challenged with an abrupt stop of nutrient supply……80
Figure 3-18: Loss of *vacuolinC* led to elevated mRNA levels of residual isoforms *vacuolinA* and B in *vacC^{KO}*……82
Figure 3-19: Moderate increase of vatA localization at *M. marinum* compartment in *vac^{KO}* mutants……83

Figure 3-20: Single knock out of vacuolin isoforms had no influence on p80s presence at the *M. marinum* compartment 84
Figure 3-21: Impaired *vacB*^{KO} defense against *M. marinum* infection 86
Figure 3-22: VacuolinA, B and C assembled to heterogenic oligomers 87

List of Tables

Table 2-1: Technical and mechanical devices....30
Table 2-2: Labware and disposables....31
Table 2-3: Chemicals and biological reagents....32
Table 2-4: Kits....34
Table 2-5: Mutant cell lines were cultured in Hl5c medium supplemented with antibiotics....36
Table 2-6: OD600 - cfu relation....40
Table 2-7: pPCR reaction mix for SYBR Green set-up....43
Table 2-8: qPCR program for SYBR Green set-up....44
Table 2-9: Primer probes for SYBR Green qPCR....45
Table 2-10: Reaction mix for multiplex TaqMan qPCR....47
Table 2-11: Program for multiplex TaqMan qPCR....47
Table 2-12: Primer probes for TaqMan qPCR....47
Table 2-13: PCR reaction mix for GoTaq and Phusion polymerases....48
Table 2-14: PCR programs for GoTaq and Phusion polymerases....49
Table 2-15: Restriction digestion reaction mix for analytic analysis and applications....49
Table 2-16: Ligation reaction mix....50
Table 2-17: A-tailing reaction mix....50
Table 2-18: pGEM-T easy ligation mix....51
Table 2-19: Primer probes for overexpression constructs....53
Table 2-20: Cloning strategy specifics for vacuolinC knock in construct....53
Table 2-21: Primer probes for knock in construct....53
Table 2-22: Primer probes for knock out construct....54
Table 2-23: Mix for preparation of two stacking and two resolving (12%) gels....55
Table 2-24: Primary antibodies....60
Table 2-25: Secondary antibodies and fixed cell stains....60
Table 2-26: Laser lines of the confocal scanning microscope....61
Table 2-27: Filter sets used for wide-field microscope....61
Table 2-28: Software programs....62

Table 3-1: PCR amplification efficiency of vacuolin and housekeeping primer pairs in Sybr Green and TaqMan qPCR systems....65

Abbreviations

%	percent
°C	degrees Celsius
α	anti
atg	autophagy
atg1	autophagy protein 1
atg8	autophagy protein 8
BLAST	basic local alignment search tool
Bp	base pairs
CD	cluster of differentiation
CD36	cluster of differentiation 36
cDNA	complementary DNA
cfu	colony forming unit
CPS	confocal point scanning microscope
Ct	threshold cycle
Cy	cyanine dye
D.	*Dictyostelium*
Dapi	4, 6-diamidino-2-phenylindol
DDB	*Dictyostelium* data base
ddH_2O	double distilled water
DDT	dichlordiphenyltrichlorethan
DHHC	protein motif containing Asp-His-His-Cys
DMSO	dimethylsulfoxide
DNA	desoxiribonuclein acid
Dnja	DnaJ (Hsp40) homolog
dNTP	desoxyribonucleoside 5-triphosphate
DupA	dual role protein A
E.	*Escherichia*
EDTA	ethylene diamine tetraacetic acid
elf6	eukaryotic translation initiation factor 6
et al.	et alii (and others)
FACS	fluorescence activated cell sorting
FTTB	fourteen - three – three like protein B
g	gram; gravitational force
gadph	glyceraldehyde 3-phosphate dehydrogenase
gDNA	genomic DNA
GFP	green fluorescent protein
GOI	gene of interest
H^+-ATPase	proton pump ATPase
h2b	histone 2B
hpi	hours post infection
HspD	heat shock protein D
ig7	mitochondrial large subunit rRNA
iliM	induced after Legionella infection
IMPA1	inositol mono phosphatase
in.ind.	interferon-induced

inf.	infection
K.	*Klebsiella*
KI	knock in
KO	knock out
LB	Luria Bertani
L.	*Legionella*
Litaf	LPS-induced TNF alpha factor
log2	base 2 logarithm
LPS	lipopolysaccharide
M	mole
m	milli
M.	*Mycobacterium*
MAPKs	mitogen-activated protein kinases
Mekk	mitogen activated Kinase Kinase
mCherry	red fluorescent protein
min	minute
ml	milliliter
mock	pseudo control in infection experiements
mRNA	messengerRNA
ms	millisecond
msp	*Mycobacterium* strong promoter
msp12	*Mycobacterium* strong promoter 12
n	nano; number of specimen/experiments
nalp	type of NOD-like receptor
NEB	New England Biolabs
ng	nanogram
Nod	nodal modulator
nramp	natural resistance-associated macrophage protein
nt	nucleotide
OD	optical density
p	pico
p62	alternative gene name for sequestosome-1
pah	phenylalanine hydroxylase
PBS	phosphate buffered saline
PCR	polymerase chain reaction
pH	potential of hydrogen
qPCR	quantitative real time PCR
RanA	ras-related nuclear protein A
RNA	ribonucleic acid
s	second
SN	supernatant
sRNA	small RNA
SYBR Green	cyanine dye
TAE	tris base, acetic acid, EDTA
TirA	toll/interleukin-1 receptor A
TirC	toll/interleukin-1 receptor C
TNF	tumor necrosis factor
Traf6	TNF receptor-associated factor 6
U	units
UV	ultraviolet

V	volt
VacA	vacuolinA
VacB	vacuolinB
VacC	vacuolinC
vatA	subunit of H^+-ATPase
wfdc	WAP four-disulfide core
WHO	World Health Organization
WRKY	DNA binding domain contains conserved WRKYGQK amino acid residues
wt	wild type
x	times
µ	micro
µg	microgram
µl	microliter
µM	micromolar

1 Introduction

1.1 Tuberculosis

1.1.1 Prevalence, morbidity and mortality

Tuberculosis (TB) is a disease of antiquity [52]. As early as 2700 before Christ, a disease similar to TB was described in Chinese literature. In the following centuries, TB caused as much as half of human deaths in Europe and North-America [209]. Friedrich Schiller († 1805), Frederic Chopin († 1849), Franz Kafka († 1924) and George Orwell († 1950) were victims of a disease at that time known as consumption [62]. In his speech „Aetiologie der Tuberculose“ held on march 24th in 1882, Robert Koch was the first to describe an infectious bacterium called *Mycobacterium tuberculosis* as the causative agent of the disease [110]. Of all bacteria, *Mycobacterium tuberculosis* is one of the most effective human pathogens that still belongs to the greatest killers worldwide: According to the world health organization (WHO) 8.6 million people fell ill with TB and 1.3 million died from TB in 2012 [137]. About one third (about 2 billion) of the world's population has latent TB, meaning that these people are infected but do not develop the disease. 10% of them will develop the disease during their lifetime and thus provide a large reservoir for active TB; a progressive hazard that will last for decades [11]. TB occurs worldwide (fig. 1-1). In 2012, the largest number of new TB cases arose in Asia comprising 60% of new cases globally.

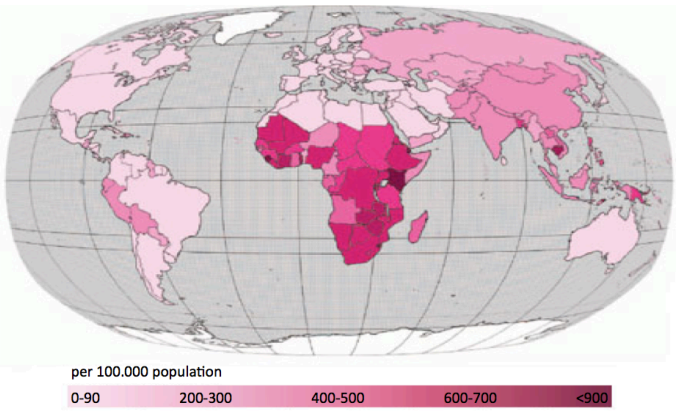

Figure 1-1: Disproportional prevalence of tuberculosis. According to estimations of the world health organization (WHO) tuberculosis occurs worldwide. Countries in sub-Saharan Africa and Asia have the highest tuberculosis prevalence. These areas are marked in dark shades of pink. Prevalence is shown in case per 100.000 population. Map was adapted from http://www.nature.com/news/specials/tb/index.html#map

However, the highest proportion of new cases per population, over 255 cases per 100.000 population, was estimated in sub-Saharan Africa. In comparison, due to efficient public health systems, the estimated mortality of TB cases per 100,000 population in Germany was 0.35 in 2012 [137]. Nowadays, active TB is treatable via a long-term therapy with a combination of four antimicrobial drugs: isoniazid, rifampicin, pyrazinamide and ethambutol [217]. Since 1995, more than 56 million people have been cured.

Emerging multidrug resistant *M. tuberculosis* strains complicate antibiotic treatment and have become incurable in some parts of the world [150]. Thus, from a global point of view TB remains a major health problem in the 21th century.

1.1.2 Impact on society and economy

From the disproportional distribution of TB prevalence it becomes clear that its impact primarily affects the developing world (fig. 1-1). In other words TB is the prototype of a disease of poverty [55, 68]. The high-burden countries identified by the WHO include China and India. Thus two of the largest emerging economies collectively accounted for more than one third of all new TB cases in 2009 [205]. Poor living and working conditions lead to enhanced risk of TB transmission, while factors such as malnutrition and diabetes impair the host's defense against TB [55]. In addition to these area restricted socio-economic risk factors HIV/AIDS and emerging antimicrobial resistance became driving forces towards a global TB pandemic. Particularly observed in recent years in South Africa, HIV/AIDS infections had a considerable effect on TB incidence [69, 112]. Due to application of chemotherapy against TB and improper use of antibiotics increased levels of multi drug resistant (MDR) and extremely drug resistant (XDR) strains appear [17, 150]. These patients are increasingly hard to cure along with higher expenses [189].

1.1.3 Pathology, clinical symptoms and diagnosis

In 90% of infected patients TB affects the lungs. Symptoms of patients with active lung infection are cough, often with sputum and blood, shortness of breath, fever, night sweats and weight loss [218]. The most common test to diagnose TB still is microscopic analysis of sputum, known as the sputum smear test, which has a sensitivity of 34-80% [46]. More sensitive is the sputum culture test, however it takes weeks to receive results. Diagnosis in children is particularly difficult, due to the lack of sputum production. Only recently, Boehme *et al.* developed a highly sensitive molecular test for *M. tuberculosis* (GeneXpert MTB/ RIF). The results can be obtained within two hours and simultaneous detection of rifampicin resistance is ensured. Rifampicin is one of the main antibiotics used to treat TB. The resistance against rifampicin serves as a marker for multidrug resistant bacteria [15]. However, its use cannot detect latent disease. Identification of persons with latent TB is an important factor to track *M. tuberculosis* reservoirs and stop risks of further spreading. Widely used is the tuberculin skin test (TST), which lacks specificity and can lead to false-positive results from environmental *M. marinum* and prior BCG vaccinations [56, 102, 167].

1.1.4 Prophylaxis, treatment and vaccines

To date an attenuated form of *M. bovis Bacille Calmette-Guérin* (BCG) is the sole vaccine against TB available. It was developed in 1921 and protects young children against TB meningitis and partially against severe forms of pediatric TB [1, 107]. The reasons remain unknown but unfortunately BCG does not protect against the diseases' highest burden

worldwide, the classical pulmonary form of TB [159]. Beyond the search for an efficient vaccine, which surely would reduce susceptibility to infection, only early diagnosis and efficient drug treatment can cut off transmission and thus remain a top priority for TB control [55].

1.1.5 The causative agent, *Mycobacterium tuberculosis*

M. tuberculosis, the causative agent of human TB is a member of the *M. tuberculosis* complex. Further members are, *M. africanum* that causes TB in some parts of Africa, *M. bovis*, which causes tuberculosis in mammals including cattle and humans, *M. microti* that infects voles but is avirulent in humans and mice and *M. canettii,* whose infection is rare [41]. *Mycobacteria* are rod shaped, acid-fast bacteria. In comparison to other bacterial species, *Mycobacteria* have a very unique cell wall structure. It is composed of a thick inner layer of arabinogalactan and an outer waxy layer of mycolic acids [73]. *M. tuberculosis* is a facultative intracellular pathogen, that parasitizes macrophages [196]. The loss of cell wall component correlates with intracellular survival [122, 136].

1.1.5.1 The *M. tuberculosis* life cycle

Current knowledge of the *M. tuberculosis* infection and life cycle is based on observations from human TB as well as research on animal models [63, 158]. The cycle starts when a patient with pulmonary disease coughs and exhales small droplets containing *M. tuberculosis* in the atmosphere. These aerosols abide airborne for several hours [159]. Infection of a host is initiated with inhalation of contagious aerosols [106]. Once in the lung, TB bacteria are presumably internalized through phagocytosis by alveolar macrophages that induce a local proinflammatory response followed by recruitment of mononuclear cells from near blood vessels (fig. 1-2). Subsequent events are rather complex and include macrophage differentiation into multinucleated giant cells, foamy macrophages and epithelioid macrophages that assemble to form granulomas or tubercles [159, 160]. These highly organized structures, can be further stabilized by accumulation of a fibrous cuff of extracellular matrix that exclude blood vessels. The accrued granuloma structure defines the disease [145]. The host's attempt to control the infection leads to a balance in which invaded bacteria are kept in check. In approximately 90% of the cases latent TB persists but is controlled and active disease never develops [65]. The precise perturbation of the immune system that leads to a TB reactivation is not known. In the case of HIV co-infection, alcoholism or treatment with α-TNF antibodies the immune deficiency is apparent, however, the majority remains unclear [40, 58]. Progression towards an outbreak is characterized by loss of vascularization, necrosis and accumulation of caseum in the center of the granuloma. Ultimately the granuloma ruptures and releases thousands of infectious bacilli into the airways [159].

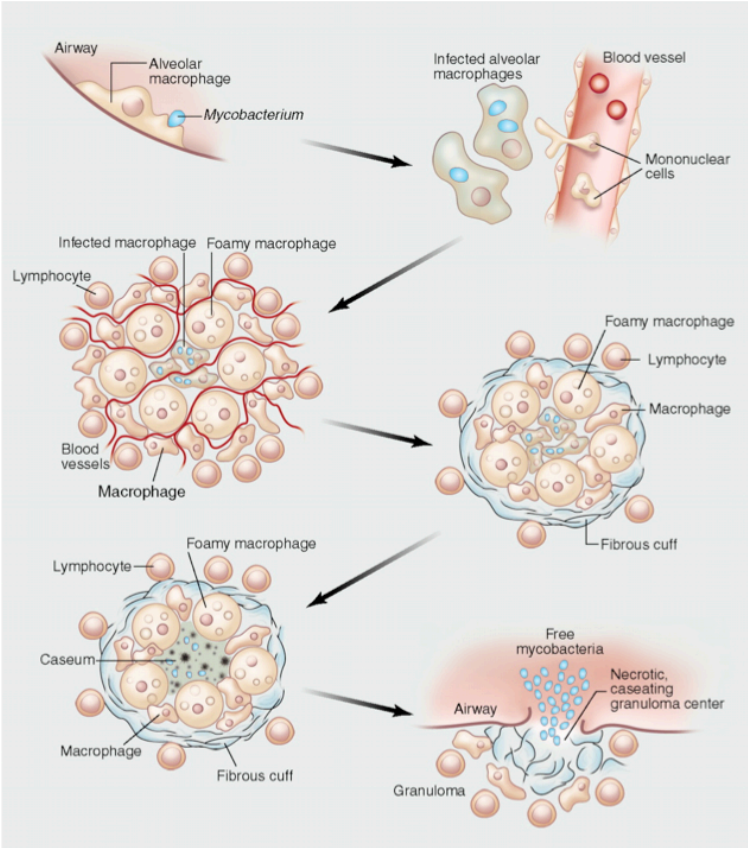

Figure 1-2: The *M. tuberculosis* life cycle. Airborne aerosols containing infections *M. tuberculosis* bacilli are inhaled and reach the lumen of the lungs. It is assumed that alveolar macrophages internalize bacteria. Instead of being killed, *M. tuberculosis* proliferates intracellular. A local proinflammatory response leads to the recruitment of mononuclear cells from near blood vessels. While *M. tuberculosis* replicates, recruited macrophages and lymphocytes surround infected macrophages. These cells then undergo complex differentiations and assemble to a granuloma. A surrounding fibrous cuff stabilizes the structure. In 90% of the cases a balance is kept at this stage, which is called latent infection. Reactivation of the infection is induced by necrotic detachment of the granuloma and rupture. Liquefied internal compounds including *M. tuberculosis* bacilli reach the airways and can be exhaled; starting a new round of infection. Figure was taken from Russell *et al.* 2010, *Science*

1.2 New models to study mycobacterial pathogenicity

M. tuberculosis is a strictly human pathogen. Additionally, due to the risk of accidental exposure, *M. tuberculosis* has to be handled at biosafety level 3. That bears obstacles in terms of research. The animal model that most closely imitates a human TB infection (active and latent) is the macaque [26]. Crossing ethical boundaries and cost considerations limit the use of that model. From all mammalian models, the mouse traditionally is the most used organism and contributed largely to insights into genetics and immunology of *M. tuberculosis* infection. However mice do not develop comparable granulomas.

More recently a zebrafish model was successfully developed and used to study granuloma formation [42, 184]. Another surrogate host, *Drosophila*, provides excellent genetic tools and RNAi screens [51]. Rapid accessions into intracellular biology of the mycobacterial infection enable investigations of the social ameba *Dictyostelium discoideum* [82, 170]. Next to surrogate hosts surrogate pathogens have proven an important tool in the study of infectious diseases. Mycobacterial models like *M. marinum, M. bovis* and *M. avium* are increasingly used to study mycobacterial virulence and pathogenicity [163]. A combination of both surrogate pathogen and surrogate host has the advantage of reduced safety risks and the potential to contribute new aspects that may help to decipher yet unknown details of host-pathogen interaction and enhance the discovery of improved treatment and prevention strategies

1.2.1 *M. marinum* a model to understand *M. tuberculosis* pathogenicity

In 1954, *M. marinum* was responsible for cutaneous granulomatous lesions of 80 people that swam in a contaminated swimming pool. This was the largest outbreak with human victims caused by *M. marinum* and the reason why the disease is now called swimming pool or fish tank granuloma [74]. According to 16sRNA gene sequence analysis *M. marinum* is a close relative to *M. tuberculosis* with above 85% nucleotide identity (fig. 1-3) [187]. It naturally infects amphibians, fishes and opportunistically humans [125]. Both species share mechanisms of virulence and cause indistinguishable pathologies and lesions [186]. One of the common genetic features is the ESX-1 secretion system required to export proteins across their complex cell walls. The coding region encompasses a known virulence gene cluster, RD1, which if knocked out, leads to decreased virulence in both species. Redundant protein functions were emphasized by expression of *M. marinum* homologues in *M. tuberculosis* knock out strains and vice versa [70, 71].
Moreover, immunization of mice with *M. marinum* resulted in protection from *M. tuberculosis* challenge [39]. Various studies show that *M. marinum* is an adequate model to investigate pathogenicity and virulence of *M. tuberculosis* [12, 173, 178].

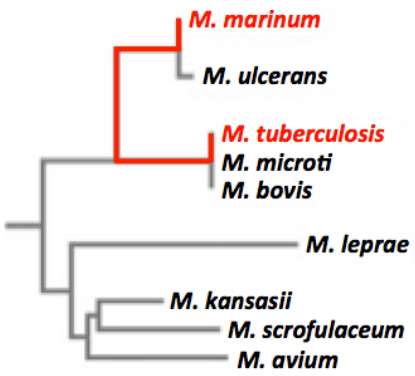

Figure 1-3: *M. marinum* is closely related to the *M. tuberculosis* complex. Phylogenetic analysis based on 16sRNA gene sequences reveal that *M. marinum* is a close relative to *M. tuberculosis* with above 85% nucleotide identity. Adapted from Stamm & Brown, 2004, *Microbes and Infection*

1.2.2 The model organism *D. discoideum*

D. discoideum is a fascinating member of the amoebozoa. Phylogenetic analysis based on protein sequences revealed that *D. discoideum* evolved from the animal/fungal lineage after the plant/animal split. *D. discoideum* harbors a complex genome and conjuncts more of the ancestral genome than either animals or plants [57]. Its natural habitats are terrestrial ecosystems. *D. discoideum* can be found in forest soil and decaying organic matter, where it tracks prey by chemotaxis [22]. As a professional phagocyte independent single *D. discoideum* cells feed on bacteria and yeast and ingest, kill and digest microorganisms [43]. *D. discoideum* cells are able to digest approximately 300 bacteria in one hour, a phagocytic capability, which easily exceeds that of neutrophils [162]. In regard to the phagocytosis process many correlations between *D. discoideum* and human phagocytic cells are present [19, 123]. Tracked bacteria are engulfed by actin-dependent phagocytosis and enclosed in a newly formed vacuole, the phagosome. Immediately after internalization p80, a putative copper transporter is recruited to the phagosome [149]. Within ten minutes after uptake the vacuolar H^+-ATPase complex is found in phagosome membranes [36, 34]. The multi-subunit enzyme transports protons across the

membrane into the phagosome via hydrolysation of ATP. The resulting proton gradient serves the transport of small molecules and the acidification of these organelles. Additional fusion with lysosomes results in the development of a phagolysosome that contains degradative enzymes such as proteases, which start to digest bacterial compounds. Fission events lead to removal of the vacuolar H^+-ATPase and lysosomal proteins; the vacuole re-neutralizes and matures to a post-lysosome [27, 36]. The post-lysosome is specific for *D. discoideum* and not found in macrophages [92]. A characteristic post-lysosomal element is membrane associated vacuolin [148]. It was reported that vacuolin may be involved in inducing exocytosis [116]. In *D. discoideum* and marcophages exocytosis of indigestible compounds terminates the phagocytosis process.
Phagocytosis also comprises the core function of innate immunity. In spite of the amoeba branched from the tree leading to metazoan after plants diverged, many specific functions remain conserved. Thus a basic skeleton of phagocytosis mechanisms equally exists in *D. discoideum* and mammalian macrophages.

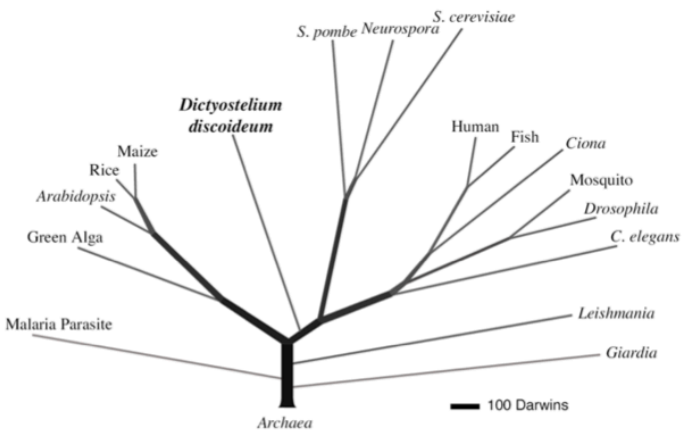

Figure 1-4: *D. discoideum* diverged from the animal/fungal lineage after the plant/animal division. Proteome based phylogenetic analysis of selected model organisms, humans, plants and pathogens. Relative lengths are depicted in Darwins, (1 Darwin= 1/2000 of the divergence between *S. cerevisiae* and humans). Species that are not specified are *Plasmodium falciparum* (malaria parasite), *Chlamydomonas reinhardtii* (green alga), *Oryza sativa* (rice), *Zea mays* (maize), *Fugu rubripes* (fish), and *Anopheles gambiae* (mosquito) Figure was taken and cited from Eichinger *et al,* 2005, *Nature*

This correlation is supported by the high degree of conservation between *Dictyostelium* and human proteomes [57]. It is presumed that basic features of pathogenic virulence and host defense mechanisms evolved in ancient co-evolution before the split of animals or plants and are still used in both, amoeba and mammalian phagocytic cells [43, 76]. Proteomic analysis using the fully sequenced *D. discoideum* genome identified at least 33 genes as orthologs of disease related human genes [57]. For example, the *D. discoideum* genome encodes potential homologues to innate immunity proteins, including Toll-like Interleukin Receptor (TIR)-domain containing proteins, WRKY transcription factors and potential LRR-domain receptors [29, 57]. Over ten years ago, when *D. discoideum* was first used as a model host for *L. pneumophila*, the list of pathogens for which *D. discoideum* was successfully used as a host constantly increased. By now it includes *S. typhimurium, P. aeroginosa* and the *Mycobacteria* species *M. avium, marinum* and *tuberculosis* [44, 82, 83, 98, 165, 170, 171]. The major benefit of *D. discoideum* as a model host relies on the analysis of host cell factors that are involved in the infection. For corresponding studies a large number of knock out mutants are freely available at the *D. discoideum* stock center [90].

1.2.2.1 The *D. discoideum* life cycle

In their vegetative state, cells divide by binary fission. Upon nutrient depletion single cells undergo a process called development and form a multicellular organism that comprises differential cell types (fig. 1-5) [30].

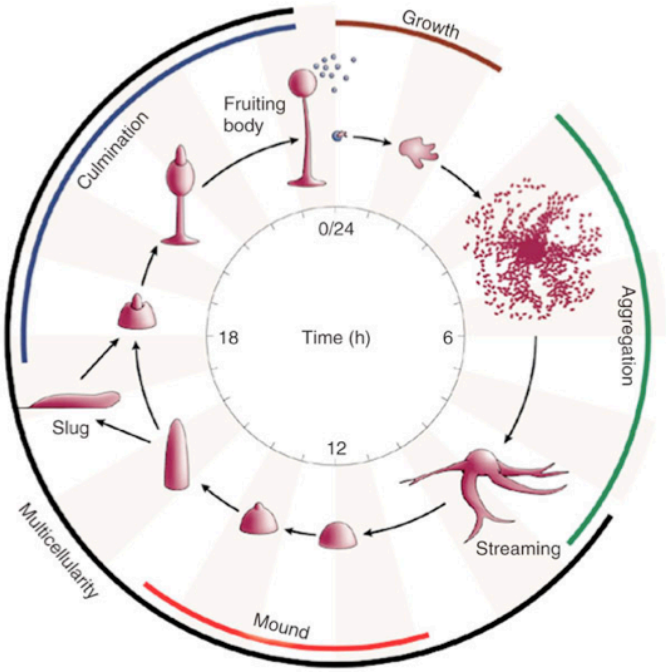

Figure 1-5: *D. discoideum* has a second life. Starting at the moment of nutrient deficiency an astonishing and unique developmental process starts. Via cell to cell signaling single cells start to stream together, forming a multicellular organism that is able to move towards light sources. The process completes within 24 hours marked by spores arising at the top of a little trunk, well harbored in a protective capsule. Spores can persist over long time periods and hatch if the conditions improve. Figure was taken from http://www.nature.com/nprot/journal/v2/n6/images/nprot.2007.178-F1.jpg

The first step towards multicellularity is the aggregation of ~10^5 cells that stream together. The driving force in the streaming process is chemotaxis towards cyclic adenosine 3', 5'- monophosphate (cAMP). As the mound forms, differentiation of pre-spore and pre-stalk cells begins. Development proceeds with the formation of a tip, which extends to a finger-like structure with an anterior-posterior polarity. Extended fingers can fall to form a motile slug that is phototactic and migrates towards light sources. Ultimately at a stage defined as culmination, finger or slug contract and the anterior tip rises to form a fruiting body, consisting of a slender stalk bearing on top a capsule filled with spores. In this process, pre-stalk cells differentiate into stalk cells that elongate and die and pre-spore cells differentiate into spores. Spores are well shielded inside a fruiting body and insensible against heat and drought. The entire process from starvation of vegetative cells to the formation of a mature fruiting body takes 24 hours [108]. The life cycle recommences when under improved conditions spores hatch to single cells [108]. Within the course of development, the phagocytic potential of cells gradually declines. Ultimately, from the migrating slug only 1% of the cells, the so called sentinel cells, exhibit the ability to phagocytize [29]. Sentinel cells migrate through the slug and phagocytize bacteria and toxic substances, representing a primitive innate immunity system.

1.2.3 *D. discoideum – M. marinum* infection model

The *D. discoideum – M. marinum* model system combines two organisms that can be handled comfortable in a laboratory. Both organisms are genetically accessible; especially *D. discoideum* harboring a haploid genome facilitates genetic manipulations. As a surrogate macrophage *D. discoideum* is infected with *M. marinum,* which has a generation time of four hours during logarithmic growth, in contrast to more than 20 hours of *M. tuberculosis* [186]. In addition BSL 2 safeguards are sufficient for *M. marinum* culture and infection studies with the model. Both, *M. marinum* and *M. tuberculosis* survive and replicate in macrophages and *M. marinum* replicates in *D. discoideum*. Common features of *M. tuberculosis* infection of macrophages in regard to the pathogens' manipulation of the host and the host defense strategies are equally found in the *D. discoideum – M. marinum* model system, respectively. Conservations of genetic programs that translate into shared virulence and protection patterns allow detailed investigation of the mechanisms of intracellular host pathogen crosstalk. It is known that *Mycobacteria* interfere with host trafficking pathways and presumed that replication takes place in a protected niche, the mycobacterial phagosome [89]. More recently, the idea that bacteria are also able to grow in the cytoplasm has gained recognition [124, 191]. In the following paragraphs current knowledge about the *Mycobacteria* intracellular life cycle is discussed describing similarities and differences of surrogate and natural hosts.

1.2.3.1 *Mycobacterial* intracellular life cycle

The intracellular life cycle of *Mycobacteria* is initiated by binding to the cell surface via specific phagocytosis receptors that are localized in the macrophage plasma membrane [61]. *M. tuberculosis* is recognized from macrophages by Mincle a C-type lectin receptor. Mincle binds the mycobacterial glycolipid, trehalose-6'6'-dimycolate part of the cell wall a known cord factor of *M. tuberculosis* immunostimulatory components [95]. It is not known if subsequent signaling cascades can be manipulated by the *Mycobacteria* for their benefit or not [113, 127]. In *D. discoideum*, genes encoding potential receptors for phagocytosis exist. In a genome wide comparative study of transcriptomes, Sillo *et al.* found a carbohydrate - binding membrane protein, a putative scavenger receptor, and a few other putative membrane proteins strongly up-regulated upon phagocytosis of *E. coli* [164].

A progressive surrounding of plasma membrane marks the ingestion of *Mycobacteria*, eventually a new vesicle called phagosome originates. This process can be very rapid, within less than 60s in *D. discoideum* [35]. Once internalized by phagocytosis, instead of being killed, *M. tuberculosis* and *M. marinum* replicate in macrophages and *D. discoideum*. This ability is instrumental in regard to the establishment of an infection. Many factors are involved in remodeling the intraphagosomal environment aimed to kill phagocytized bacteria into a convenient mycobacterial environment. The central role in the process is the block of phagosomal maturation.

The *M. tuberculosis* containing phagosome in macrophages fuses with early endosomes shortly after phagocytosis [86, 181]. This leads to the accumulation of the small GTPases Rab5, however, its conversion to Rab7, as it occurs in normal phagosomal maturation,

does not follow [197]. Amongst a variety of functions, Rab GTPases, control vesicle budding and fusion [175]. Without the presence of Rab7 fusion with late endosomes and lysosomes is impaired with consequence that markers such as cathepsin or LAMP are not found at the mycobacterial vacuole [37]. Moreover, Rab5 recruits the kinase that generates phosphatidylinositol 3-phosphate (PI3P) [143]. PI3P is suspected to be a target of a mycobacterial secreted factor [194].

Mycobacterial effectors are still being uncovered, however it is known that *M. tuberculosis* secretes an acid like phosphatase (SapM) and tyrosin phosphatases (PtpA and B) that interfere with host trafficking processes [9, 78, 161]. SapM may hydrolyze phosphatidylinositol 3-phosphate (PI3P) another major player in phagosomal trafficking events [156, 195]. PtpA binds to the cytosolic subunit H of the macrophage vacuolar-H^+-ATPase multisubunit protein complex initially found at internalized phagosomes. Next, PtpA dephosphorylates VPS33B a member of the class C VPS complex, responsible for regulation of membrane fusion within the endocytic pathway [10, 153, 211]. Inactivation of VPS33B inhibits further fusion with lysosomes [9]. Circumvention of lysosome delivery and the accompanied exposure of bactericidal components prevents degradation and subsequent presentation of mycobacterial antigens to the immune system [5, 85, 139, 144].

Characteristic for the mycobacterial phagosome is the lack of late endosomal markers such as Rab7 or Lamp1 and due to insufficient delivery of vacuolar H^+-ATPase, an elevated pH of 6.2 to 6.4 [31, 181]. Besides impaired phagosomal biogenesis, the compartment remains connected to the endocytic pathway: Transferrin receptors travel to and from the mycobacterial phagosome allowing the scavenging of iron [31, 180]. In parallel, an identical strategy of mycobacterial survival is observed in the *D. discoideum – M. marinum* model system: the phagosomal maturation arrest [82]. This is specific to pathogenic *Mycobacteria*, as non-pathogenic *Mycobacteria* such as *M. smegmatis* or prey undergo phagosomal maturation (fig.: 1-6). In contrast, *M. marinum* circumvents phagosomal maturation and remodels the vacuole into a replication niche (fig.: 1-6). Initial accumulation of the vacuolar H^+-ATPase at the *M. marinum* containing vacuole is a transient matter and the complex is removed quickly. Similar to macrophage infections acidification is strongly reduced. Also, due to inhibited lysosomal fusion cathepsinD is not present in the *M. marinum* compartment [82]. Specific to *D. discoideum* is the recruitment of p80, a putative copper transporter to the *M. marinum* containing phagosome and at later time points the accumulation of vacuolin [82]. It is assumed for *D. discoideum* and macrophage hosts that *M. marinum* replication takes place in the compartment and that the bacteria subsequently escape into the cytosol by rupturing the replication niche [82, 166, 174]. Ultimately, reported for the *D. discoideum – M. marinum* model system, *M. marinum* exit the host in a non-lytic fashion through an actin-based structure, the ejectosome [81].

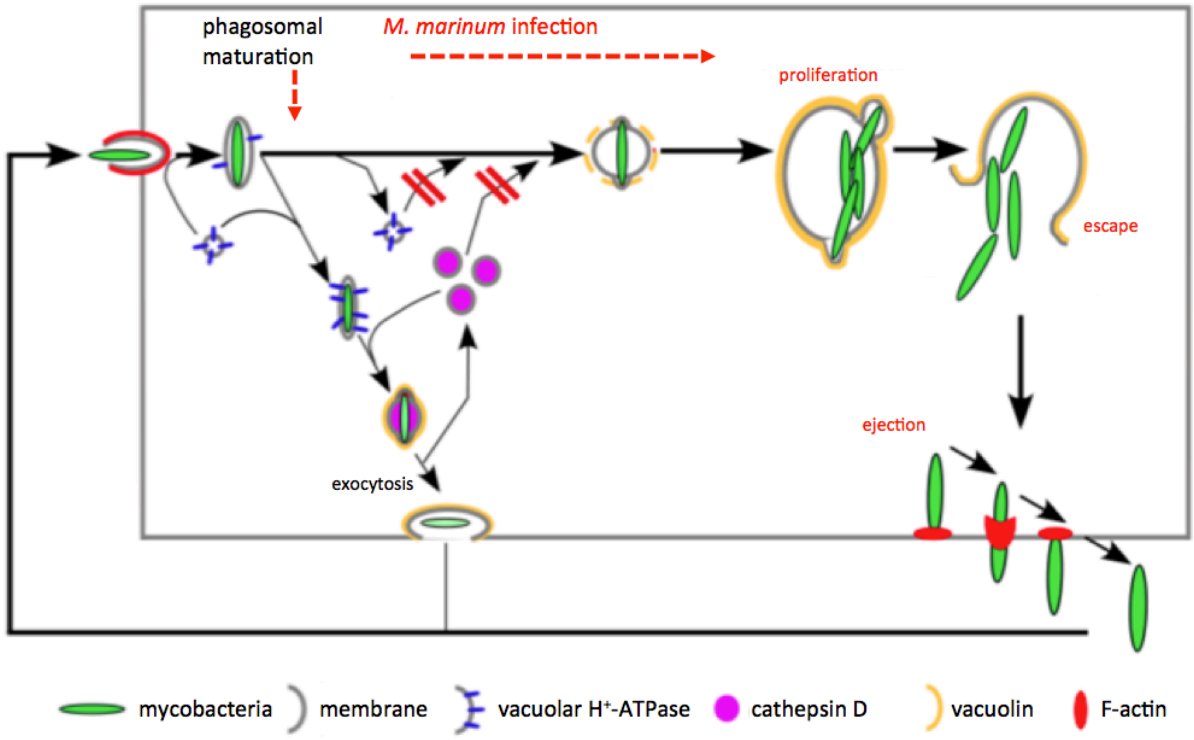

Figure 1-6: Course of infection in the *M. marinum – D. discoideum* model system. Bacteria are internalized via phagocytosis**.** In the case of prey or non-pathogenic *M. smegmatis* a process called phagosomal maturation takes place leading to degradation and exocytosis. In the case of pathogenic *M. marinum* the initially recruited vacuolar H^+-ATPase (small blue rods) is removed from the compartment. Additionally, the fusion with lysosomes is blocked. Thus lysosomal proteases such as cathepsinD (pink) are not released into the replication niche. 12 hours post infection (hpi) vacuolin (yellow) starts to accumulate at the *M. marinum* containing compartment. The bacteria proliferate in their customized replication niche that finally ruptures. *M. marinum* escapes into the cytosol and ultimately exits the cell in a non-lytic fashion through an actin-based structure called ejectosome. Figure was adapted from Hagedorn *et al.* 2009, *Science*

1.3 The well conserved vacuolin / flotillin family

The *D. discoideum* genome encodes three isoforms of vacuolin, *vacuolinA, B* and *C*. Their DNA sequences are strikingly similar: while *vacuolinA* and *B* share an identity score of 78.1%, *vacuolinB* and *C* share 86.3%. According to dictybase gene information sheets, only *vacuolinA* and *B* are expressed in vegetative *D. discoideum* cells. Both proteins localize to membranes of late endosomes and patches of the plasma membrane [148, 207]. Their localization is partially mediated by the small GTPase RacH [172]. In the *D. discoideum – M. marinum* model system vacuolin is a marker of the maturing mycobacterial compartment and suggested to play a role its establishment and maintenance [81, 82].

While the knock out of *vacuolinA* does not lead to effects in the endocytic pathway nor in *M. marinum* infection the lack of *vacuolinB* has a rather strong impact on both: In regard to the endocytic pathway the process of re-neutralization is impaired and a drastic enlargement of late endosomal vacuoles occurs. For these reasons a role of *vacuolinB* in the coordination of exocytosis was postulated [96]. More important is the effect of *vacuolinB* deficiency on the course of *M. marinum* infection in *D. discoideum,* where it leads to an improved resistance against *M. marinum* infection [82]. Characteristic protein domains shared by all vacuolin family members is an evolutionary conserved prohibitin homology (PHB) domain located at the intermediate part of the protein and a coiled-coil

domain (CC) at the C-terminus (fig. 1-7: A). The latter is responsible in mediating oligomerization to homo- and hetero oligomers [172]. Based on structural domain organization *D. discoideum* vacuolin isoforms were categorized as homologues to mammalian flotillins [207].

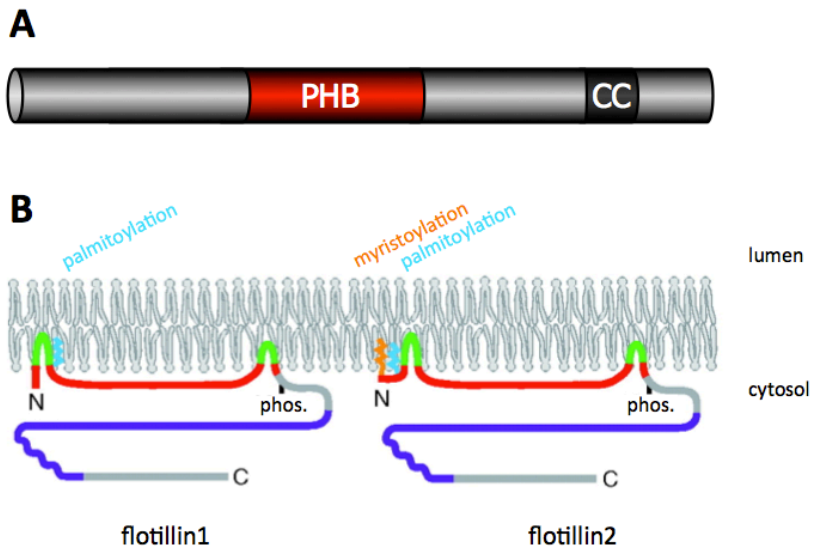

Figure 1-7: *D. discoideum* vacuolin isoforms and their human homologues flotillins consist of well conserved protein domains and localize to the cytoplasmic leaflet of membranes. (**A**) In all three vacuolin isoforms, the prohibitin homology (PHB) domain is located at the intermediate part of the protein and the coiled-coil domain (CC) at the C-terminus. (**B**) Palmytoylation and myristoylation have been shown to strengthen membrane attachment of human flotillins.

The human homologues, flotillin1 and 2 also comprise of a PHB and CC domain but the PHB domain is located at the N-terminus of the protein closely followed by the CC domain. Proteins that contain a PHB domain are categorized to the SPFH superfamily [8, 154].

The SPFH superfamily of proteins is a very diverse family of prokaryotic and eukaryotic membrane proteins that all carry the evolutionarily conserved domain called SPFH (named after the proteins Stomatin, Prohibitin, Flotillin and HflK/C) [24]. Members of this superfamily can be found in all species including bacteria, archaea and eukaryotes and are universally expressed [8]. Despite intense research their function remains not clear and various functions such as coordinating of fusion and fission events, scaffolding proteins and active signaling partners have been proposed [64, 135, 169, 132].

All members of this protein group are enriched in detergent-resistant fractions and classified as lipid raft proteins. The presence of PHB also in prokaryotic proteins suggests a possible ancient lipid recognition motif [130].

Localization of the integral membrane proteins flotillins to the cytoplasmic leaflet of endosomal membranes is facilitated by loops of the protein that intercalate with one lipid bilayer but not traverse it (fig. 1-7: B). Post translational palmytoylation and myristoylation support and strengthen membrane localization [154]. It was reported that their organization in membrane microdomains could induce plasma membrane invagination [64]. Importantly flotillins are a common target of pathogenic organisms; the protozoan *L. donovanii* prevents flotillin1 delivery to its intracellular compartment, the parasite *P. falciparum* exports its own homologue and *S. meliloti*, a nitrogen-fixing bacteria that infects plants, induces a strong up-regulation of host flotillins [49, 84, 87].

1.4 Project introduction

Despite decades of intense research the specifics of *M. tuberculosis* intracellular development are mostly unknown. Especially, major knowledge is lacking of the essential steps during phagosomal maturation arrest and the establishment of the replication niche. Better understanding of host-pathogen interaction could aid the evaluation of new vaccine candidates and improve diagnostic capabilities.

The first objective of this study was to use the *M. marinum – D. discoideum* infection model to find host cell genes that undergo alteration of mRNA production in response to the infection. A bioinformatic approach and the annotated genome provided *D. discoideum* gene candidates that were hypothesized to be involved in the immune response. First, to measure mRNA levels, the establishment of the methodological backbone, a quantitative real time PCR (qPCR) was planned. Via qPCR, baseline transcription patterns of gene candidates should be compared to transcription patterns from *D. discoideum* infected with *M. marinum.* Additional, comparisons to other pathogenic and non-pathogenic bacteria sould be analyzed to disclose *M. marinum* specific responses.

The second objective was to evaluate the impact of the most promising candidate-genes in respective to the course of infection in a spatial and temporal fashion. For this, a wide range of methods, including genetic manipulation, fluorescence microscopy and protein biochemistry should be used to examine translation, localization and function of the candidate-gene products in the *D. discoideum* - *M. marinum* model system.

2 Materials and Methods

2.1 Materials

2.1.1 Technical and mechanical devices

Table 2-1: Technical and mechanical devices

Type	Model	Manufacturer/Distributor
Agarose gel electrophoresis chamber	Horizon® 58 PerfectBlue™	Gibco, Karlsruhe, Germany PEQLAB, Erlangen, Germany
Analytical scale	PCB 1000-1	Kern & Sohn, Balingen, Germany
Cell culture incubator	Innova 42	Eppendorf, Hamburg, Germany
Centrifuges	5415 R 5415 D 5417 GS-6KR	Eppendorf, Hamburg, Germany Eppendorf, Hamburg, Germany Eppendorf, Hamburg, Germany Beckmann, Krefeld, Germany
Digital camera	C4742-95	Hamamatsu, Herrsching
Flow cytometer (FACS)	Accuri C6 Calibur	BD, Franklin Lakes, USA BD Bioscience, Heidelberg, Germany
Fluorescence binocular	SMZ 800	Nikon, Duesseldorf
Freezing container	Mr. Frosty	Thermo Fisher, Waltham, USA
Magnetic stirrer	Combimag RCT	IKA Labortechnik, Staufen, Germany
Microscopes - basic light microscope - basic model wide-field - advanced model wide-field - confocal point scanning	 CKX41 Axiovert 200 cellR Imaging System FluoView 1000	 Olympus, Hamburg, Germany Zeiss, Jena, Germany Olympus, Hamburg, Germany Olympus, Hamburg, Germany
Microwave	R-234	Sharp Electronics, Osaka, Japan
NanoDrop	NanoDrop 2000	Thermo Scientific, Wilmington, USA
Neubauer counting chamber	Neubauer-improved	Marienfeld, Lauda-Königshofen, Germany
PCR machines	MJ Mini™ T3000	Bio-Rad, Munich, Germany Biometra, Goettingen, Germany
Photometer	BioPhotometer	Eppendorf, Hamburg, Germany
pH meter	pH Level 1	inoLab, Weilheim, Germany
Pipetting aid	Matrix	Thermo Fisher, Waltham, Germany

Type	Model	Manufacturer/Distributor
Pipettes	P2 P10 P20 P100 P200 P1000	Gilson, Middelton, USA Rainin, Gießen, Germany Gilson, Middelton, USA Rainin, Gießen, Germany Gilson, Middelton, USA Rainin, Gießen, Germany
Power supplies	Consort E835 Consort EV231 EPS 3500	Consort, Turnhout, Belgium Consort, Turnhout, Belgium Amersham Bio. Freiburg, Germany
Scale	Handy H51	Sartorius, Göttingen, Germany
Shaker	Innova™ 4400 KS250 Basic	New Brunswick, Nuertingen, Germany IKA Labortechnik, Hamburg, Germany
Sterile benches	Kojair 2009 Herasafe	Kojair, Vilppula, Finnland Heraeus Instruments, Osterode, Germany
Tweezer	Pinzette Inox Nr. 5	neoLab Migge Laborbedarf-Vertriebs GmbH, Heidelberg, Germany
UV bath	Sonorex Super	Bandelin, Berlin, Germany
UV transilluminator	UV-Flaechenstrahler	Konrad Bender, Wiesloch, Germany
Vacuum pump	Laboport	KNF, Freiburg, Germany
Vortexer	VF2 Vortex Genie 2	IKA Labortechnik, Hamburg, Germany Scientific Industries Inc, New York, USA
Water bath	FBH 604 SW 20	Fisherbrand®, Schwerte, Germany Julabo, Seelbach, Germany

2.1.2 Labware and disposables

Table 2-2: Labware and disposables

Type	Specification	Manufacturer/Distributor
Cell culture dishes	35 x 10 mm 100 x 20 mm	BD, Franklin Lakes, USA BD, Franklin Lakes, USA
Cell culture plates	24-well	Sarstedt, Nümbrecht, Germany BD, Franklin Lakes, USA
Coverslips	round 12 mm, No. 1	Assistent, Sondheim, Germany
Cryo tube vials	1.5 ml	Thermo Fisher, Waltham, USA
Cuvettes	Halbmikro-Einmalkuevette 1.5-3 ml	Sarstedt, Nümbrecht, Germany
Falcon tubes	15 ml and 50 ml	Sarstedt, Nuernbrecht-Rommelsdorf, Germany

Type	Specification	Manufacturer/Distributor
Filters	0.22 µm, 500 ml	TPP, Trasadingen, Switzerland
Glass-beads	4 mm	Sigma-Aldrich, St. Louis, USA
Latex-beads	1 µm	Polysciences, Warrington, USA
Microscope slides	SuperFrost® Polysine slides	Roth, Karlsruhe, Germany Mentel GmBH, Braunschweig, Germany
Needles Object-slides	Sterican 76 x 26 mm	Braun, Melsungen, Germany Engelbrecht, Edermünde, Germany
Parafilm	Parafilm ‚M'®	American Can Company, Greenwich, Great Britain
Pasteur pipets	---	Brand, Wertheim, Germany
Petri dishes	10 cm	Sarstedt, Nuernbrecht-Rommelsdorf, Germany
Plastic pipet tips	10µl / 200µl / 1000 µl	Sarstedt, Nuernbrecht-Rommelsdorf, Germany
Plastic pipets	5 ml / 10 ml / 25 ml	Sarstedt, Nuernbrecht-Rommelsdorf, Germany
Reaction tubes	1.5 ml / 2 ml 1.5 ml Nerbe PCR Softtubes 0.2 ml	Eppendorf, Hamburg, Germany Nerbe plus, Winsen/Luhe, Germany Biozym, Oldendorf, Germany
Syringes	BD-Micro-Fine 0.5 ml	BD Medical, Franclin Lakes, USA

2.1.3 Chemicals and biological reagents

Table 2-3: Chemicals and biological reagents

Chemical or biological reagent	Manufacturer/Distributor
1 kbp DNA marker	Roth, Karlsruhe, Germany
7H11	BD, Franklin Lakes, USA
7H9	BD, Franklin Lakes, USA
Agarose	Bio&Sell, Nuernberg, Germany
Ampicillin	Sigma-Aldrich, Taufkirchen, Germany
Antibodies	see Table 2-24 and 2-25
Aqua ad iniectabilia Delta Select	Delta Select GmbH, Pfullingen, Germany
Blasticidin	InvivoGen, San Diego, USA
Bromephenol blue sodium salt	Merck, Darmstadt, Germany
Calcium chloride	Sigma-Aldrich, Taufkirchen, Germany
Calf intestinal phosphatase (CIP)	New England Biolabs, Frankfurt, Germany
Chloramphenicol	Sigma-Aldrich, Taufkirche, Germany
Cycloheximide	Sigma-Aldrich, Taufkirche, Germany
Dimethylsulfoxide (DMSO)	Sigma, Steinheim, Germany
Disodium hydrogen phosphate (Na_2HPO_4)	Merck, Darmstadt, Germany
DNase I, Amplification Grade I	Life Technologies, Carlsbad, USe
dNTP-Mix	Roth, Karlsruhe, Germany

Chemical or biological reagent	Manufacturer/Distributor
D-Sorbitol	Roth, Karlsruhe, Germany
EDTA sodium salt (ethylene diamine tetraacetic acid)	Biomol, Hamburg, Germany
EGTA sodium salt (ethylene glycol tetraacetic acid)	Roth, Karlsruhe, Germany
Ethanol (100%)	Roth, Karlsruhe, Germany
Ethidiumbromide (1%)	Biomol, Hamburg, Germany
Foetal Bovine/Calf Serum (FCS)	GE Healthcare, Chalfont St Giles, GB
Formaldehyde	Merck, Darmstadt, Germany
Gelatin	Sigma-Aldrich, Taufkirchen, Germany
Gentamicin	Formedium, Hunstanton, USA
Glucose	Roth, Karlsruhe, Germany
Glutaraldehyde	Sigma-Aldrich, Taufkirchen, Germany
Glycerol	Roth, Karlsruhe, Germany
HL5-C supplemented with glucose	Formedium, Hunstanton, USA
Hydrochloric acid (37%)	Roth, Karlsruhe, Germany
Hygromycin	InvivoGen, San Diego, USA
Hyperladder DNA markers	Bioline, Luckenwalde, Germany
Isopropanol	Roth, Karlsruhe, Germany
Kanamycin	Formedium, Hunstanton, USA
LB-Agar (Lennox)	Roth, Karlsruhe, Germany
LB-Media (Lennox)	Roth, Karlsruhe, Germany
LightCycler® 480 SYBR Green I Master	Roche Diagnostics, Manheim, Germany
Lysozyme (from hen egg white)	Roche Diagnostics, Mannheim, Germany
Magnesium chloride	Roth, Karlsruhe, Germany
Magnesium sulfate	Roth, Karlsruhe, Germany
Maxima® SYBR Green qPCR Master Mix (2x)	Thermo Fisher, Waltham, USA
Methanol	Roth, Karlsruhe, Germany
Mounting Medium, ProLong Gold	Life Technologies, Carlsbad, USA
OADC	BD, Franklin Lakes, USA
Paraformaldehyde	Sigma-Aldrich, Taufkirchen, Germany
Penicillin/Streptomycin-Mix (100x)	Life Technologies, Carlsbad, USA
Phusion™ High Fidelity DNA polymerase	Finnzymes/New England Biolabs, Frankfurt am Main, Germany
Potassium acetate	Sigma-Aldrich, Taufkirchen, Germany
Potassium chloride	Roth, Karlsruhe, Germany
Protein markers (PageRuler)	Thermo Fisher, Waltham, USA
Restriction enzyme buffers	New England Biolabs, Frankfurt, Germany
Restriction enzymes	New England Biolabs, Frankfurt, Germany
Saccharose	Sigma-Aldrich, Taufkirchen, Germany
Sodium acetate	Biomol, Hamburg, Germany
Sodium chloride	Roth, Karlsruhe, Germany
Sodium iodide	Roth, Karlsruhe, Germany
T4 DNA ligase	New England Biolabs, Frankfurt am Main, Germany
Taq polymerase (GoTaq)	Promega, Mannheim, Germany
Tetracycline	Sigma-Aldrich, Taufkirchen, Germany

Chemical or biological reagent	Manufacturer/Distributor
Tris	Biomol, Hamburg, Germany
Tris-HCl	Biomol, Hamburg, Germany
Triton X-100	Sigma-Aldrich, Taufkirchen, Germany
Trizol	Life Technologies, Lohne, Germany
Tween 80	Sigma-Aldrich, Taufkirchen, Germany

2.1.4 Kits

Table 2-4: Kits

Kit	Manufacturer/Distributor
High Pure PCR Template Preparation Kit	Roche Diagnostics, Manheim, Germany
Maxima® First Strand cDNA Synthesis Kit for RT-qPCR	Thermo Fisher, Waltham, USA
NucleoSpin® Extract II	Macherey&Nagel, Dueren, Germany
NucleoSpin® Plasmid	Macherey&Nagel, Dueren, Germany
PureLink® RNA Mini Kit	Life Technologies, Lohne, Germany

2.2 Methods

2.2.1 Cell biology

In general the handling of all living organisms in this study was carried out under sterile conditions.

2.2.1.1 Culture and seeding of *D. discoideum*

The *D. discoideum* strain used in this study was the AX2 wild type (Strain ID: DBS0235534) described by Watts and Ashworth in 1970 [201].
The cells were obtained from the Dicty Stock Center at the Northwestern University in Chicago, IL, USA. Adherent axenic AX2 cells were kept in culture in 10 ml HL5-C medium supplemented with 100 U/ml penicillin and 100 µl/ml streptomycin in 10 cm culture dishes at 22°C. Every two to three days, before reaching confluence, cells were diluted. To detach cells from the dish the media was decanted and the dish was gently knocked at the front of the sterile bench. For the running culture, detached cells were taken up in 10 ml fresh HL5-C media, the desired volume of cell suspension was reseeded in 10 cm culture dishes topped up to 10 ml with fresh HL5-C media. Alternatively, the cell number was determined using a Neubauer counting chamber and dilutions appropriate for seeding of 24-well dishes were prepared. Between 0.5 and $1x10^6$ cells were seeded either on coverslips in 24-well plates or directly into IBIDI dishes. Mutant cell lines were constantly kept under selection by adding the appropriate antibiotic.

***D. discoideum* culture medium**

HL5-C medium including glucose	26.55 g/l in ddH_2O
(Formedium, Hunstanton, UK)	→ autoclave
Penicillin	100 U/ml
Streptomycin	100 µl/ml

2.2.1.2 *D. discoideum* stock preparation

Since a continuous culture is exposed to genetic drift, cells for experiments were used for the period of one month. Also, an established cell line is a valuable resource and its replacement is very time consuming. Thus it was important to freeze and preserve all cell lines for long-term storage. *D. discoideum* can be cryopreserved in the form of single cells or spores.

2.2.1.2.1 Cell cryopreservation

D. discoideum cells were grown to late log phase. At a confluency of 80%, which comprises about $2x10^7$ cells per ml, cells were harvested. The supernatant was discarded and the cells were detached and taken up in 10 ml HL5-C medium before being pelleted by centrifugation (500 g, 5 min. 22°C). Next, the pellet was gently suspended in 2 ml HL5-C medium containing 10% DMSO (v/v). Aliquots of 1 ml cell suspension in freezing vials were placed in a Thermo Scientific Nalgene Mr. Frosty 1°C freezing container (Cat. No. 5100-0001). Mr Frosty provides a simple-to-use system designed to achieve a rate of cooling very close to 1°C per minute (which is optimal conditions for freezing live cells). 24 hours later the aliquots were transferred to liquid nitrogen storage tanks.

2.2.1.2.2 Spore cryopreservation

D. discoideum cells were developed according to the protocol described in paragraph 2.2.2.1. Sori (Sporeheads of the fruiting bodies) containing the spores were collected in the lid of the dish by tapping it on the surface of the bench and taken up in 1x Sørensen buffer. In order to release the spores, pooled sori were ruptured by intensive pipetting. Exact spore numbers were determined using a Neubauer counting chamber. Spores were pelleted by centrifugation at 1000 g and aliquots of $1x10^7$ spores were prepared in 1 ml 10% glycerol in 1 x Soerensen buffer. As described above, they were placed in Thermo Scientific Nalgene Mr. Frosty boxes at -80°C for 24 hours before the transfer into to liquid nitrogen storage tanks.

2.2.1.3 Transfection of *D. discoideum*

The transfection of *D. discoideum* was carried out via electroporation. All transgenic *D. discoideum* strains were generated by transfecting freshly thawed and recovered AX2 wild type cells. For episomal expression in the cells, the gene of interest was cloned in *D. discoideum* expression plasmids [193]. To generate transgenic *D. discoideum* cell lines, the respective constructs were created and linearized prior to transfection.

General transfection procedure

Twenty – 40 µg DNA were precipitated by adding 1/10 volume 3 molar sodium acetate (pH adjusted to 5.2) and a 2.5 fold volume of absolute ethanol. The solution was mixed thoroughly and incubated for 15 min at -20°C. Next, the mixture was pelleted for 5 min at maximum speed in a tabletop centrifuge for 15 minutes at 4°C. The supernatant was discarded and the DNA pellet washed once with 70% ethanol. Again, the DNA was pelleted for 5 min at maximum speed in a tabletop centrifuge for 15 minutes at 4°C and allowed to air dry for 5 -10 minutes. Finally the DNA was dissolved in 100 µl electroporation (EP) buffer and stored on ice until later usage.

Fresh AX2 wild type *D. discoideum* cells were grown to late log phase. At a confluency of 80 to 90% cells were washed once with 5ml pre-chilled EP buffer. Cells were then detached and taken up in 1.5 ml EP buffer, transferred in 2 ml Eppendorf tubes and pelleted by centrifugation (500 g, 5 min, 4°C). The supernatant was discarded and the cells suspended in pre-chilled 100 µl EP buffer containing the respective DNA. The suspension was transferred to a pre-chilled electroporation cuvette (BTX, 2mm) and incubated for 10 minutes on ice. The electroporation was done in the LV-mode, five times with 250 volts and two milliseconds pulse length in intervals of one second. Immediately afterwards, the cuvette was placed on ice and incubated for 10 minutes. Total volume was then topped up to one milliliter with HL5-C media and distributed equally to two or three 10 cm dishes with 10 ml HLL5-C media supplemented with 200 U/ml penicillin and 200 µl/ml streptomycin. Freshly transfected cells were allowed to recover at 22°C for 24 hours, after which, transfected cells were selected for with the appropriate antibiotic (table 2-5).

1 x EP buffer

K_2HPO_4/ KH_2PO_4 (Roth, Karlsruhe)	10 mM
Sucrose (Sigma-Aldrich, Taufkirchen)	50 mM
	→ pH 6.2

Table 2-5: Mutant cell lines were cultured in Hl5c medium supplemented with antibiotics

Mutant cell line	Antibiotic
GFP::vacuolinA (episomal overexpression)	gentamicin (7 µg/ml)
GFP::vacuolinB (episomal overexpression)	gentamicin (7 µg/ml)
GFP::vacuolinC (episomal overexpression)	gentamicin (8 µg/ml)
vacuolinA knock out mutant	blasticidin (5 µg/ml)
vacuolinB knock out mutant	blasticidin (5 µg/ml)
vacuolinC knock out mutant	blasticidin (5 µg/ml)

2.2.1.4 Subcloning of transgenic *D. discoideum* cells

Antibiotics treatment selected for transgenic cells. Nevertheless, it had to be confirmed that the respective construct had integrated at the designated location in the genome. To obtain clonal cell lines, a plaque assay was performed after the pre-selection via the antibiotic treatment. For this, 400 ml *Klebsiella aerogenes* overnight culture was harvested by centrifugation (4500 rpm, 10 min), reduced to a volume of 2 ml in 1x

Sørensen buffer and autoclaved. The suspension was then mixed gently with either 50 or 100 transfected and pre-selected transgenic cells and evenly distributed on Sørensen agar plates. The plates were allowed to dry and were subsequently incubated upside down at 22°C. Approximately after 7 days of incubation, *D. discoideum* plaques originating from a single cell appeared on the plates. These clones were picked, brought back into adherent culture and the genomic DNA analyzed by site-specific PCR.

2.2.1.5 Control of gene integration into target locus by site-specific PCR

The constructs used for *D. discoideum* transfection carried sequences targeting the transgenic region for integration into the genome of the cells. Due to the high extent of homology in the vacuolin genes as well as random integrations, the genomic DNA of individual subclones was tested for the correct integration of the transgene by PCR. Primers are listed in table 2-21 for the vacuolinC knock in and in table 2-22 for the vacuolinC knock out. In general, GoTaq polymerase was used for analytic PCRs. However, for PCR amplifications longer than 1500 bp, Phusion polymerase was used.

2.2.1.6 Lipopolysaccharide exposure of *D. discoideum*

Macrophages treated with LPS show an increased IL-12 response, a key modulator of immune function. In order to elucidate if the exposure of *D. discoideum* to lipopolysaccharide (#L4005, *E.coli* 055) induced changes in mRNA abundance, for each time point one dish at a 70 – 80% confluence (logarithmic phase) was overlaid with 10 ml HL5-C supplemented with 5 µl LPS (2mg/ml) and incubated at 22 °C for indicated intervals. Cells were harvested, suspended in 10 ml HL5-C and subsequently centrifuged for 5 min at 500 g. Pellet were reconstituted in 1 ml TRIzol®, incubated for 5 min at room temperature before being stored at -80 °C.

2.2.1.7 Cell culture of *Mycobacteria*

Mycobacteria marinum

The wild type strain and all mutants of *M. marinum* were cultivated in running cultures were kept either in 50 ml cell culture flasks at a volume of 12-20 ml 7H9 culture medium or (in preparation of infections) in 200 ml cell culture flasks at a volume of 30-60 ml 7H9 culture medium supplemented with appropriate antibiotics. Cultivation was mostly carried out in suspension at 32°C while the flasks were shaken at 120 rpm. In order to avoid cluster formation of the bacteria, the culture medium was supplemented with 0,05 % Tween 80. In addition, 20-30 glass beads with a diameter of respectively 4 mm were added.

For infections, fresh *M. marinum* aliquots were thawed. The stock was prepared by growing a 100 ml culture to an OD_{600} of 1. Bacteria were then centrifuged at 3000 g for 20 min at 4°C. The pellet was gently suspended in 90 ml 7H9 containing 50 % glycerin and 1 ml aliquots were stored at -80 °C.

Mycobacterial culture medium (7H9)

7H9 powder (Roth, Karlsruhe)	4.7 g
glycerol (Sigma-Aldrich, Taufkirchen)	2 ml
	900 ml ddH_2O
	→ autoclave; cool down
OADC (BD, Franklin Lakes)	100 ml
Tween 80	0.5 ml
	→ sterile filter, store in the dark at 4 °C

Mycobacteria smegmatis

Mycobacteria smegmatis mc2 155 was kindly provided by Dr. Gareth Griffith (University of Oslo, Norway). The strain corresponds to the catalog number 700084 and can be found in the American Type Culture Collection (ATCC, Manassas, USA). *M. smegmatis* was isolated of human smegma. Similar to *M. marinum*, *M. smegmatis* belongs to the organisms of risk group 2. Culturing was performed as described for *M. marinum*. Due to shorter division rates, *M. smegmatis* cultures were diluted more often.

2.2.1.8 *Mycobacteria* stock preparation

For all *Mycobacteria* strains used in this study, aliquots were prepared for long-term storage. For that, 100 ml of culture was incubated until the bacteria reached their stationary growth phase and the optical density measured at 600 nm (OD_{600}) reached approximately 3. Cells were then centrifuged (3000 g, 20 min, 4°C) and the pellet was suspended in 6 ml 7H9 containing 50% glycerin. Subsequently, 1 ml aliquots were stored for long-term preservation at -80°C.

2.2.1.9 Cell culture of *Legionella pneumophila*

All *Legionella* experiments were carried out in the laboratory of Prof. Dr. Hubert Hilbi (LMU, Munich) under the guidance of Eva Rothmeier. Briefly, *L. pneumophila* was grown for 3 days on *Charcoal Yeast Extract* (CYE) agar plates containing charcoal yeast extract, buffered with N-(2-acetamido)-2-amino ethanesulfonic acid (ACES). Liquid cultures were inoculated in AYE medium at an OD_{600} of 0.1 and grown at 37°C to an OD_{600} of 3.0 (21–22 h) [cited from 157].

2.2.1.10 *D. discoideum* phagocytosis assay

This assay is used to quantify the number of phagocytized fluorescent particles per cell. To begin with, cells were detached from a confluent dish and suspended in 10 ml of HL5-C medium. Cells per ml were calculated using a Neubauer counting chamber and adjusted to a density of 2 x 10^6 cells in 5 ml medium. Subsequently, the cells were incubated at 22 °C while shaking at 150 rpm for 2 hours in a well of a 6-well dish. This step is used to acclimate cells to the different culture conditions and to obtain synchronized starting conditions for the experiment. Particle uptake was started by adding green fluorescent beads (1 µm, #17458, polysciences) to the cell suspension at a

ratio of 10:1. A 300 µl sample was withdrawn directly before bead addition (biol. control) and subsequent probes were taken at 10, 20, 30, 40, 50, 60, and 90 min after adding the beads. Samples were processed on ice and pre-cooled material was used. Taken samples were first gently mixed with an equal volume of Soerensen/sorbitol buffer (SSB) supplemented with 5 mM sodium azide and centrifuged (4 min, 500 g, 4 °C). Pellets were gently suspended in 500 µl SSB and stored on ice until analyzed by flow cytrometry (see pargraph 2.2.1.13 for description and settings). Over time, the number of cells that internalized beads increased and towards the end of the experiment the majority of cells had internalized beads (fig. 4-1).

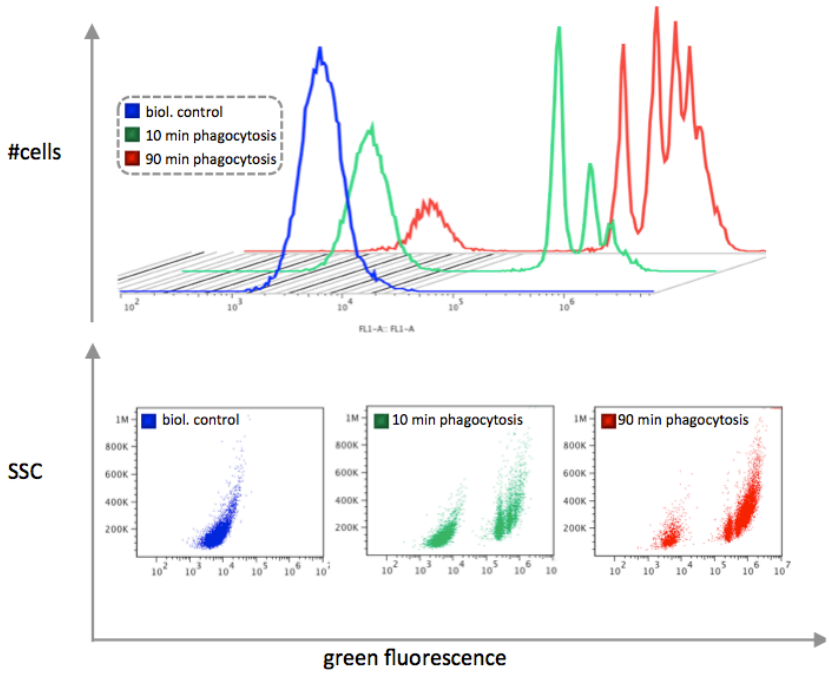

Figure 2-1: Changing ratio of cells that internalized fluorescent beads versus those that did not. FACS analysis of the number of cells (#cells) and dot plots of side scatter (SSC) against green fluorescence before bead addition and after (10 and 90 min). The cell's fluorescence shifted depending on the number of phagocytosed fluorescent beads. SSC depicts the granularity of each cell.

50 x Soerensen buffer (SSB)

Potassium phosphate KH_2PO_4	99.86 g
Sodium phosphate Na_2HPO_4	13.61
	→ up to 1 l ddH_2O;pH 7.4

2.2.1.11 *D. discoideum* development

Cells from a dish (axenic culture) with approximately 85% confluency were detached and suspended in 10 ml HL5-C medium. The cell number was determined using a Neubauer counting chamber and the equivalence of 2.8 x 10^6 cells was pelleted in 2 ml Eppendorf tubes by centrifugation (3 min, 500 g). The supernatant was removed and the pellet reconstituted in 200 µl of 1 x SSB. Subsequently, the cell suspension was dispensed evenly on Soerensen agar plates (diameter: 60 mm). The liquid on the surface was allowed to dry until the surface appeared shinny in the center but dry around the edges. Plates were subsequently put upside down into a black box (exclusion of light)

with a damp tissue at the bottom and incubated motion-free at 22 °C. One plate was prepared and gently removed for each time point to be analyzed.

2.2.1.12 Infection of *D. discoideum*

2.2.1.12.1 Infection of *D. discoideum* with *Mycobacteria*

Approximately 15 hours before the infection, adherent *Dictyostelium* cells were adjusted to reach 2,5 x 10^7 cells per 10 cm culture dish at infection time and incubated without any supplements overnight. Infection was performed with a shaking *Mycobacteria* culture at an OD_{600} of approx. 0.8-1. An equivalent volume of 5 x 10^5 cells, which equals a *multiplicity of infection* (MOI) of 200 with one dish of *Dictyostelium* cells, was passaged through a 50 µm filter to remove larger *Mycobacteria* clusters. From the OD_{600}, the amount of colony forming units (cfu) per volume, and thus, the amount of bacteria per 1 ml was could be estimated with table 2-6 kindly provided by Dr. T. Soldati.

Table 6-6: OD_{600} - cfu relation

OD_{600}	cfu [x 10^8]
0.60	0.9
0.70	1.1
0.80	1.2
0.85	1.5
0.90	1.7
0.95	1.8
1.00	1.9

The filtered *Mycobacteria* were pelleted (3000 g, 5 min, 25°C), suspended in 500 µl HL5-C for each dish to be infected and passaged six times through a 26-gauge needle to obtain single cells. Adding the *Mycobacteria* onto the *Dictyostelium* cells marked the beginning of the infection (t = 0). Dishes were sealed with parafilm and the bacteria were centrifuged on the *Dictyostelium* cells for 4 times (3 min, 500 g, 25 °C). This step allows a fast and synchronic method of infection. Between centrifugation steps, the dishes were gently turned a quarter in order to reassure a uniform distribution of the bacteria, leading to maximum distribution of centrifugal force affecting all areas of the dish. Subsequently, the culture dishes were incubated 45 min at 25°C to allow detached cells to settle and enable further phagocytosis of bacteria.
If a 0.5 hours post infection (hpi) sample was required, it was directly taken without any washing steps. Otherwise at 45 min post infection extracellular bacteria were removed by washing the cells repeatedly with 3 ml fresh HL5-C using 10 ml serologic pipette. At regular intervals a light microscope was used to check for the presence of extracellular bacteria. Infected cells were ultimately supplied with 10 ml HL5-C medium and incubated at 25°C before harvested at desired time points. To prevent growth of extracellular bacteria during the infection the media was supplemented with 5 U/ml penicillin and 5 µg/ml streptomycin. For microscopic analysis, infected cells were suspended in 10 ml HL5-C medium, the cell number was estimated with a Neubauer

counting chamber and 6 x 10^4 cells were seeded into 24 well plates with one cover slip per well and the volume was adjusted to 500 µl HL5-C. For the analysis at 24 hpi, 2 x 10^4 infected cells were seeded per well. At the sampling time points, the infected cells were fixed.

2.2.1.12.2 Infection of *D. discoideum* with *L. pneumophila*

Legionella experiments were carried out in the laboratory of Prof. Dr. Hubert Hilbi under the guidance of Eva Rothmeier. Briefly, *D. discoideum* was infected with *L. pneumophila (*grown for 21–22 h in AYE broth) *at an MOI of 50.* The infection was synchronized by centrifugation (450×*g*, 10 min, RT), and the infected phagocytes were incubated at 25°C for the time indicated in the experiments [cited from 157].

2.2.1.13 Fluorescence activated cell sorting (FACS)

With a flow cytometer, cells can be analyzed based on their light scattering and fluorescent features. The forward scatter (FSC) determines the relative size of each cell and the side scatter (SSC) detects the granularity. In addition, the use of lasers with the appropriate filters allows the measurement of fluorescence. Infection and phagocytosis rates were estimated using the BD Accuri™ C6 FACS machine. First, using the SSC on the y-axis and the FSC on the x-axis, live cells were gated which enabled the exclusion of debris and other small particles of the suspension. By setting the green fluorescence on the x-axis, the population could be divided into two groups, namely cells that did not internalized fluorescent particles (green fluorescent beads or bacteria) and cells that did.

For cell sorting the pre-cooled (4 °C) BD FACS Aria™ III equipped with a nozzle size 70 nm was used. *M. marinum*::msp12^{gfp} infected *D. discoideum* cells were suspended in ice-cold HL5-C medium and passaged through sterile 50 µm CellTrics® filters. All samples were kept on ice before, during and after the process. *M. marinum*::msp12^{gfp} infected *D. discoideum* cells were sorted into 3 ml RNA*later*® RNA stabilization solution. Approximately 10^6 cells per sample were collected, pelleted by centrifugation (10 min, maximum speed), suspended in 1 ml TRIzol® and incubated for 5 min at room temperature before being stored at -80 °C. All FACS data collected was analyzed using the FlowJo software (TreeStar).

2.2.1.14 Quantification of colony forming units (cfu)

To determine the intracellular growth of *M. marinum* in *D. discoideum, M. marinum* colony-forming units (cfu) were counted over the course of infection. For each time point, 3 x 10^5 infected cells were seeded in small culture dishes (35 mm) with a final volume of 1 ml HL5-C medium (supplemented with 5 U/ml penicillin and 5 µg/ml streptomycin to prevent extracellular proliferation of bacteria) each and incubated at 25°C.

In order to isolate the *M. marinum* from *D. discoideum*, at respective time points, infected cells were suspended in their culture media, 300 µl of the suspension was transferred into a 1.5 ml Eppendorf tube and centrifuged (4900 g, 4 min, 22°C). Subsequently, *D. discoideum* cells were lysed by suspension in 300 µl lysis buffer (0,1% Trition in PBS)

and immediate vortexing for 10 sec. Cell lysis was continued by an incubation at room temperature for 10 min, followed by another vortexing step for 30 sec. Then, a serial dilution (1:10 to 1:100) of the *Mycobacteria* at a final volume of 300 µl was pipetted in lysis buffer. 15 µl of each dilution plus the non-diluted samples were plated per quarter of mycobacterial 7H11 agar plates and evenly spread. The plates were then incubated in a humid chamber for 5-12 days at 32°C.
After *Mycobacteria* colonies appeared, samples containing 10 to 200 bacterial colonies were included for analysis. For the graphical evaluation using Prism Software, the amount of bacteria per 1 ml bacteria suspension was estimated with respect to the given dilutions. The bacterial growth was displayed as fold change over 3 hpi.

Mycobacterial culture plates (7H11)

7H11 powder (Roth, Karlsruhe)	21 g
glycerol (Sigma-Aldrich, Taufkirchen)	5 ml
	900 ml ddH_2O
	→ autoclave; cool down
OADC (BD, Franklin Lakes)	100 ml
	→ pour plates, store in the dark at 4 °C

2.2.2 Molecular biology

2.2.2.1 Extraction of genomic DNA from *D. discoideum*

For the extraction of genomic DNA, *D. discoideum* cells were harvested at late log phase. About $1.5x10^7$ cells were pelleted by centrifugation (500 g, 22 °C, 5 min). The pellet was either stored at -20 °C until use or processed directly. Genomic DNA was obtained by applying the High Pure PCR Template Preparation Kit (Roche Diagnostics, Manheim, Germany) according to the manufacturer's instructions.

2.2.2.2 Extraction of total RNA from *D. discoideum*

Total RNA from infected or non-infected *D. discoideum* cells was extracted using the PureLink™ RNA Mini Kit (Life Technologies, Lohne, Germany) with slight modifications. Briefly, about $3x10^6$ – $2x10^7$ cells were harvested by centrifugation (500 g, 23 °C, 5 min), suspended in 1 ml TRIzol® (Life Technologies, Lohne, Germany) and incubated for 5 min at room temperature. Samples were then stored at -80 °C or processed directly using the PureLink® RNA Mini Kit according to the manufacturer's instructions with slight modifications. Briefly, the cells were lysed in TRIzol® instead of the provided lysis buffer and incubated at room temperature for 5 min to allow a complete dissociation of nucleoprotein complexes. Subsequently, to digest DNA contamination an on-column PureLink™ DNase I treatment was performed.

2.2.2.3 Nucleic acid quantity quality control

Purity and concentration of all extracted nucleic acids were analyzed via NanoDrop. To determine RNA purity, a SYBR Green I qPCR run was performed for all RNA samples that subsequently were used for cDNA synthesis and qPCR analysis. Hereby, the intron spanning housekeeping gene glyceraldehyde 3-phosphate dehydrogenase (*gapdh*) primer pair was used with 5ng RNA as template.

2.2.2.4 Revers transcription of mRNA – cDNA synthesis

To generate cDNA the Maxima® First Strand cDNA Synthesis Kit for RT-qPCR was used according to the manufacturer's instructions. 1 µg of total RNA was used for each 20 µl reaction. Amplification was carried out for 30 min at 30 °C in a PCR machine. Synthetized cDNA was stored at -20 °C for up to 3 months.

2.2.2.5 Quantitative real time PCR (qPCR)

The quantitative real time PCR (qPCR) allows detection and quantification of cDNA amplification after each polymerase chain reaction (PCR) cycle. To minimize inaccuracy due to pipetting, each reaction was carried out in duplicates or triplicates. All qPCR reactions were performed using the RotorGene 3000 (Corbett Life Science) equipped with the 72-size rotor.

2.2.2.5.1 SYBR Green I

The SYBR Green I system uses SYBR Green I that intercalates into double stranded DNA. SYBR Green I emission increases proportional to amplified PCR products and thus can be used for cDNA quantification. For qPCR, either the Maxima® SYBR Green qPCR Master Mix (Thermo Scientific) or the LightCycler® 480 SYBR Green I Master (Roche) was prepared in a final volume of 10 µl per reaction. In total, 45 amplification cycles were programmed including a touch down of the annealing temperature, starting at a temperature of 64°C it dropped down 0.5 °C each cycle to maintain a final annealing temperature of 60°C throughout the remaining cycles. The specificity of each SYBR Green I reaction was confirmed using melting curve analysis. Via melting curve analysis primer-dimers can be detected because they exhibit a lower melting temperature than the amplicon. In addition, gDNA contamination can be visualized with the use of intron spanning primer pairs.

Table 2-7: pPCR reaction mix for SYBR Green set-up

Component	Maxima® SYBR Green	LightCycler® 480 SYBR Green
cDNA template (5 ng)	1 µl	1 µl
Master mix (2x)	5 µl	5 µl
sense primer (10 pmol/µl)	0.5 µl	0.5 µl
anti-sense primer (10 pmol/µl)	0.5 µl	0.5 µl
H_20	ad 10 µl	ad 10 µl

Table 2-8: qPCR program for SYBR Green set-up

Phase	Temperature	Time
Activation of hot start polymerase	95 °C	15 min
Cycles (45)		
Melting	95 °C	30 sec
Annealing	64 - 60 °C	30 sec
Elongation	72 °C	30 sec
Melting curve analysis	95 °C	1 min
	67 - 95 °C	8 sec / step
Cool down	40 °C	20 sec

Sequences of used oligonucleotides are listed in table 2-9. For analysis of qPCR data the Rotor-Gene real time Analysis software 6.0 was used. First, the cycle of threshold (Ct) was set in the logarithmic amplification phase. The Ct value complies with a fluorescence signal that exceeds the background signal. Ct values were set individually for each primer pair and used for all qPCR runs. The correlation of Ct values of the housekeeping gene (HKG) as a reference in relation to the gene of interest (GOI) was calculated with the following formula:

$$\Delta Ct = Ct(GOI) - Ct(HKG)$$

Hereby the HKG serves as a reference to normalize the cDNA concentration in each reaction. In this study, the constitutively expressed glyceraldehyde 3-phosphate dehydrogenase (*gapdh*) was used as the HKG. Subsequently the ΔCt from the mock control was subtracted from the infection ΔCt:

$$\Delta\Delta Ct = \Delta\mathrm{Ct(infection)} - \Delta\mathrm{Ct(mock\ control)}$$

The relative difference of expression of the GOI comparing a mock-control sample with an infection sample both normalized to the HKG was subsequently calculated using the following formula:

$$Relative\ expression = 2^{-\Delta\Delta Ct}$$

This scheme of calculation presumes that all given templates double in each cycle, a theoretical scenario that is given when the primer efficiency is optimal. In the case of vacuolin measurements, the efficiency of the PCR reactions was included to calculate the relative expression. For this, the respective primer pair efficiency (gapdh 1.99; vacA 1.98; vacB 1.96; vacC 1.97) was inserted into the following formula:

$$Relative\ expression = \frac{efficiency\ HKG^{Ct\ HKG}}{efficiency\ GOI^{Ct\ GOI}} * 1000$$

Table 2-9: Primer probes for SYBR Green qPCR

Internal reference	Target	Sequence 5´- 3´
1	H2B_fw	atg gta ttc gtt aaa ggt caa aag aaa gc
2	H2B_rev	tta gtt ttt gct ttc agt tgg att gta ctt g
3	MM_8-9L3_fw	ACCGCTACGAGGTCAACAAT
4	MM_8-9R3_rev	ATTCGACGAACTCCACCAAG
5	IG7_fw	TGATCCAATAGTTCTGTGTGG
6	IG7_rev	ATGTGTTAAGCCGACATCGA
7	Q-GAPDH_fw	GGTTGTCCCAATTGGTATTAATGG
8	Q-GAPDH_rev	CCGTGGGTTGAATCATATTTGAAC
9	Litaf_FwI	TGG TCA ACC ATC AAG TCC AC
10	Litaf_RevI	TGT TGT GGA TAA CCT TGT GGT G
13	DupA_FwI	CAA ACA CAA ATT CTA CAA CAC CAA T
14	DupA_RevI	GGT GTA GCT AAT TTA GGA ATG GTA GG
17	VacA_FwI	ATC ACT GCT GAG GCT CAA AAG AAA GC
18	VacA_RevI	GAT GTA AAG GGT GGC ATT TTT GAG G
19	VacB_FwI	TTG CAA TGG CAC ATC GTA AT
20	VacB_RevI	GTT TAC CGA ATG AGC CGA AA
21	VacC_FwI	CCG AAG CTT TAA AAA GTT CAA CA
22	VacC_RevI	TGT TTT CCA AGC ATT CTT TCC
25	pah_FwI	CCC TTC AAG AAA GTT CAA ACC A
26	pah_RevI	TGA AGC ACC TGG ATG ATC TG
27	CalA_FwI	GGT CAA AAC CCA ACT GAA GC
28	CalA_RevI	TGC TTC ACG GAT TTC TTC TTC
73	MEKK3_fw	GCACCTCCACTCAGAACTCC
74	MEKK3_rev	TGAACCTGGTGGTGTACGAA
75	Traf6_fw	AAATCCCAATCACTGTGCAAT
76	Traf6_rev	ATCTTCCCCAACTCCAATCC
77	WRKY_fw	CCAAATCCAACAAGAACATGG
78	WRKY_rev	TGCTCTTTGTCGACTTGCAT
79	NOD_fw	CACGACATTGGAACTCTCACA
80	NOD_rev	CTCTTCGGCACCCTCATTAC
81	CD36_fw	ATGCCACTGCCGAACTCTAT
82	CD36_rev	TGACCTGTGAAAATGGTGGA
83	hspD_fw	AAGCTCAAGCTCTCCGTGAC
84	hspD_rev	CGATGAATACGTGAAGCAAATG
85	actin_fw	CGTTGCCATTCAAGCCGT
86	actin_rev	CCGTGGTACGACCAGAGG
90	tirA_fw	CTGGTTGTAATTGGAGAGCTGA
91	tirA_rev	TTGGATCGATTTGAACTGATTG
92	tirC_fw	TTTGAAATGGGATTTGAACCA
93	tirC_rev	AAAAGCTTTATTATCGGGTGACA
94	TNF as-fac 3_fw	TGAATGCCCACAATGTAGATG
95	TNF as-fac 3_rev	CTCCAAATGATGTCGGATGA
96	nramp1_fw	GGTATCAGTTTTCGCTAAAGGATT
97	nramp1_rev	CGAGCATTGACCAGCACTAA
98	nalp_fw	CAACCACAAGGTGACACAGG

Internal reference	Target	Sequence 5´- 3´
99	nalp_rev	GACCACCACTACCACCATCA
100	inter-ind-Dnjac3_fw	ATCTGCAACCCCTGAAGAAA
101	inter-ind-Dnjac3_rev	ACCACCTTGACCACCTTGAC
102	VatM_fw	CACCACGAAGAGGAACATGA
103	VatM_rev	GCCAATGAAAGAGCCCATAA
104	VatA_fw	TCCACCAAAGGAAATGGGTA
105	VatA_rev	CAACCAAAAGCACCTGGAAT
111	atg8l_fw	CTCCAAGATCAGATGCACCA
112	atg8l_rev	GCAGCAGTTGGTGGGATAGT
115	atg1_fw	TCACGCCTCTTCACTTCCTT
116	atg1_rev	CGGTTGTTGGATTGTAGTTGAT
117	p62_fw	TTGAAAATCGCACAACCAAC
118	p62_rev	AGGAACCCTTTGGAATGACA
119	iliM_fw	GGACCAGCAGGACTTTCATT
120	iliM_rev	CCCATCCTTATTTGCAATCG
121	eIF6_fw	GGTGCTCTCGTTCATCCAAT
122	eIF6_rev	TCAGTGGCAGTGGTATCAGC
123	lipocalin1_fw	AAAATGGTATGAAATCGCTCGT
124	lipocalin1_rev	AACCAGCATAAAATGGACCAA
125	lipocalin2_fw	CAGAAGGAGTTCATGCCGTTA
126	lipocalin2_rev	TTCGTCCGAGCCATTTACA
127	serine protease inhib. 1_fw	CAAGTGAGCCAAAGAAACCA
128	serine protease inhib. 1_rev	TTTCACCGACTTTCCAATCA
131	wfdc_fw	TGAGTATTTGTGGGGTAACATCTG
132	wfdc_rev	TGATGAGGGTTTTACAAATCCAG
133	interferon ind. 281639_fw	ACCCAGATTCAAACCACGAT
134	interferon ind. 281639_rev	TCTACATGCCCACATCCAAA
148	RanA_fw	CCCAAATTGTTTTCCATCGT
149	RanA_rev	AGCAGCATCAGCGACTTCTT
150	fttb_fw	ATCGTTTCATCAGCCTCTGG
151	fttb_rev	GGTGGGTTGGTGGTAATTCA
152	aif_fw	ACTGGTGAAATGGCTGGTTC
153	aif_rev	AGGATGGCTTCTCCCAAACT
154	impa_fw	GGGGTAATGAACCAACATGG
155	impa_rev	TTAAAAAGGCACCACCACCT

2.2.2.5.2 Multiplex TaqMan qPCR

The more sophisticated TaqMan qPCR system was mostly applied to analyze vacuolin mRNA abundance. In this approach a gene-specific probe is included in the PCR reaction which allows the differentiation of very similar target sequences. Thereby, a gene-specific probe, labeled with a fluorophore at the 5'-prime and a quencher at the 3'-prime end were designed with melting temperatures that were 10 °C higher than those of the corresponding primer pairs. The fluorescent signal of intact probes is extremely weak due to the close proximity of fluorophore and quencher. Since different fluorophores were used for all probes, and no impact of efficiency was detected, the reaction was

multiplexed to minimize inaccuracy due to pipetting. During annealing, primers and probes annealed specifically to their target sequence and during elongation the probe was hydrolyzed by the 5'-3' exonuclease activity of the taq-polymerase, separating fluorophore and quencher. Thus, the fluorescent signal only occured if the target sequence was amplified while non-specific products were not detected. Increasing amplification was hence directly proportional to the fluorescent signal and was used for quantitative analysis. For TaqMan qPCR reactions the HotStarTaq Master Mix Kit (Qiagen) was used. In general, analysis was performed as described above for the SYBR Green I systems. In addition, the efficiency of the PCR reactions was included to calculate the relative expression. For this, the respective primer pair efficiency (gapdh 1.98; vacA 1.94; vacB 1.96; vacC 1.99) was inserted into the following formula:

$$Relative\ expression = \frac{efficiency\ HKG^{Ct\ HKG}}{efficiency\ GOI^{Ct\ GOI}} * 1000$$

Primers and probes were received from Eurofins MWG and are listed in table 2-12.

Table 2-10: Reaction mix for multiplex TaqMan qPCR

Component	HotStarTaq Master Mix Kit
cDNA template (5 ng)	1 µl
master mix (2x)	10 µl
$MgCl_2$ (25mM)	1 µl
sense primer (600 nM)	0.5 µl (each)
anti-sense primer (600 nM)	0.5 µl (each)
probe (200 nM)	1 µl (each)

Table 2-11: Program for multiplex TaqMan qPCR

Phase	Temperature	Time
Activation of hot start polymerase	95 °C	15 min
Cycles (50)		
Melting	95 °C	15 sec
Annealing	64 - 58 °C	30 sec
Elongation	72 °C	30 sec
Cool down	40 °C	20 sec

Table 2-12: Primer probes for TaqMan qPCR

Internal reference	Target	Sequence 5´- 3´
212	GapDH_fw	AAT GGT GAA TTT GTT GTA AAT GG
213	GapDH_rev	ATA AAA AGA GAC CAG TTG ATT CTA C
214	vacA_fw	GCT TCT GAA TTA CAA GGT GAA CTC TAC ACT
215	vacA_rev	GCA CCA GCA TCT TGA GGA GTG ATG

Internal reference	Target	Sequence 5´- 3´
216	vacB_fw	CAT CAT CTG AAA ATT CAA TTG GTA GT
217	vacB_rev	TAT TCT TTA TAC CTT CAT TGA ATC TCT CT
218	vacC_fw	CGT TTA GAT TCA AGT TAT TTT GCT TTA A
219	vacC_rev	CAC CAT TGT ATT CGA TGA TAG TG
220	GapDH probe	CY5 - AAT CCA CGT TTT CGC TGA AAA AGA CCC A - BHQ2
221	VacA probe	ROX - AGC TGA AGC CCT CAA AAA TGC CAC CCT - BHQ2
222	VacB probe	FAM - CTT CAG AAC ATG AAA ATG GTG ATC AAT CCC TTA CCA - BHQ1
223	VacC probe	JOE - AAT CGT GAC AAA GTT GCT GAA TTA TTC GAT CCA CG - BHQ1

2.2.2.6 Cloning of plasmids and preparation for transfection

General procedure

For cloning procedures, the following steps were performed:

- RNA extraction and cDNA synthesis (see paragraph 2.2.2.4)
- PCR (see paragraph 2.2.2.6.1)
- Restriction digestion and purification of PCR-products and vectors (see paragraph 2.2.2.6.2)
- Ligation (see paragraph 2.2.2.6.4)
- Transformation of *Escherichia coli* (see paragraph 2.2.2.6.6)
- Plasmid extraction (see paragraph 2.2.2.6.7)
- Analytic restriction and sequencing (see paragraph 2.2.2.6.2 & 2.2.2.6.8)

2.2.2.6.1 PCR

Sequences of all primer pairs for cloning procedures were designed to have a melting temperature of 50 to 68 °C and were ordered from Sigma (Sigma-Aldrich, Taufkirchen). Gene fragments were amplified using either Go Taq (analytical purposes) or Phusion High Fidelity (further cloning steps) DNA polymerase. Lyophilized oligonucleotides were suspended to 100 pmol/µl stock-solutions from which 10 pmol/µl working solutions were prepared with DNase-free ampuva water (Fresnius, Bad Homburg). Both solutions were stored at -20 °C.

Table 2-13: PCR reaction mix for GoTaq and Phusion polymerases

Component	GoTaq	Phusion
DNA template	50-300 ng	50-300 ng
Reaction buffer (5x)	5 µl	5 µl

Component	GoTaq	Phusion
dNTPs (10 mM GC; 20 mM ATP)	2 µl	2.5 µl
sense primer (10 pmol/µl)	2 µl	2.5 µl
anti-sense primer (10 pmol/µl)	2 µl	2.5 µl
$MgCl_2$ (50mM)	2 µl	---
H_20	ad 50 µl	ad 50 µl

Table 2-14: PCR programs for GoTaq and Phusion polymerases

Step	GoTaq			Phusion		
	Temperature	Time	Cycles	Temperature	Time	Cycles
Initial DNA denaturation	95 °C	3 min	1x	98 °C	3 min	1x
DNA denaturation	95 °C	1 min	25x	98 °C	1 min	30x
Annealing	55 °C	30 sec min		55 °C	1 min	
Elongation	68 °C	2-5 min		72 °C	2-5 min	
Final elongation	68 °C	5-10 min	1x	72 °C	5-10 min	1x
Storage	4 °C	indefinitely	1x	4 °C	indefinitely	1x

2.2.2.6.2 Restriction digestion of DNA

PCR products and plasmids were restriction digested with the appropriate enzymes for 1 hour at 37 °C in a thermocycler. On manufactures recommendation, BSA was either added to the reaction or not.

Table 2-15: Restriction digestion reaction mix for analytic analysis and applications

Component	Analysis	Linearization for transformation
DNA	1-2 µg	15-40 µg
Restriction enzyme	10 U	80 U
Buffer (10x)	2 µl	5 µl
BSA (2 mg/ml)	2 µl	5 µl
dH_2O	ad 20 µl	ad 50 µl

If the following ligation was not directional, respectively only one enzyme used, linearized vectors were dephosphorylated with Antarctic Phosphatase from NEB, exactly following the manufactures' protocol.

2.2.2.6.3 Agarose gel electrophoresis

In order to purify DNA and/or to determine the size of DNA fragments and vectors, agarose gel electrophoresis was performed. Since the speed with which DNA fragments move through the agarose gel is indirectly proportional to the logarithm of their molecular weight, smaller fragments move faster through the gel than large fragments. Depending on the expected size, either a 1% or 1.5% gel was prepared by dissolving the agarose in 1 x TAE buffer by boiling. The cooled suspension was supplemented with

0.1µg/ ml ethidiumbromide, a dye that intercalates dsDNA. Exposed to ultraviolet light, bound ethidiumbromide is fluorescent and the DNA can be visualized. DNA samples were supplemented with loading dye prior loading of the gel. 1 x TAE buffer was used for running the gels and, depending on the gel size, an 80-120V voltage was applied for 30 to 60 minutes.

2.2.2.6.4 Extraction of DNA fragments

To extract DNA fragments from agarose gels, bands were cut out using a sterile blade and purified using the GeneJET Gel Extraction Kit (Thermo Scientific) according to the manufacturer's instructions. Subsequently, a 1 µl aliquot of the eluted DNA was used to confirm purification and to determine the concentration of the DNA using the NanoDrop instrument.

2.2.2.6.5 Ligation of DNA fragments into plasmids

For each ligation reaction 50-100 ng restriction digested vector was used. The amount of digested insert added the liagtion reaction calculated with the following formula: 50-100 ng vector * x bp of insert * 3 / y bp of vector = z ng insert. Incubation with appropriate enzymes was performed for 2-4 h at 37 °C or overnight at 4 °C.

Table 2-16: Ligation reaction mix

Component	Volume
T4 ligase (400 U)	1 µl
Ligase buffer (10x)	1 µl
Insert	x µl
Vector (50 - 100 ng)	y µl
ddH_2O	ad 10 µl

A-tailing

Ligation into pGEM®-T easy is mediated by a 3'-T-overhang of the vector. If Phusion-polymerase was used to amplify the inserts, the addition of several deoxyadenosines to the blunt 3'-end were added via Go-Taq-polymerase. Incubation took place for 30 min at 70 °C.

Table 2-17: A-tailing reaction mix

Component	Volume
PCR product	5 µl
Taq polymerase buffer (10x)	1 µl
$MgCl_2$ (25 mM)	1 µl
dATPs (1 mM)	2 µl
Taq polymerase	1 µl

Inserts were then ligated into the pGEM®-T easy vector for 2-4 h at 37 °C or overnight at 4 °C.

Table 2-18: pGEM-T easy ligation mix

Component	Volume
Rapid ligation buffer (10x)	5 µl
pGEM®-T easy (50 ng/µl)	1 µl
ligase	1 µl
A-tailing reaction mix	3 µl

2.2.2.6.6 Generation of and transformation into electroporation competent *E. coli* bacteria

Ligated plasmids were transformed into electroporation competent *E. coli* XL1 gold bacteria. Generation of electroporation competent bacteria was carried out on ice and pre-cooled reagents and labware were used. A 30 ml LB medium liquid culture with 15 µg/ml tetracycline was grown overnight at 37 °C. The following morning, 12.5 ml of the culture were added to 2x 500 ml of LB medium with antibiotics and grown until an OD_{600} of 0.5 – 0.9 was reached. After incubation on ice for 10 min the bacteria were pelleted at 4500 rpm for 10 minutes at 2°C and suspended in 2 x 400 ml ice-cold water. They were pelleted at 5000 rpm for 10 minutes at 2°C and suspended in 400 ml ice-cold water. Next centrifugation steps were at 5500 (cells were suspended in 400 ml ice-cold water); 6000 rpm (cells were suspended in 20 ml ice-cold 10% glycerol) and finally 6000 rpm for 15 min. Cells were then suspended in 10 ml ice-cold 10% glycerol. By these sequential centrifugation steps the bacteria were washed free of salts and concentrated. Aliquots of 40 or 80 µl were then frozen down immediately in liquid nitrogen and stored at -70°C.

Aliquots for transformation were thawed on ice immediately prior to use and transferred into a sterile electroporation cuvette (0.2 cm). To 40 µl of electroporation competent bacteria 1 – 3 µl of purified plasmid DNA in DNase-free ampuva water was added and incubated on ice for 5 min. Directly after one pulse of approx. 5 ms at 1700 V 1 ml of LB medium (37 °C) was added and transformed bacteria plated on LB agar plates containing antibiotics to select for the transformed plasmid. To account for varying transformation success, and therefore growth density, different volumes of the mixture were plated. Depending on plasmid sizes, 50 - 200 µl were plated on the first and the remaining suspension on a second plate. Agar plates were incubated at 37°C overnight.

Luria-Bertani medium (LB)

LB broth (Sigma) — 20 g/l in ddH_2O
→ autoclave; cool down

LB selection plates

Agar (Sigma) — 15 g/l in LB
→ autoclave; cool down

Ampicillin (100 mg/ml) — 1 ml
→ pour plates, store in the dark at 4 °C

2.2.2.6.7 Small-scale extraction of plasmid DNA

For initial analysis, transformed *E. coli* XL1 gold clones were used to inoculate overnight cultures in 3-5 ml LB selection medium. Plasmid purification was performed using NucleoSpin® Plasmid kit according to the manufacturer's instructions.

2.2.2.6.8 DNA sequencing

Plasmid DNA samples were sequenced by SeqLab (Göttingen, Germany).

2.2.2.6.9 Large-scale extraction of plasmid DNA

Overnight cultures of *E. coli* XL1 gold clones harboring plasmids used for *D. discoideum* transfection were used to inoculate 50-100 ml LB selection medium and grown in liquid culture overnight at 37 °C. Bacteria were harvested by centrifugation and their plasmid DNA extracted with the Nucleobond® Plasmid PC100 kit according to the manufacturer's instructions.

2.2.2.6.10 Linearization for transfection

Concentration of a plasmid DNA obtained by large-scale extraction was measured with the Nanodrop and a volume equaling approximately 20 µg was digested with KpnI (for vacuolinC knock out construct) or BbsI and SacI (for vacuolinC::gfp knock in construct). A detailed pipetting scheme can be reviewed in paragraph 'Restriction of DNA'.

2.2.2.6.11 DNA precipitation

Prior transformation of *D. discoideum*, the DNA was purified and concentrated by precipitation. First, 1/10 (v/v) of sodium acetate (pH 5.2) was added and mixed well. Second, 2.5 x (v/v) 100% ethanol was added, the solution mixed and stored at -20 °C for 20 min. DNA was then pelleted by centrifugation with maximum speed at 4 °C and washed once with 70% ethanol. Ten minutes of air drying allowed remaining ethanol to evaporate before the DNA was dissolved in 100 µl EP- buffer and stored on ice until transformation.

2.2.2.7 Specific cloning strategies

All genes were initially cloned into pGEM®-T easy or pJET and sequenced. Each step was analyzed by sequencing (after PCR amplification) or restriction.

2.2.2.7.1 Overexpression constructs

All vacuolin genes were then sub-cloned into pDM317 for N-terminal tagging with a green fluorescent protein tag (GFP) and into pDM323 for C-terminal tagging with GFP. The pDM - vector sets are customized for expression in *D. discoideum* [193] and received from the dicty-stock center [90]. Vectors and *vacuolinA*-insert were linearized using BglII and SpeI, while *vacuolinB* and *C*-inserts were restricted with BglII and XbaI. XbaI introduces compatible ends to SpeI, therefore a site specific ligation ensured directed cloning.

Table 2-19: Primer probes for overexpression constructs

Internal reference	Target	Sequence 5´- 3´
45	VacA-N`BglII_FW	aga tct att gaa ggt agt ggt agt aaa act c
46	VacA-N`SpeI_Rev	act agt tta att ctt ttt ttg ttg aat ag
47	VacB-N`BglII_FW	aga tct att gaa agt agt tca ttt atg
49	VacC-N`BglII_FW	aga tct att gaa agt aaa atc cct tca c
50	VacC-N`XbaI_Rev	tct aga tta act ttt aat gtt ggt ttg ttg
51	VacA_C'BglII_FW	aga tct aaa atg att gaa ggt agt gg
52	VacA_C'SpeI_Rec	act agt att ctt ttt ttg ttg aat ag
54	VacB_C'XbaI_Rev	tct aga ttt ttc taa ttt ttg ttg gtg tcc
56	VacC_C'XbaI_Rev	tct aga act ttt aat gtt ggt ttg ttg ttt tcc
65	VacB_N XbaI_rev	tct aga tta ttt ttc gaa ttt ttc ttg gtg tcc
66	VacB_C BglII_fw	aga tct aaa atg att gaa agt agt tca ttt atg
67	VacC_C BglII_fw	aga tct aaa atg att gaa agt aaa atc cc
87	vacB_C_sequencing_fw	CAAGAACCATTTATAAACCATTCAAC
88	vacA_sequencing_fw	GGTGAAGGTCCACATGTTATCATTG

2.2.2.7.2 Knock in construct

In order to attach a GFP-tag to the endogenous *vacuolinC* gene, a construct was designed that was flanked by two regions (flankI and II) homologous to the respective genomic regions. The flanks were used to target insertion of the *gfp* gene and a gentamicin resistance into the genome by homologous recombination. For this approach, flank I, II and the GFP-tag were PCR amplified. An overview of the cloning strategy is depicted in table 2-20.

Table 2-20: Cloning strategy specifics for vacuolinC knock in construct

Vector	Linearization sites used	Insert	Restriction sites used	Ligated into
flank I in pGEM®	NdeI, SacI	flank I	NdeI, SacI	Flank I + II in pGEM®
gfp in pJet	BamHI, SalI	resistance cassette	BamHI, XhoI	gfp+resistance cassette in pJet
Flank I & II in pGEM®	BglII, SpeI	gfp_resistance cassette	BglII, XbaI	Final construct in pGEM®

Before the construct was used for *D. discoideum* transfection it was linearized as described in paragraph 2.2.2.6.2.

Table 2-21: Primer probes for knock in construct

Internal reference	Target	Sequence 5´- 3´
106	pGem_gfp_fw	CAGATCTAGTACTAGTAGTGGTAAAGGAGAAG
107	pGem_gfp_rev	CGATAAGCTTTATCTTTTTGATTTTCATACTCTTTGGC
108	pGem_gfp(xhoI)_rev	CTCGAGTTGGATCCAGATTACTTGTATAGTTCATCCATG
109	pJet_gfp_fw	GAGCTCGGTACCAGATCTAGTACTAGTAGTGGTAAAG

Internal reference	Target	Sequence 5´- 3´
110	pJet_gfp(salI)_rev	GTCGACTTGGATCCAGATTACTTGTATAGTTCATCCATG
144	FI(-TAA) VacC fw	CCTCAAATTGCACTCACTAAATTAGG
145	FI(-TAA)_bglII VacC rev	AGATCTACTTTTAATGTTGGTTTGTTGTTTTCC
146	NdeI_XhoI_FII VacC fw	CATATGCTCGAGAATATTTCAATAGTATAAC
147	FII_XhoI_SacI VacC rev	GAGCTCCTCGAGTGTCAATCTTAATTAATAG
171	VacC_KI_control_1_fw	TCACAACCAAACAAGCAACGC
172	VacC_KI_control_1_rev	ATCACCTTCACCCTCTCCACTGAC
173	VacC_KI_control_2_fw	TTTCATTTTATAATCTCAGAAACCTCA
174	VacC_KI_control_2_rev	CCGCACATATTTGCAGTATTC
188	VacC_KI_control_3_rev	ACTCAAAAAAATGAGCAGATTTTTTTTTTGGTGAC
189	VacC_KI_control_4_rev	GAACGACTACCAATTGAATTTTCAGATG
190	VacC_KI_control_5_fw	CAAGATCGTGTAAAATCTCATTTGGC
191	VacC_KI_control_6_fw	CACCCATGGTTTGAAAATTTCAATC

2.2.2.7.3 Knock out construct

For the generation of a *D. discoideum vacuolinC* knock out mutant the StarGate® cloning system with the pKOSG-IBA-Dicty1 vector was used. The system allows a one-step assembly of the flanks, the selection marker and the vector by recognizing and combining the respective starCombinase™ recognition areas. Placement of the four starCombinase™ recognition areas at the exact 5'-end of each primer is important. The first 409 bp of vacuolinC were chosen to be amplified as flank I and the last 369 bp were chosen to be amplified as flank II. A KpnI restriction site was selected to be included for linearization of the transfection construct. All steps were performed according to the manufacturer's instructions [206].

Table 2-22: Primer probes for knock out construct

Internal reference	Target	Sequence 5´- 3´
161	VacC_KO_FI fw	AGCGCGTCTCCAATGGGTACCATTGAAAGTAAAATCCCTTCACAATTTTC
162	VacC_KO_FI rev	AGCGCGTCTCCGTTGGTATAAAGTGAAATAACGACTAGTTTTTGG
163	VacC_KO_FII fw	AGCGCGTCTCCCTTC TTGTAAAAGAATATGATATCAAAACCAC
164	VacC_KO_FII rev	AGCGCGTCTCCTCCCGGTACCTTAACTTTTAATGTTGGTTTGTTGTTTTC
182	VacC_KO_control_1_fw	TATCTGATTTATTTAAAAAAACCAGTGGAG
183	VacC_KO_control_2_rev	CCGATAATATTAAGTTGATTTTCTTTTTTAATACAAG
184	VacC_KO_con_3_blast_fw	ATATTTGAGTGGAATGAGTTCTTCAATC
185	VacC_KO_con_4_blast_rev	ATGGATCAATTTAACATTTCTCAACAAGATC

2.2.3 Protein biochemistry

2.2.3.1 Protein extraction from *D. discoideum*

Cells from a 60-80% confluent 10 cm dish were suspended in 10 ml HL5-C and the cell number was determined using a Neubauer counting chamber. Equivalent volume to 1 x 10^6 was taken and pelleted by centrifugation (5 min, 500g). Cells were washed once with 1 x Soerensen buffer and subsequently suspended in 2 x Lämmli buffer (95 °C). Samples were incubated for 5 min at 95 °C and immediately frozen in liquid nitrogen if not loaded directly on to the gel. Aliquots of 20 µl were used to load gels.

Lämmli buffer (2x)

Tris-HCL (Biomol)	125 mM
SDS (Biomol)	2 % (w/v)
Glycerol (Biomol)	20 % (v/v)
DTT (Biomol)	20 mM
Bromophenol blue sodium salt (Merck)	0.0001 % (w/v)
	→ pH 6.8

2.2.3.2 SDS-polyacrylamide gel electrophoresis (SDS-PAGE)

According to their molecular mass, proteins enclosed in SDS complexes were separated in a discontinuous system via gel electrophoresis under denaturating conditions. Samples were mixed in a volume ratio of 1:1 with Lämmli buffer (2x) and denatured for five minutes at 95 °C prior to loading into the gel wells. For SDS-PAGE gels that were used for Coomassie staining, 5 µl of unstained PageRuler™ Protein Ladder (10 – 200 kDa; Fermentas) were used while for subsequent immunoblot analysis, 5 µl prestained PageRuler™ Protein Ladder (10 – 170 kDa; Fermentas) were added. SDS-PAGE was performed in 1x running buffer at 25 mA for each gel. Components for preparation of resolving and stacking gel are listed in table 2-23 for two gels each.

Table 2-23: Mix for preparation of two stacking and two resolving (12%) gels

Component	Stacking gel	Resolving gel (12%)
Gel buffer	1.25 ml	2.5 ml
30 % acrylamide (Biomol)	650 µl	4 ml
ddH_2O	3.05 ml	3.4 ml
25 % APS stock solution	25 µl	50 µl
TMED (Biomol)	5 µl	5 µl

Running buffer (10x)

Tris-HCl (Biomol)	0.25 M
Glycerol (Biomol)	0.5 M
SDS (Biomol)	1 % (w/v)

Resolving gel buffer

Tris-HCL (Biomol)	1.5 M
SDS (Biomol)	0.4 % (w/v)
	→ pH 8.8

Stacking gel buffer

Tris-HCL (Biomol)	0.5 M
SDS (Biomol)	0.4 % (w/v)
	→ pH 6.8

APS stock solution

APS (Biomol)	25 % (w/v)

Long term storage at – 20 °C

2.2.3.3 Coomassie staining of protein gels

Protein gels were stained following the protocol by Weber *et al* [202]. Incubation in staining solution took place for at least one hour or overnight with constant shaking. The application of the destaining solution followed under shaking condition until only the protein bands remained. Subsequently the gels were washed with water two times and finally mounted and left to dry between two layers of cellophane foil.

Coomassie staining solution

Coomassie brilliant blue R250 (Sigma)	0.1 % (w/v)
Methanol (Roth)	40 % (v/v)
Acetic acid (Roth)	10 % (v/v)

Destaining solution

Methanol (Roth)	20 % (v/v)
Acetic acid (Roth)	10 % (v/v)

2.2.3.4 Silver staining of protein gels

Silver staining is a highly sensitive method to visualize nanogram levels of proteins. To prevent residual protein contamination, prior to silver staining, all equipment was soaked in 1% SDS solution (10 g / l) and washed thoroughly with ddH_2O. All buffers have to be prepared fresh on the day of usage. SDS gels were prepared and proteins separated as described above. The gel was fixed overnight in fixing solution with constant shaking at 100 rpm before it was washed 3 times in 50 % ethanol. For sensitization, the gel was incubated for 1 min in sensitization solution. Subsequently, the gel was washed 3 times for 20 min in ddH_2O and incubated for 20 min with impregnation solution. Next, the gel was washed shortly three times for 20 sec in ddH_2O. For development of the stain, the gel was briefly incubated with developing solution, which was decanted and fresh developing solution was added to the gel until the intensity of protein bands was optimal. The reaction was stopped by a10 min incubation in fixing solution. Finally, the gel was washed in 50% methanol for two minutes and stored in ddH_2O at 4 °C until the gel was mounted for drying.

Fixing solution

Methanol (Roth)	50 % (v/v)
Acetic acid (Roth)	12 % (v/v)

Sensitization solution

Sodium thiosulphate (in solution) $Na_2S_2O_3$	5 % (v/v)
	12 % (v/v)

Impregnation solution

Silver nitrate $AgNO_3$ (Sigma)	0.1 g
Formaldehyde (Roth, 37%)	37.5 µl
	→ up to 50ml ddH_2O

Developing solution

Sodium carbonate Na_2CO_3 (Sigma)	15 g
Sodium thiosulphate (in solution) $Na_2S_2O_3$	130 µl - 5 % (v/v)
Formaldehyde (Roth, 37%)	125 µl
	→ up to 250ml ddH_2O

2.2.3.5 Immunoblot analysis

The protein samples for Western blot analysis were separated via SDS-PAGE until the dye front had passed through the resolving gel. Prior to assembling the blotting sandwich, all used equipment was equilibrated in transfer buffer, including the membranes. The proteins were subsequently transferred onto a nitrocellulose membrane by wet blotting in transfer buffer (1x) for less than one hour at 400 mA. Free protein binding sites were blocked with 5 % milk powder (Roth) dissolved in TBS for one hour at room temperature on an orbital shaker. The incubation with the primary antibody in 2.5 % milk powder in TBS-T was performed overnight at 4 °C. Unbound antibodies were removed via triple washing of the membrane with TBS-T for five minutes per wash at room temperature. Next, the membrane was incubated for one hour with a horseradish peroxidase (HRP) coupled secondary antibody (1:5000) in 2.5 % milk powder in TBS-T at room temperature. Subsequently, the triple washing of the membrane with TBS-T for 5 minutes per wash at room temperature was repeated. Under exclusion of light, the membrane was incubated for 2 minutes with 500 µl of the substrate solution, a 1:1 mixture of both reagents from the chemiluminescence kit Femto (Super Signal® West Femto). The solution was carefully dabbed off. The chemiluminescent signal was then visualized by exposure (30 seconds to 20 minutes) to and the subsequent development of X-ray films (Fujifilm Super RX, Fujifilm USA). For reanalysis, all attached antibodies could be removed by incubation with 5 ml Restore™ Western Blot Stripping Buffer (Pierce) for 10 minutes, which was afterwards washed away via four washing steps using TBS-T for five minutes per wash.

2.2.3.6 GFP Trap M co-immunoprecipitation

With the aid of co-immunoprecipitation it becomes possible to isolate GFP::fusion proteins together with their associated interaction partners. In order to identify interaction partners of vacuolins, the GFP Trap M kit from Chromotek was used in this study according to the manufacturer's instructions. In principal this method is based on magnetic beads coupled to GFP binding antibodies that bind to GFP::fusion proteins.

For the assay, approximately 5 x 10^7 log-phase cells were harvested in 10 ml 1x Soerensen buffer (SSB) and a few drops were collected in an IBIDI dish containing 200 µl HL5-C (for microscopic analysis). The remaining cells were washed once with SSB (3 min, 500 g), the supernatant (SN) was decanted; the pellet suspended in 1ml SSB and transferred to a 1.5 ml Eppendorf tube. After another centrifugation step, the SN was removed completely using a blue tip.
To lyse the cells, 480 µl ice-cold 1x lysis buffer and 120 µl ice-cold 1x RIPA buffer were added; the cells were dispersed by thoroughly pipetting the suspension up and down. Subsequently, the cell suspension was incubated for 30 min on a rotating disc at 4 °C. During this incubation time, infection rates were determined visually and the magnetic beads were equilibrated in the following way: bead suspensions were vortexed before 25 µl per samples were removed and each aliquot was transferred into 250 µl lysis buffer. The suspensions were then magnetically separated until the SNs were clear and beads were washed two more times with 250 µl lysis buffer, replicating the procedure.
Lysates were centrifuged (5 min, 4 °C, maximum speed) in order to separate soluble (lysate) and non-soluble (pellet) contents. Next, lysates were transferred into new pre-cooled tubes. Pellets were resuspended in 50 µl pre-heated (95 °C) 1 x NuPAGE® LDS sample buffer (= non soluble fraction) and 30 µl lysate were added to 30 µl pre-heated (95 °C) 2 x LDS sample buffer (= input). Both samples were incubated for 5 min at 95 °C and immediately transferred into liquid nitrogen. The remaining majority of the lysates were added to the beads and incubated for 2 hours on a rotating wheel at 4 °C. The suspension was then magnetically separated until SN was clear and 30 µl SN were added to 30 µl pre-heated (95 °C) 2 x LDS sample buffer (= non bound fraction). Remaining SNs were discarded and beads were washed twice with 500 µl RIPA buffer and 3 times with 500 µl lysis buffer, as described above. After the last washing step, the beads were suspended in 30 µl pre-heated (95 °C) 1 x LDS sample buffer (=bound fraction), incubated for 5 min at 95 °C and immediately transferred into liquid nitrogen.

Lysis buffer

Tris, pH 7.5 (Sigma)	50 mM
Sodium chloride, NaCl (Sigma)	150 mM
EDTA (Roth)	5 mM
* PI – cocktail (Roche)	1 tablet
* ATP	5 mM
* DTT	1 mM

RIPA buffer

1 x lysis buffer	10 ml
Triton X 100 (Sigma)	150 mM
Sodium deoxycholate (≥97%, Sigma)	5 %
SDS (pellets, Sigma)	0.5 %
* PI – cocktail (Roche)	1 tablet

* add freshly prior utilization

2.2.3.7 Indirect immunofluorescence analysis (IFA)

2.2.3.7.1 Fixation

For all immunofluorescence experiments, coverslips with adherent *D. discoideum* cells were fixed in 500 µl 4 % paraformaldehyde (PFA) for one hour at 4 °C. Subsequently, the fixation-solution was removed and replaced with 1 ml PBS. Fixed coverslips were then stored at 4°C.

2.2.3.7.2 Immunolabeling

In order to stain fixed cells, coverslips were incubated for 15 min with blocking solution, which contained gelatin to saturate free and unspecific binding sites. The advantage thereof is that the relevant epitopes are targeted with higher efficiency. During the incubation process, a fixing chamber was prepared by placing wet paper towels in the box to create a humid atmosphere that prevents evaporation of the antibody solutions. In addition, the box was wrapped in aluminum foil to exclude light.
Subsequently, 30 µl droplets of the respective primary antibodies in blocking solution were placed onto the parafilm and coverslips were placed, cells down, on top of the antibody solution. Incubation with the primary antibodies took place for 1 hour at RT. Next, the coverslips were washed by gently dipping into PBS and placed back into the 24-well plate with the blocking solution for 10 min. Secondary antibodies and fixed cell stains were also diluted in blocking solution and placed in 30 µl drops on a fresh strip of parafilm. Coverslips were incubated on the second droplets in the same manner as before for 1 hour at RT. Last, the coverslips were gently dipped in PBS and the edge of each coverslip was put on a paper towel to draw off the excess buffer. The coverslips were placed with the cell-covered side on a drop of mounting-medium on an ethanol-cleaned glass slide. In order to allow the embedding medium to harden, slides were kept in the dark overnight at RT before ultimately stored at 4 °C.

10 x PBS (phosphate buffered saline)

Sodium chloride, NaCl (Sigma)	80 g
Potassium choride, KCl (Sigma)	2 g
Sodium phosphate, NaHPO4 (Sigma)	14. 2 g
Potassium phosphate KH2PO4 (Sigma)	2.4 g
	→ up to 1 l ddH2O, pH 7.4

Blocking solution

Gelatin (Sigma)	0.2 g
Triton X 100 (Sigma)	0.2 ml
Sodium deoxycholate (≥97%, Sigma)	→ up to 200 ml PBS

2.2.3.7.3 Antibodies and fixed cell stains

All primary antibodies used for IFA are listed in table 2-24. Secondary antibodies and fixed cell stains are listed in table 2-25.

Table 2-24: Primary antibodies

Antibody	Species	Dilution	Clone	Manufacturer/ Distributor
α-GFP (# 598)	chicken	1:500	polyclonal	MBL, Woburn, USA
α-p80 (H161)	mouse	1:10	monoclonal	Dr. Pierre Cosson, University of Geneva, Swiss
α-VatA (22.35.2)	mouse	1:10	monoclonal	Prof. Dr. Markus Maniak, University of Kassel, Germany

Table 2-25: Secondary antibodies and fixed cell stains

Antibody	Species	Dilution	Clone	Manufacturer/ Distributor
α-chicken Alexa Fluor® 488	goat	1:1000	polyclonal	Life Technologies, Carlsbad, USA
α-chicken Alexa Fluor® 568	goat	1:1000	polyclonal	Life Technologies, Carlsbad, USA
α-chicken Alexa Fluor® 647	goat	1:500	polyclonal	Life Technologies, Carlsbad, USA
α-mouse Alexa Fluor® 488	goat	1:1000	polyclonal	Life Technologies, Carlsbad, USA
α-mouse Alexa Fluor® 568	goat	1:1000	polyclonal	Life Technologies, Carlsbad, USA
α-mouse Alexa Fluor® 647	chicken	1:500	polyclonal	Life Technologies, Carlsbad, USA
DAPI	---	1:100	---	Sigma-Aldrich, Taufkirchen, Germany

2.2.4 Microscopy

2.2.4.1 Confocal point scanning microscope

In a confocal scanning microscope the excitation laser produces a single point spotlight on the sample. In this way phototoxicity and bleaching is reduced to that exact illumination point. However, the entire sample has to be scanned dot by dot, which is why the method is best suited for fixed cells.

The microscope used in this study was built around an Olympus IX81 base and images were acquired using either an Olympus 60x Plan-Apochromat 1.35 or an Olympus 100x UPlanSApo 1.4 Oil objective in combination with the Olympus Fluoview software version 1.7b. The fluorescence of fluorophores was excited by successive stimulation by the relevant lasers (see table 2-26). Laser intensities were kept as low as possible but varied from sample to sample in a range of 8- 60%. Photomultiplier tubes detected emitted fluorescence light whereby their sensitivity was not raised above 800. The size of the pinhole was set automatically, and offset and gain were set to zero and one, respectively. Images were acquired in either a 512 x 512 or a 1024 x 1024 pixel format. The dwell time was set to 10 µs and the image was avergaged three times (Kalman 3 x).

Table 2-26: Laser lines of the confocal scanning microscope

Laser	Used for excitement of	Manufacturer
405 nm diode	DAPI	Olympus, Hamburg, Germany
488 nm argon	GFP, Alexa Fluor® 488	Olympus, Hamburg, Germany
559 nm diode	mCherry, Alexa Fluor® 568	Olympus, Hamburg, Germany
635 nm diode	Alexa Fluor® 647	Olympus, Hamburg, Germany

2.2.4.1.1 Micrograph processing

In general, enhancement of images was kept to a minimum and was performed for the complete image without changing any information relayed by the image. Scale bars were added to images using either the program they had been acquired with, FluoView software or during image processing with Imaris software. Clipping as well as false coloring were done using Imaris software. To make images widely readable they were exported from their original format (.oif) into either .tif or .avi files using the Imaris software.

2.2.4.2 Wide-field microscope

The luminous source used in wide-field fluorescence microscopy creates light of different wavelengths, ranging across the whole spectrum. Specificity is generated by passage through different filter sets, which are adapted to the respective fluorophores before excitation and detection. Due to the possibility to illuminate a large area, the image information of an entire view field is immediately available. The cellR Imaging System that was used for this study, was the inverted microscope Olympus IX81 equipped with an Olympus 100x/1,4 UPlanSApo oil objective, an MT20-I- fluorescence illumination system including a xenon burner and two filter sets (table 2-27).

Table 2-27: Filter sets used for wide-field microscope

Filter set	Used for excitement of	Manufacturer
Excitation HC 479/22 Emission 512	GFP, Alexa Fluor® 488	Olympus, Hamburg, Germany
Excitation HC 555/20 Emission 612	mCherry, Alexa Fluor® 568	Olympus, Hamburg, Germany

2.2.4.3 Quantification analysis of infected *D. discoideum* strains

For quantification of marker association with the *M. marinum* replication vacuole, *D. discoideum* cells were infected and stained as described in paragraph 2.2.2.2 and 2.2.4.7. At least 3 technical and biological independent samples were examined for each time point by using the wide-field fluorescence microscope. Included in each analysis were at least 100 bacteria or bacterial aggregates distributed in random areas of the slide. Counting criteria were categorized in two groups: no association or association. Partial association of markers was counted to the association category.

2.2.5 *In silico* biology, databases and software programs

2.2.5.1 Databases and web-links for sequence retrieval

D. discoideum AX2 wild type genomic DNA, cDNA and protein sequences were retrieved from dictyBase database at http://dictybase.org/.

2.2.5.2 Generation of oligonucleotides

All primers were generated using the Primer3 software http://primer3.ut.ee/.

2.2.5.3 Sequence analysis

BLAST similarity searches were performed via http://dictybase.org/tools/blast or http://blast.ncbi.nlm.nih.gov/Blast.cgi?PROGRAM=blastn&PAGE_TYPE=BlastSearch&LINK_LOC=blasthome. Protein domains and prediction of putative modification sites were analyzed by SMART http://smart.embl-heidelberg.de/, motif scan http://myhits.isb-sib.ch/cgi-bin/motif_scan and UniProt http://www.uniprot.org/.

2.2.5.4 *In silico* cloning

All cloning steps were performed *in silico* using MacVector™ software, version 12.01.

2.2.5.5 Software programs

Table 2-28: Software programs

Software program	Version	Used for
Endnote	X.5	Literature management
FlowJo	7.6.3	Analysis of FACS-data
GraphPad Prism	5.0.b	Graphs, statistical analysis, normalization
Microsoft Office 2011	14.3.2	Calculations, writing, figures

3 Results

Despite decades of tuberculosis research many questions remain in regard to composition and maintenance of the mycobacterial replication niche. The initially successful host defense represented by a macrophage phagocytizing the pathogen is alternated by the pathogen before the invasive bacteria would be killed by digestion in a phagosome. By bypassing further phagosomal maturation *Mycobacteria* are capable of reorganizing the phagosome into a replication niche and establishing an infection. In respect to these early host pathogen interactions many factors of the host defense and bacterial survival strategy are still unknown. Better knowledge of these processes might contribute to improved development of new drug targets to fight tuberculosis infection. With the *Dictyostelium discoideum* – *Mycobacterium marinum* model system a new perspective on both, the pathogen and the host emerges. Using this model system, the aim of this study was to identify and characterize host proteins that are actively involved in the response to a mycobacterial infection. It is anticipated that the results obtained from this model system can be transferred to macrophages fighting against a *M. tuberculosis* infection.

3.1 Expression analysis of infected *Dictyostelium discoideum*

3.1.1 Design and evaluation of a quantitative real-time PCR system

Host-pathogen interactions lead to several changes of the host cell. First, infected host cells modulate their gene expression in response to the invaded pathogen mostly followed by the production of proteins to control the infection [105]. Here, the analysis of *D. discoideum* transcriptional response to the *M. marinum* infection provided potential information about the mechanism used by host cells to control a mycobacterial infection or pathways which are targeted by the pathogen. An expression profile of handpicked candidate-genes of infected *D. discoideum* cells was generated via quantitative real-time PCR (qPCR). Therefore two qPCR systems using two types of PCR amplification detection were established. The SYBR Green system was based on random fluorescence signals from double-strand DNA while TaqMan system relies on fluorescence signals from sequence-specific templates. In addition, several parameters were optimized making the qPCR systems a powerful tool to monitor transcriptional changes in response to the infection by determining mRNA abundance of infected *D. discoideum* cells in comparison to non-infected *D. discoideum* cells.

3.1.1.1 Primer design and evaluation

Specific oligonucleotide pairs for each candidate-gene and potential housekeeping genes were designed using Primer3 software. All oligonucleotide pairs were thoroughly checked in terms of melting temperature, ability to form secondary structures and self-priming tendency, strictly avoiding the last two points. Specificity was verified in silico

via BLAST analysis to ensure that oligonucleotides solely match to the gene of interest (GOI). The vacuolin gene subset showed very high DNA sequence similarities. Therefore, to absolutely exclude false positive signals each vacuolin primer pair was challenged with full-length *vacuolinA*, *B* and *C* genes as PCR templates, respectively. No cross-reactivity was detected; consequently all vacuolin primer pairs were specific for their target sequence [data not shown]. In order to check efficiency of the amplification reaction in the different PCR setups a tenfold dilution series of known template concentrations was performed for housekeeping and vacuolin primer pairs (fig. 3-1: A). Based on data points of the Ct values a linear regression was performed and the slope of the reaction was calculated (fig. 3-1: B). To determine the exponential amplification efficiency the slope was inserted into the formula: $E = 10^{(-1/slope)}$. Accordingly, an amplification factor of two has the slope of -3.322, representing a 100% efficient amplification reaction by doubling the PCR product in each cycle. Amplification efficiencies of used primer pairs are quoted in table (tab. 3-1).

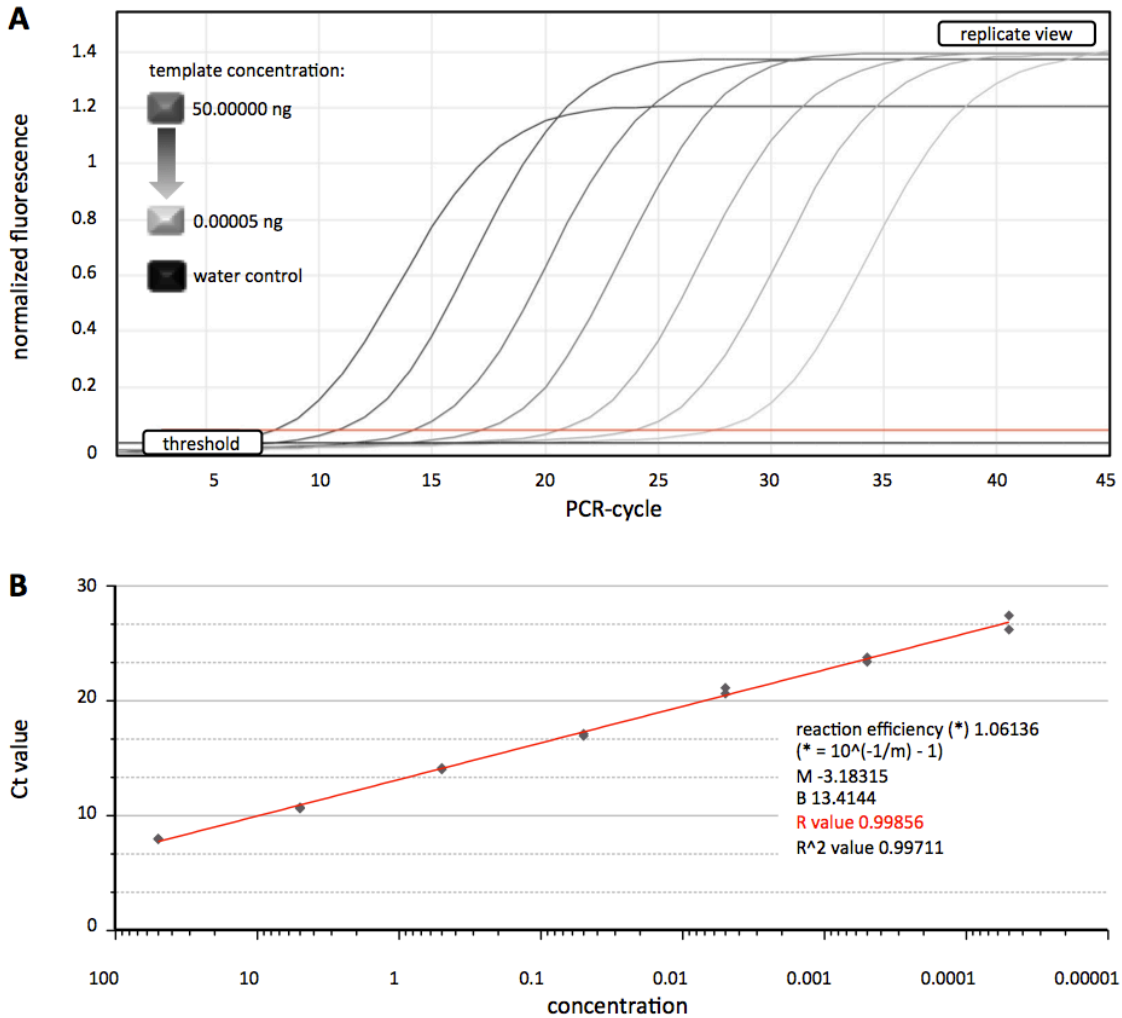

Figure 3-1: *Gapdh* primer pair revealed an excellent amplification efficiency of 99%. Primer pair amplification of a 7-log template dilution series is representatively shown for the housekeeping gene *gapdh* (*glyceraldehyde 3-phosphate dehydrogenase*). (**A**) Increasing fluorescence signal per PCR cycle display amplification of PCR products. A threshold was set automatically in log-phase to determine Ct values (**B**) Ct values of each template dilution plotted against template concentration to calculate reaction efficiency. A slope (M) of -3.183 and a correlation coefficient (R Value) of 0.9986 were calculated.

Table 3-1: PCR amplification efficiency of vacuolin and housekeeping primer pairs in Sybr Green and TaqMan qPCR systems

primer pair	efficiency [%]	
	Sybr Green	TaqMan
gapdh	99	98
vacuolinA	98	94
vacuolinB	96	96
vacuolinC	97	99

3.1.1.2 *glyceraldehyde 3-phosphate dehydrogenase* (gapdh): a reliable internal control

For relative quantification an internal control (housekeeping gene) was required to normalize variations of RNA input. Since the complete analysis was built on that signal the choice of housekeeping gene was an important part of the experimental setup. The transcription level of the ideal internal control stayed steady throughout proliferation and experimental procedures as well as differential cell types. Therefore, the potential of *gapdh*, *ig7, h2b*, *calmodulin* and *pah* was evaluated to comply with these parameters. Only *gapdh* fulfilled all criteria and did not show an influence on Ct values comparing samples from non-treated cells (biological control), cells that underwent the complete infection procedure without any pathogens (mock control) and cells that were infected (fig. 3-2). Thus, *gapdh* was suitable for internal normalization of the following qPCR analysis.

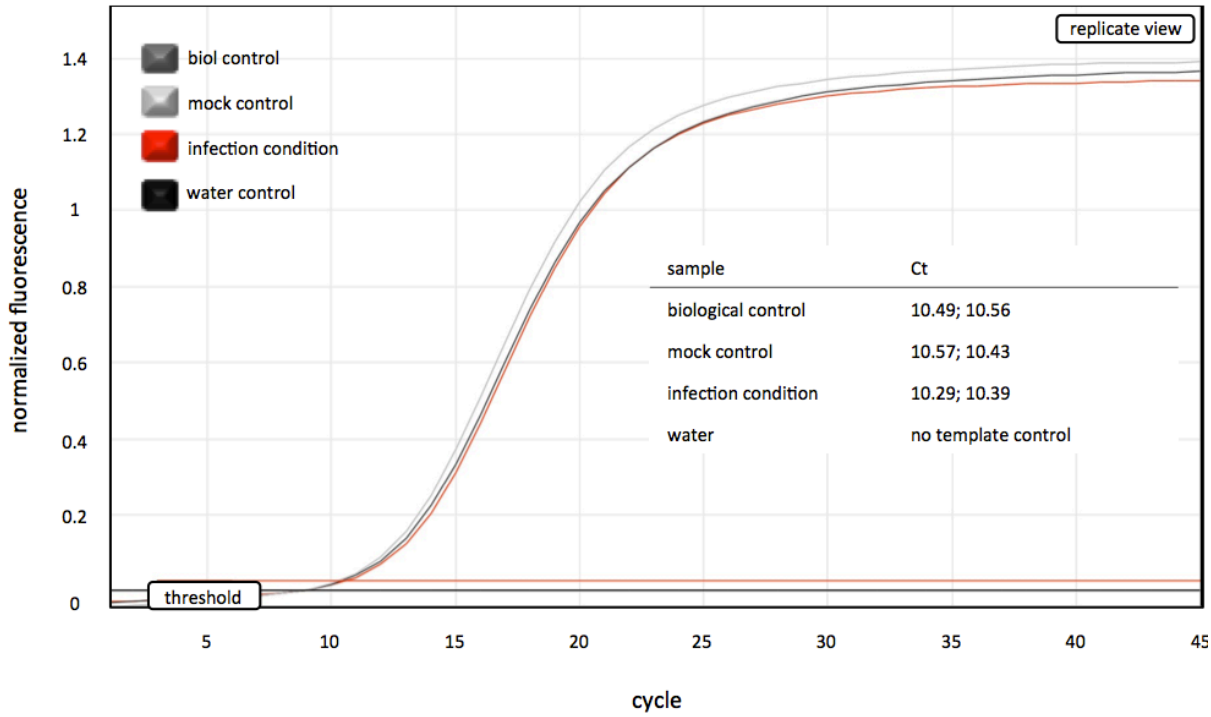

Figure 3-2: Validation of *gapdh's* potential for qPCR normalization. Stable Ct values of gapdh PCR products of axenic, mock-treated and infected samples confirmed gapdh's capacity to serve as a non-regulated normalizer. Total RNA of all samples was isolated, reversely transcribed and the cDNA was used as template for qPCR. Amplification was monitored by fluorescent SYBR Green signal detection and plotted against PCR cycle number. Threshold was set in log-phase of fluorescent SYBR Green signal.

3.1.1.3 Infection for quantitative real-time PCR analysis

In order to profile transcriptional changes of *D. discoideum* induced by *M. marinum* the *D. discoideum* cells had to be highly infected in a synchronized fashion. Since differences between infected and non-infected samples were analyzed by comparing total RNA of the population, clearly any changes became more assessable if the infection rate was above 60% threshold. In order to increase efficiency of infection some parameters of the original infection protocol were changed [82].

Even though the course of infection differed from that described by Hagedorn and Soldati [82]. First, the multiplicity of infection (MOI), the ratio of bacteria to infective *D. discoideum,* was increased from ten to 150. Second, the centrifugation procedure was adjusted to warrant high infection rates. Last, changes were made concerning *D. discoideum* culture conditions by keeping cells adherent instead of a suspension under shaking conditions.

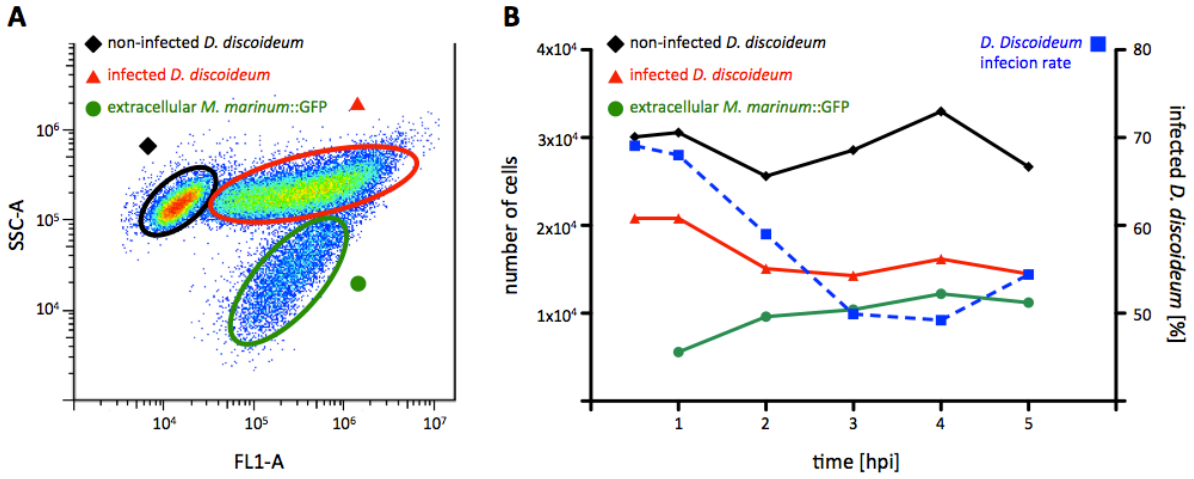

Figure 3-3: Dismissal and re-uptake of bacteria led to asynchronous infection. (**A**) Representative FACS analysis plot of non-infected and infected *D. discoideum* cells as well as extracellular *M. marinum::*msp12^{gfp} showing the different cell populations as indicated. (**B**) Hourly FACS analysis enabled monitoring of population dynamics in the course of infection: The total numbers of non-infected *D. discoideum* (left y-axis, black) cells increased more rapidly then infected *D. discoideum* cells (left y-axis, red), which led to a decline of the infection rate (right y-axis, blue) within one to three hours post infection (hpi). In parallel, quantity of extracellular bacteria constantly increased (left y-axis, green). Due to re-uptake of initially exocytosed bacteria the infection rate increased again from four to five hpi.

To characterize the infection rate during the course of the infection under the new conditions, wild type *D. discoideum* were infected with green fluorescent *M. marinum*::msp12^{gfp}. Subsequent FACS analysis was used to distinguish between infected *D. discoideum*, uninfected *D. discoideum* and extracellular *M. marinum*::msp12^{gfp} (fig. 3-3). Over time, the number of infected *D. discoideum* cells slightly decreased and the number of non-infected *D. discoideum* increased. In parallel, the population of extracellular bacteria increased, which could then be rephagocytosed by *D. discoideum.* Subsequently, prolonged cultivation led to an asynchronous infection. Despite of the optimized infection and cultivation conditions, the usual infection rate at 30 minutes

post infection still did not reach the 60% mark regularly. However, for repetition of experiments one time point, two hours of infection (hpi), was selected at which infected *D. discoideum* cells were enriched via FACS sorting. Thereafter, infected cells could be enriched to 90%.

3.1.2 Screening revealed potential candidate-genes that respond to *M. marinum* infection

Based on a bioinformatic approach the *D. discoideum* proteome a search was performed for protein domains known to be directly or indirectly involved in pathogen triggered immune response of eukaryotes. Since the *D. discoideum* genome is fully annotated respective genes were traced back resulting in a list of *D. discoideum* genes putatively involved in pathogen response. From this repertoire, candidate-genes originating from orthologs in plant immunity (I) and animal immunity and scavenger receptors (II) were selected for the qPCR screening approach. In addition, genes known to be regulated upon *D. discoideum* infection with *L. pneuophila* (III) or are involved in bacterial response (IV) were included. In total, 34 candidates were analyzed for transcriptional regulation upon the mycobacterial infection at two hpi (fig. 3-4).

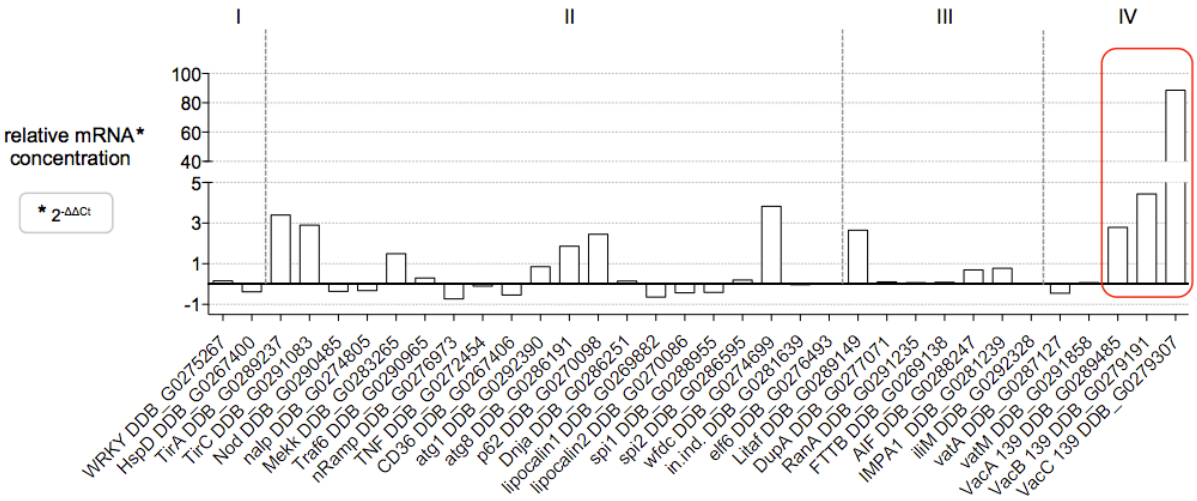

Figure 3-4: SYBR Green qPCR screening of 34 candidate-genes revealed a new insight into *D. discoideum* transcriptional response to *M. marinum* infection. The screening was performed at two and four hours post infection (hpi). mRNA abundances of candidate-genes originating from orthologues in plant immunity (I) and animal immunity and scavenger receptors (II) as well as two categories representing genes involved in *D. discoideum* response to *L. pneumophila* (III) and bacteria infection (IV) were determined by qPCR analysis and subsequent $2^{-\Delta\Delta Ct}$ calculation using *gapdh* for normalization. To emphasize down regulation results were normalized using the formula: Y=Y-K with K=1.0.

For group I, putative *D. discoideum* immunity genes derived from plant immunity genes, neither the gene coding for the transcription factor *wrky* nor the gene coding for *hspD* were highly influenced and transcriptionally regulated. The second group consisting of putative *D. discoideum* immunity genes derived from animal immunity orthologues (II) show a transcriptional regulation at almost every functional subset. The relative mRNA concentration of two *D. discoideum* Toll/interleukin (TIR) receptor domains (fig.3: *tirA* and *tirC*) both were increased by a factor of three. These highly conserved intracellular signaling domains mediate protein-protein interactions between Toll-like receptors and

signal transduction components. In *D. discoideum, tirA* expression is known to increase in sentinel cells and involved in sustained growth on bacteria and in pathogen response to virulent bacteria [29]. Increasing amounts of mRNA were also measured for *mekk*, coding for a protein serine/threonine kinase that is a part in the MAPKs signaling pathway. Interestingly, transcription of *nramp1* and *cd36*, encoding the natural resistance-associated macrophage protein and a putative scavenger receptor, was down-regulated. A moderate increase of relative transcription was measured for *litaf*, the *D. dicoideum* ortholog of the conserved lipopolysaccharide-induced tumor necrosis factor alpha. In contrast, mRNA level of the TNF receptor-associated factor 3 (TNF) was only slightly down-regulated. Furthermore, for members of the autophagy family, precisely *atg1*, *atg8* and *p62*, a notable transcriptional increase in response to *M. marinum* infection was recorded. For one potentially secreted protein, wfdc named after a WAP four-disulfide core domain with a putative protease inhibitor activity, a comparable strong increase of mRNA amount of almost fourfold was detected. The analysis of group III, candidates derived from the *L. pneumophila* infected *D. discoideum* model, did not show significant changes of mRNA concentration. The most outstanding relative transcriptional increase occurred in the vacuolin family categorized to group IV. In particular, *vacuolinC* showed a remarkable 88 fold relative transcriptional increase. At the same time for *vacuolinB* and *vaculoinA* an increasing relative transcription of almost fivefold and twofold was calculated, respectively. *VacuolinB* and *C* up-regulation was verified with a second independent method, via deep sequencing [data not shown].

3.1.3 Up-regulation of small RNAs in response to *M. marinum*

In collaboration with the laboratory of Prof. Fredrik Söderbom at the Uppsala University (Department of Molecular Biology, Swedish University of Agricultural Sciences) we aimed to gain further knowledge of RNA changes in *D. discoideum* induced by the infection with *M. marinum.* Two independent infections and the corresponding mock treated control samples were sent for deep sequence analysis. The analysis of small RNAs uncovered an up-regulation of small RNAs with a size of 33 nucleotides (nt) in response to *M. marinum* infection (fig. 3-5).

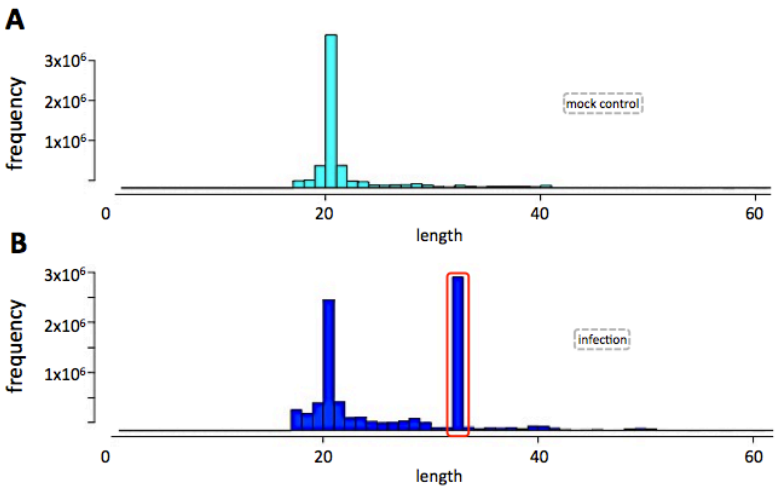

Figure 3-5: Increase of small RNAs (33 nt) in response to *M. marinum* infection. Representative excerpt of deep sequencing analysis of two independent samples, each consisting of infected and mock-treated wild type *D. discoideum* cells. Total RNA of all samples was isolated two hours post infection (hpi).

3.1.4 Verification of enhanced *vacuolin* mRNA abundance via TaqMan qPCR

Evidence is growing, that the transcription of genes in *D. discoideum* does not follow a constitutive pattern in different life cycle stages as well as during infection [32, 133, 176]. For a better understanding of these variances a sophisticated method was established and applied for the most promising candidates, the vacuolin family. Quantitative real-time PCR with TaqMan probes guarantees more specificity, a higher sensitivity to low copy genes and the possibility of multiplexing the PCR reduces variability of template input. With that method *vacuolin* mRNA levels were compared in four independent samples of *M. marinum* infected *D. discoideum* wild type at two hpi. Analysis via reaction efficiency corrected relative mRNA expression confirmed results obtained via SYBR Green screening approach and likewise demonstrated a moderate increase of relative *vacuolinA* and *B* concentrations as well as a massive increase of *vacuolinC* by the factor of 1000 (fig. 3-6: A). In figure 3-6: B the ΔCt values of the same data give further information about the respective mRNA levels: Considering the general level of *vacuolin* isoforms in non-infected cells normalized to the housekeeping gene *gapdh*, the highest abundance was measured for *vacuolinA*. About half of that amount was measured for *vacuolinB* while *vacuolinC* was close to the detection level (fig. 3-6: B; mock controls, grey bars). The increase of relative *vacuolinA* mRNA amount of about 200 (mock) to about 400 (infection) led to the lowest relative change of twofold even though the relative expression in infected cells is the highest of the vacuolin family. In contrast, the increase of relative *vacuolinC* mRNA expression of almost no expression (mock) to an over 400 fold (infection) led to the highest relative change as calculated by reaction efficiency corrected relative mRNA expression.

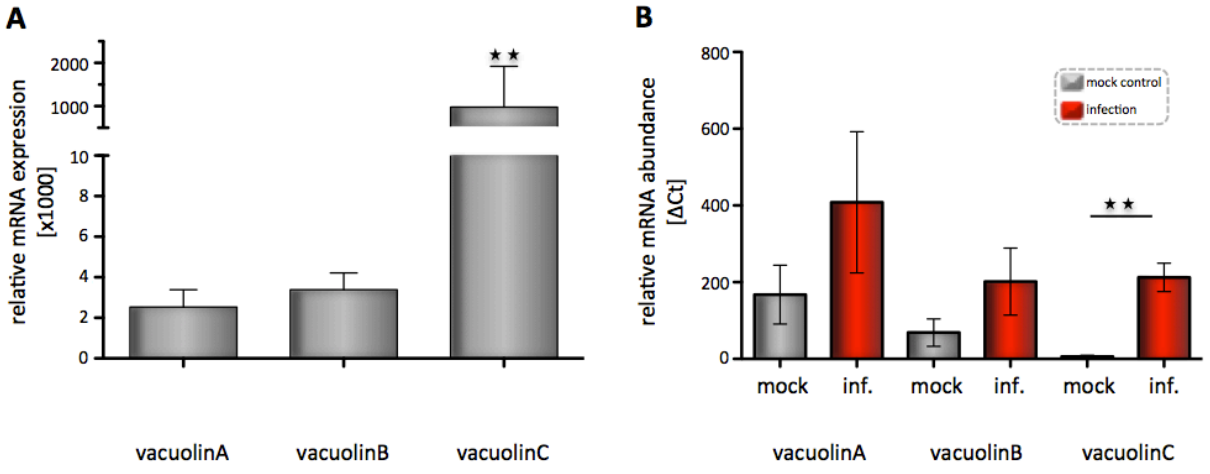

Figure 3-6: Multiplex TaqMan qPCR analysis confirmed previously described enhanced *vacuolin* transcription in response to *M. marinum* infection. Total RNA was isolated from mock treated and *M. marinum*-infected *D. discoideum* wild type cells at two hours post infection (hpi). Subsequently, transcription of mRNA to cDNA was performed prior qPCR analysis. (**A**) The relative concentration of *vacuolin* isoforms *A*, *B* and *C* was calculated via the efficiency corrected $2^{-\Delta\Delta Ct}$ method. Mean value ± standard deviation shows a statistically significant increase of *vacuolinC* mRNA abundance. (**B**) The expression rates of *vacuolinA*, *B* and *C* relative to the expression of the reference gene *gapdh* in mock treated (grey) and *M. marinum*-infected (red) samples were calculated by ΔCt. Shown are mean values ± standard deviations. Statistics were performed using the unpaired two-tailed t-test with a confidence interval of 95% in reference to the wild type control, n = 4, **p = 0.0011. mock: mock- treated samples, inf.: infection samples

3.1.5 *Vacuolins* are differentially transcribed in various *D. discoideum* infections

To obtain a detailed transcriptional overview of vacuolins during early phase of mycobacterial infection a time series was analyzed by qPCR. In addition, to monitor if differential vacuolin expression was specific to *M. marinum* infection, *D. discoideum* cells were infected with different pathogenic and non-pathogenic bacteria (fig. 3-7).

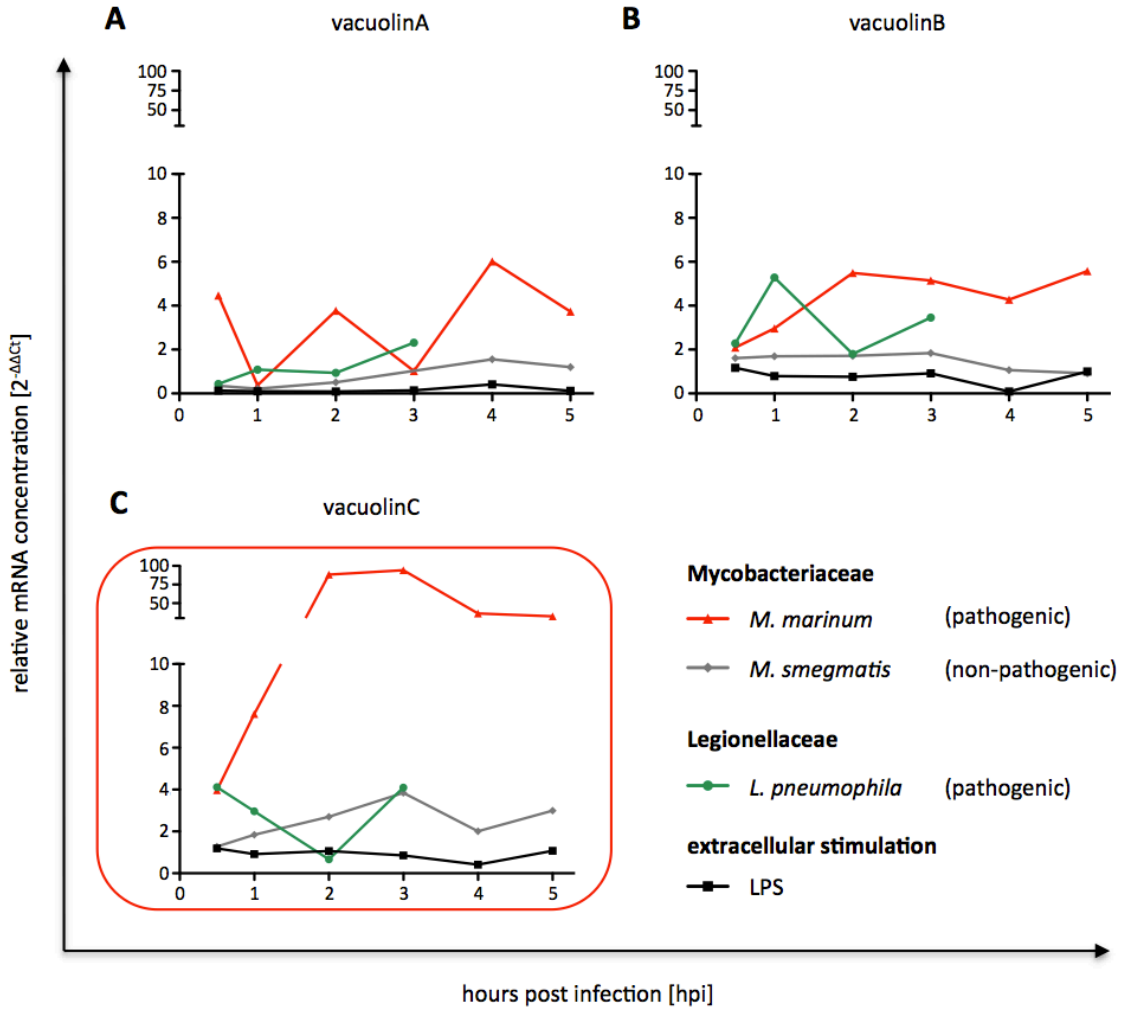

Figure 3-7: mRNA expression profile of *vacuolinC* specifically increased upon pathogenic *M. marinum* infection. *VacuolinA* (**A**), *vacuolinB* (**B**) and *vacuolinC* (**C**) mRNA abundances of *D. discoideum* wild type challenged with *M. marinum* (red), *L. pneumophila* (green), *M. smegmatis* (grey) and the exposure with LPS (black)**.** The relative concentration determined by $2^{-\Delta\Delta Ct}$ method of all vacuolin isoforms in reference to mock treated samples and normalized to the housekeeping gene *gapdh* (*glyceraldehyde 3-phosphate dehydrogenase*) was plotted over time (hours post infection; hpi). qPCR was performed using the SYBR Green-based system.

The transcription profile of *vacuolinA* revealed a very fast response specific for pathogenic *M. marinum*. 30 minutes post infection the expression level of *vacuolinA* showed a fivefold increase. In the course of the infection *vacuolinA* mRNA level followed an on and off pattern with peaks at 30 minutes, two and four hpi. No major changes were monitored in response to non-pathogenic *M. smegmatis*, pathogenic *L. pneumophila* or LPS treatment. On the contrary, *vacuolinB* mRNA level followed a different pattern in the response to the *M. marinum* infection: After a constant increase

over the first two hours up to fivefold, the elevated mRNA level was maintained. In contrast to the other vacuolin isoforms, a transient response with a peak by factor five at one hpi was monitored upon *L. pneumophila* infection. Similar to *vacuolinA* no transcriptional changes of *vacuolinB* were observed in response to uptake of either non-pathogenic *M. smegmatis* or LPS treatment. Interestingly, the transcription of *vacuolinC* was quickly up-regulated exclusively during *M. marinum* infection (fig. 3-7: C). Within two hpi an almost hundredfold increase of relative mRNA level was reached and maintained. The drop at four and five hpi could be due to decreasing infection rates that regularly occurred at four to six hpi. In summary, none of the vacuolin genes showed a strong response to non-pathogenic *M. smegmatis* infections or LPS treatment. Instead, specific transcriptional changes of all vacuolin isoforms in response to *L. pneumophila* and *M. marinum* were uncovered. Moreover, *vacuolinA, B* and *C* reacted to *M. marinum* infection with an isoform unique transcriptional profile.

3.1.6 Elevated vacuolinC protein level in response to *M. marinum* infection

The surprising increase of *vacuolinC* transcription in consequence to *M. marinum* infection obviously led to the question about its impact on protein level. Clearly, a concomitantly enhanced protein amount would emphasize the importance of vacuolinC in *D. discoideum* during *M. marinum* infection. To address this issue, a *D. discoideum* strain was generated, where the endogenous gene was tagged with a GFP encoding sequence (*D. discoideum* wild type$^{KI\ vacC:gfp}$). Therefore, a construct was designed that carried a *D. discoideum* adapted *gfp*-coding sequence and an independent gentamycin resistance cassette consisting of promotor, coding sequence and terminator, to enable screening via antibiotic pressure. The construct was enclosed by sequences targeting for an insertion upstream of the *vacuolinC* stop codon (fig. 3-8: A). With the successful integration of the construct into the *D. discoideum* wild type genome by homologous recombination the endogenous gene was coupled in frame to a *gfp*-tag via a small flexible linker sequence. After transfection of the linearized knock-in construct and sub-cloning of the transgenic *D. discoideum* wild type$^{KI\ vacC:gfp}$ cells by single-cell separation, genomic DNA was extracted and tested for integration of the construct at the expected loci (fig. 3-8: B). For two of the three loci selected for genomic analysis, one specific primer was used that could only yield a PCR product if the transgene had integrated. According to the PCR screen, 35% of tested sub-clones were confirmed to have the construct successfully integrated at the right place. With the wild type$^{KI\ vacC:gfp}$ strain, a powerful tool to observe the expression and localization patterns of endogenous vacuolinC protein was generated. First, to substantiate the hypothesis of an augmented presence of vacuolinC upon *M. marinum* infection the wild type$^{KI\ vacC:gfp}$ strain was infected to create a vacuolinC protein expression profile. For this, whole cell lysates of infected wild type$^{KI\ vacC:gfp}$ cells were prepared at hourly intervals and analyzed by immunoblotting (fig. 3-8: B). Indeed, the α-GPF antibody detected a signal at the expected size of the vacuolinC::GFP fusion protein in all samples. More importantly, an enhanced expression of vacuolinC occurred in transient waves upon infection with the strongest signal intensity peaks ranging from two to four hpi and from eight to ten hpi.

In accordance with the qPCR data, this immunoblot analysis confirmed the increased vacuolinC expression in response the *M. marinum* infection on protein level.

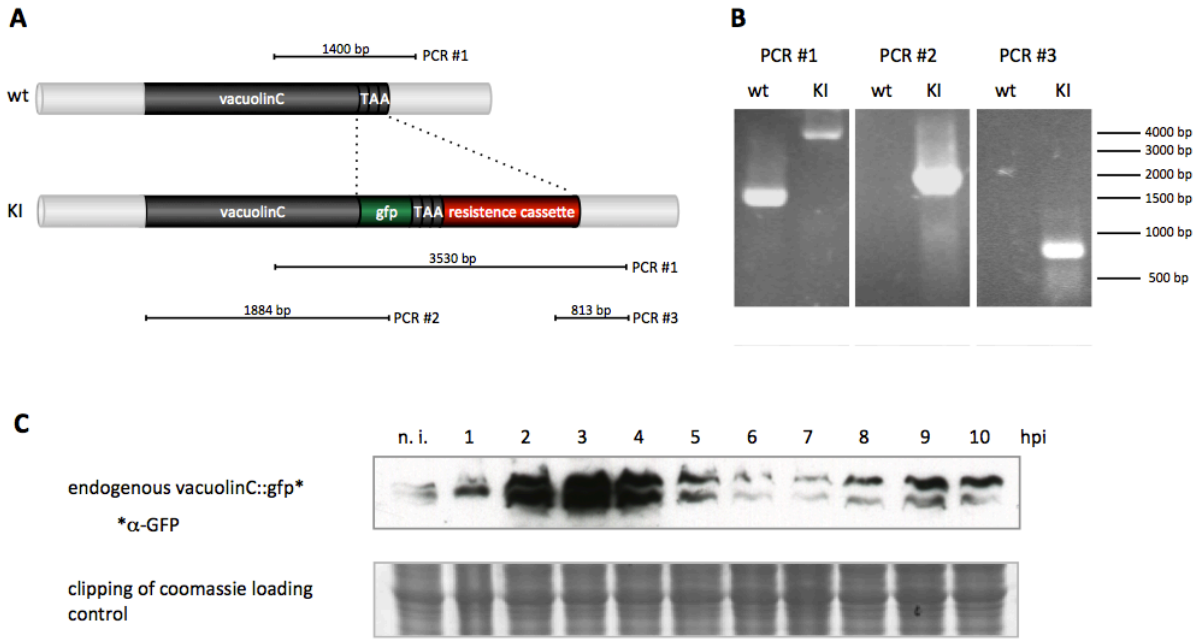

Figure 3-8: *M. marinum* infection induced elevated vacuolinC protein level in wild type$^{KI\ vacC::gfp}$. (**A**) Schematic overview of wild type$^{KI\ vacC::gfp}$ cloning strategy. The endogenous stop codon of *vacuolinC* was replaced in frame with the coding sequence of *gfp* including a 3' stop codon followed downstream by a gentamycin resistance cassette consisting of the *actin6* promotor, G418 resistance and *mhcA* terminator. (**B**) Successful insertion of knock in construct *KI vacC::gfp* in *D. discoideum* genome was proven by control PCRs #1-3 using subclone gDNA and subsequent agarose gel electrophoresis. (**C**) Immunoblot analysis of infected wild type$^{KI\ vacC::gfp}$ with hourly sampling probed with α-GFP primary antibody revealed transient boost of endogenous vacuolinC::GFP protein in accordance to the qPCR data (fig. 3-7, C). Equal sample load was confirmed by coomassie staining. Wt = wild type, KI = wild type$^{KI\ vacC::gfp}$.

3.2 Localization of vacuolin isoforms

As previously presented, several data hint to a differential regulation and diverging biological function of the vacuolin isoforms in *D. discoideum.* Unfortunately, the existing antibody directed against vacuolin does not distinguish between these isoforms, which are extremely similar; thus, the microscopical dissection of the specific localization of the vacuolin isoforms via immunolabeling is currently impossible. Several attempts to raise peptide antibodies specific for vacuolinC and also new antibodies specific for full-length vacuolinB were made. However, all antisera tested reacted either with all three vacuolin isoforms or failed to recognize any protein. Accordingly, GPF::vacuolin episomal expression system and the wild type$^{KI\ vacC:gfp}$ strain were used to visualize vacuolin isoforms in *D. discoideum*.

3.2.1 Localization of overexpressed vacuolin isoforms in axenic cultured *D. discoideum*

Transgenic *D. discoideum* strains (vacA^{gfp}, vacB^{gfp} and vacC^{gfp}) were created that constitutively express green fluorescent vacuolinA, B or C fusion proteins using the vector system pDM317/323 [193]. Axenic growing cells were fixed and stained for detailed microscopic analysis. All vacuolin GFP-fusion proteins localized to endosomal membranes (fig. 3-9). In comparison to vacuolinA and vacuolinB, which both localized to distinct vacuoles of approximately two µm diameter, vacuolinC decorated smaller vacuoles of approximately one µm diameter, which occurred with high abundances in uninfected cells. Double staining of the cells with a subunit of the vacuolar H^+-ATPase, vatA, revealed that only vacuolinC co-localized together with vatA at these small vacuoles (fig. 3-9: C). The vacuolar H^+-ATPase is a multi subunit enzyme, which is highly conserved. In macrophages and *D. discoideum*, the vacuolar H^+-ATPase pumps protons across membranes and therefore drives luminal acidification at the expense of ATP [34, 80, 152]. Shortly after phagocytosis the enzyme is delivered to the phagosome via fusion events with acidic lysosomes that carry vacuolar H^+-ATPase in their membranes [20, 34, 183].

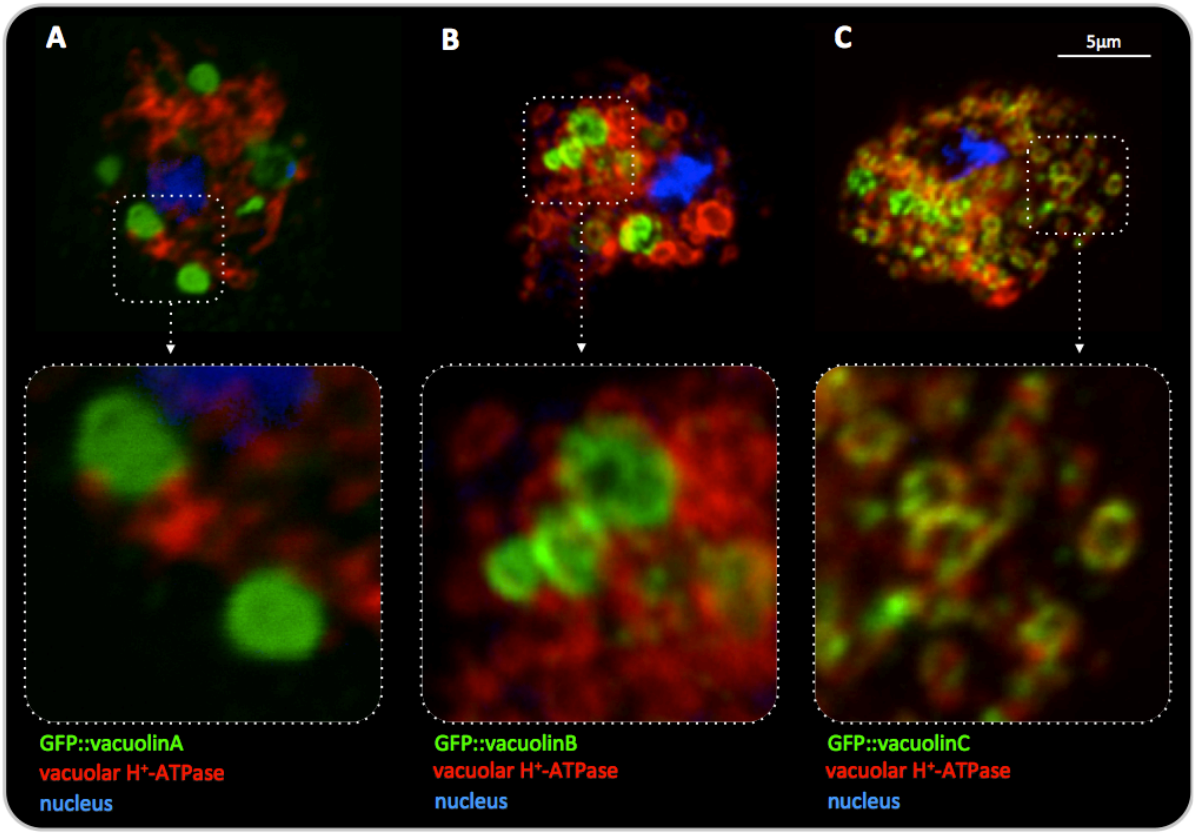

Figure 3-9: GFP::vacuolinA, B and C fusion proteins localized to endosomal vacuoles inside of axenic *D. discoideum*. Indirect immune fluorescence analysis of axenic *vacA*^{gfp} (**A**), *vacB*^{gfp} (**B**) and *vacC*^{gfp} (**C**) cells. Cells were fixed, permeabilized and incubated with monoclonal α-vatA (mouse) antibody. Red fluorescent α-mouse Alexa Fluor^{594} secondary antibody was used to visualize vatA, a subunit of the vacuolar H^+-ATPase type V. Double stranded DNA was visualized with DAPI.

3.2.2 Localization of overexpressed GFP::vacuolin fusion proteins in infected cell lines

So far, we observed that vacuolin isoforms were specifically regulated in *D. discoideum* host cells during the *M. marium* infection. To visualize vacuolin isoforms in the infection, *D. discoideum* vacA^{gfp}, vacB^{gfp} or vacC^{gfp} expressing cells were infected with red fluorescent *M. marinum::*msp12^{mCherry}, fixed and microscopically analyzed. At three hpi, GFP::vacuolinA fusion protein was not associated with *M. marinum*. As already shown in uninfected cells the protein was localized to endosomal membranes of vacuoles in the cytoplasma (fig. 3 -10: A). In addition to endosomal vacuoles about 50% of the examined bacteria were labeled with GFP::vacuolinB (fig. 3 -10: B&C).

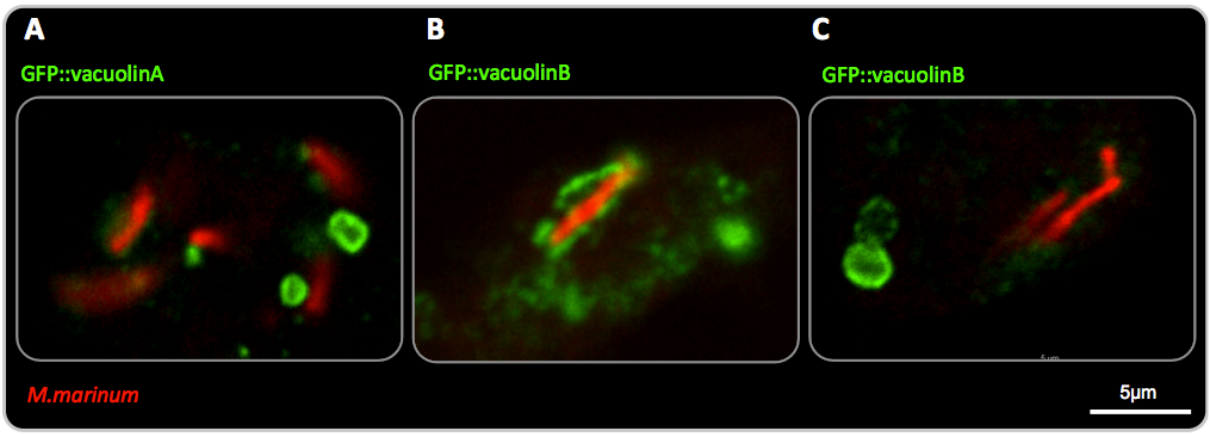

Figure 3-10: Isoform specific association behavior of GFP::vacuolinA and B fusion proteins with the *M. marinum* compartment. Confocal microscopy sections of fixed *M. marinum::*msp12^{mCherry} infected *vacA*^{gfp}(**A**) and *vacB*^{gfp} (**B** and **C**) cells at three hours post infection (hpi). While almost no association of GFP::vacuolinA with *M. marinum* vacuoles was found in *vacA*^{gfp}, about 50% of *M. marinum* containing vacuoles were decorated with GFP::VacuolinB in *vacB*^{gfp} samples.

Most importantly, in the *D. discoideum* vacC^{gfp} the majority of *M. marinum* compartments were decorated with the fusion protein (fig. 3 -11: A). At the same time the number of small vacuoles decorated with GFP::vacuolinC fusion protein was reduced. For the first time, endogenous GFP::vacuolinC fusion protein was shown to be localized at the mycobacterial compartment by confocal microscopic analysis on fixed *D. discoideum* wild type$^{KI\ vacC:gfp}$ cells infected with *M. marinum::*msp12^{mCherry}. 3D reconstruction of confocal images of the sector around the bacterial compartment demonstrated that endogenous vacuolinC localizes close to *M. marinum* in various shapes (fig. 3 -11: B). Here, the difference of the GFP signal intensity between the endogenous tagged protein and the overexpressed GFP-fusion protein became very obvious: While the target of vacuolinC, stayed the same, distribution of the signal changed from distinct structured domains decorating the bacteria in the *D. discoideum* wild type $^{KI\ vacC:gfp}$ strain (fig. 3-11: B) to a coat covering the entire bacteria in the overexpressing vacC^{gfp} cell line (fig. 3-11: A). A movie to emphasize these observations can be found in the supplemented material (CD1; movie #1 and #2).

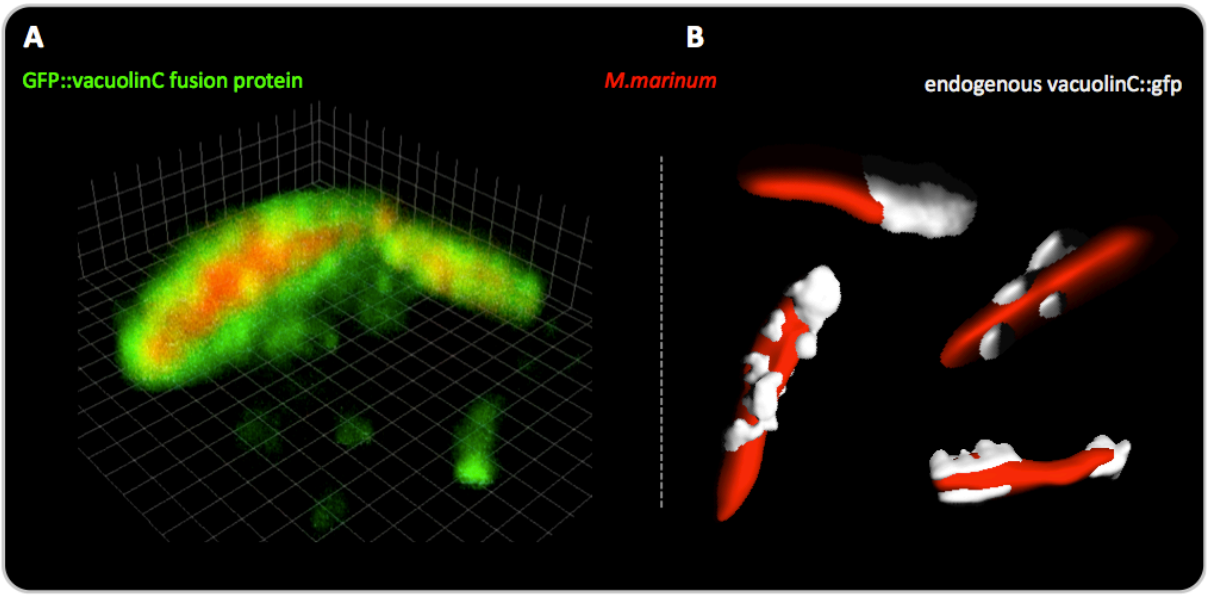

Figure 3-11: VacuolinC localized in close vicinity to *M. marinum* infected *D. discoideum*. (**A**) Episomally expressed GFP::vacuolinC fusion protein (green) accumulated at the *M. marinum::*msp12^{mCherry} (red) containing vacuole. Infected *vacC*^{gfp} were fixed three hours post infection (hpi) and prepared for microscopic analysis. Confocal images of several stacks through an infected cell were 3D reconstructed and the sector around the bacterial compartment cropped. (**B**) Wild type$^{KI\ vacC::gfp}$ was infected with *M. marinum::*msp12^{mCherry} (red). Three hpi infected cells were fixed, permeabilized and endogenous vacuolinC::GFP was labeled with α-GFP primary antibody (rabbit). α-rabbit Alexa Fluor^{488} secondary antibody was used to amplify endogenous GFP-signal. Confocal images of representative bacterial compartments were 3D reconstructed and vacuolinC::GFP was false-colored in light grey for easier detection.

3.2.3 Marker association at the mycobacterial compartment by immune fluorescence analysis

To substantiate these observations, association of GFP::vacuolin signal with the bacterial compartment was quantified in three biological samples (fig. 3-12). Therefore, *D. discoideum* knock out strains of vacuolin isoforms A, B and C were complemented with the corresponding overexpressed GFP-fusion protein, respectively, in order to minimize the functional background of the endogenous protein. Subsequently, cells were infected with *M. marinum*::msp:12^{mCherry}, fixed, stained at hourly intervals. Association of fusion protein with the *M. marinum* containing vacuole was microscopically analyzed. One late time point was included at 24 hpi. The GFP::vacuolinA localization followed a dynamic pattern. At the early onset of infection (at 30 minutes post infection) almost 60% of the bacterial compartments were associated with the GFP signal. This suggested a fast recruitment of vacuolinA in response to infection. This peak was followed by a quick drop and a stable association rate (20-30%) of GFP::vacuolinA with *M. marinum* was established from one to five hpi. At later time points (six and 24 hpi) an increase of association to 40% was counted, which is most likely due to the re-uptake of *M. marinum* (see 3.1.1.3). In contrast, the number of GFP::vacuolinB positive *M. marinum* compartments slowly rose over time. The percentage of *M. marinum* compartments decorated with GFP::vacuolinB increased in two steps, starting at 30 minutes post infection with 22%. A rate of 50% was

established from two to six hpi and the highest association rate of 85% was reached at a later stage of infection at 24 hpi.

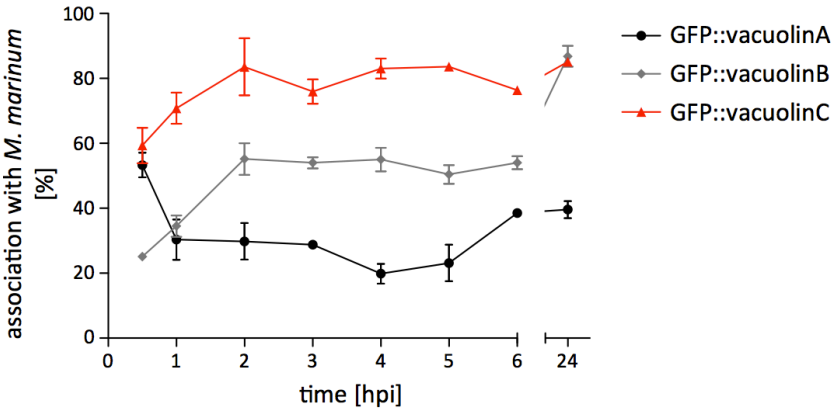

Figure 3-12: GFP::vacuolinC maintained very high association rates with *M. marinum* during the course of infection. *D. discoideum* vacA$^{KO+gfp:vacA}$, vacB$^{KO+gfp:vacB}$ and vacC$^{KO+gfp:vacC}$ were infected with *M. marinum::msp12*^{mCherry}. Samples were fixed and prepared for microscopic analysis on an hourly basis. The association of GFP::vacuolinA, B and C with one hundred *M. marinum* containing vacuoles was evaluated by microscopy for each time point and depicted with regard to time (hours post infection; hpi).

Association rates of *M. marinum* compartments and GFP::vacuolinC started with the highest number of all vacuolin isoforms with almost 60% reached at 30 minutes post infection. It steadily rose to its maximum above 80% at two hpi. This high level could be observed throughout the complete course of *M. marinum* infection (fig. 3-12).
In summary, localization pattern of each vacuolin isoform followed a distinct recruitment to *M. marinum* compartment. Especially in case of vacuolinB and C, increasing mRNA amounts in response to infection correlate with an association of vacuolin positive bacterial compartments. Thus, an isoform specific regulation in response to *M. marinum* infection was implemented.
Furthermore, results obtained with all cell lines hint towards a fundamental function of the vacuolinC protein during *D. discoideum* infection.

3.3 Functional studies of vacuolin knock out cell lines

To date vacuolinC did not receive much attention. However, its enhanced transcription upon *M. marinum* infection and its localization at the *M. marinum* compartment indicated that vacuolinC might be involved in host-pathogen interaction. Consequently, the question arises about its function. A common way to address this is to eliminate the coding region of the gene and expose the knock out cells to the situation of interest. *D. discoideum vacuolinA* and *vacuolinB* knock out strains (vacA^{KO} and vacB^{KO}) were produced in the laboratory of Markus Maniak and given to Dr. Monica Hagedorn in 2006. However, a *D. discoideum vacuolinC* knock out strain (vacC^{KO}) had to be generated.

3.3.1 Generation of a *D. discoideum vacuolinC* knock out mutant

In order to investigate the role of vacuolinC, a construct was designed to partially replace the *vacuolinC* gene locus by a resistance cassette for blasticidin (fig. 3-13 A). *D. discoideum* wild type cells were transfected with the knock out construct. The genomes of 30 to 50 sub clones per generation of transfected cells were screened before

two independent clones in the third generation were found to be positive for exact integration of *vacuolinC* knock out transgene (fig. 3-13 B).

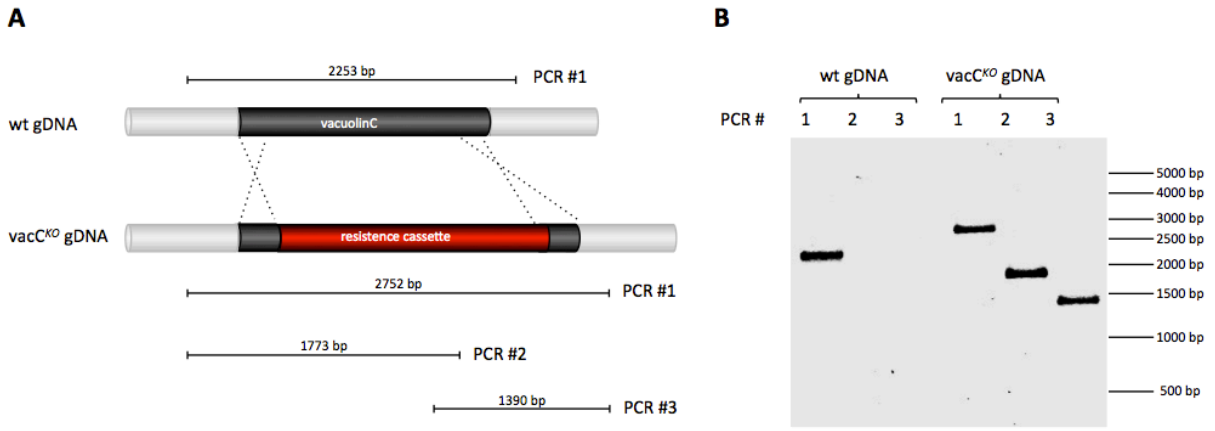

Figure 3-13: The *vacuolinC* knock out construct successfully integrated in the *D. discoideum* genome. (**A**) The majority of the endogenous *vacuolinC* coding sequence was replaced with a blasticidin resistance cassette. The knock out construct was created using StarGate® Cloning System. (**B**) Control PCR amplifications (PCR #1-3) with sub-clone gDNA templates analyzed by agarose gel electrophoresis provided proof for successful integration of the knock out construct and consequently the generation of a *D. discoideum vacuolinC* knock out strain (*vacC*^{KO}).

3.3.2 Characterizing *vacuolin* knock out mutants

The availability of all *vacuolin* single knock out strains allowed us to perform a thorough characterization under axenic and infection conditions.

3.3.2.1 Residual vacuolin transcription in *D. discoideum* knock out mutants

To find out if the lack of one vacuolin isoform had an impact on the mRNA amounts of the other two remaining vacuolins, mRNA of axenic cultured *D. discoideum* knock out cells was analyzed by multiplex TaqMan qPCR (fig. 3-14). The analysis revealed an enhanced *vacuolinA* mRNA presence in both, vacB^{KO} and vacC^{KO} (ΔCt mean value = approximately 500, respectively) in comparison to the mRNA level measured in *D. discoideum* wild type strain (ΔCt mean value = 290) (fig. 3-14: A). No difference of *vacuolinB* mRNA level was observed in vacA^{KO} and vacC^{KO} in comparison to wild type cells (fig. 3-14: B). Surprisingly, a heterogeneous picture was observed by analyzing the *vacuolinC* mRNA amount. In general, *vacuolinC* was only hardly detectable in axenic cultured *D. discoideum* and only a slightly higher *vacuolinC* level was measured in vacA^{KO}. In contrast, the lack of *vacuolinB* was accompanied by a complete reduction of *vacuolinC* mRNA (fig. 3-14: C). Subsequent PCR analysis using gDNA as templates uncovered that *vacuolinC* could not be amplified from vacB^{KO} gDNA (fig. 3-14: C, framed insert). In another sense, the combination of these findings implied that the vacB^{KO} mutant might not be a single *vacuolinB* knock out but a putative *vacuolinB* and *C* double knock out.

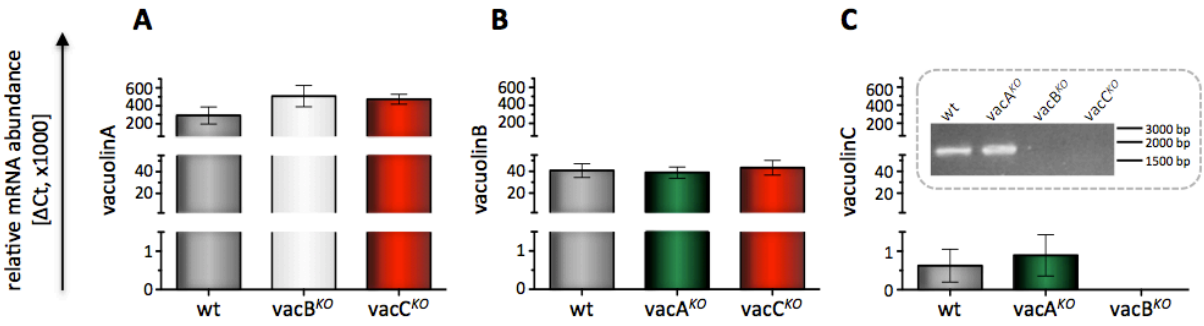

Figure 3-14: No *vacuolinC* mRNA expression in axenic *vacB^{KO}*. Multiplex TaqMan qPCR analysis of residual *vacuolin* mRNA abundance in *D. discoideum vacA^{KO}*, vacB^{KO} and vacC^{KO} mutants. Total RNA was isolated and mRNA revers transcribed. cDNA was then used as template for qPCR amplification. ΔCt values of vacuolin isoforms were calculated in reference to the housekeeping gene *gapdh* and mean values ± standard deviation was depicted. (**A**) Elevated *vacuolinA* mRNA abundance in both, vacB^{KO} (light grey) and vacC^{KO} (red) mutants in comparison to mRNA level measured in wild type (grey) cells. (**B**) Similar *vacuolinB* mRNA level in wild type (dark grey), vacA^{KO} (green) and vacC^{KO} (red). (**C**) *VacuolinC* mRNA abundance in wild type (dark grey) and vacA^{KO} (green) was very low in general with rather high natural fluctuation. No *vacuolinC* mRNA was detected in vacB^{KO}. PCR analysis of gDNA uncovered that *vacuolinC* could not be amplified from vacB^{KO} mutants.

3.3.2.2 Growth: vacB^{KO} cells show an increased proliferation rate

The cell division cycle of *D. discoideum* takes about eight to twelve hours [6]. To measure the growth rate of the single *vacuolin* knock out strains, the proliferation under axenic culture conditions was followed over time. The same number of log-phase cells were initially seeded and cultured for 48 hours. In regular intervals samples were harvested and counted using a Neubauer counting chamber. Under these conditions wild type division rates were 14 hours. The lack of *vacuolinA* did not influence the proliferation of the cells in comparison to the wild-type strain (fig. 3-15: A). In contrast, the disruption of *vacuolinB* led to an enhanced cell division rate of 10.7 hours. Within 19 hours vacB^{KO} reached significantly higher cell numbers. This discrepancy to wild type cell division rates was then maintained (24 – 48 h). VacC^{KO} cells also exhibited an accelerated cell division cycle (12.17 h) in comparison to wild type cells but not in the same dimension as seen for vacB^{KO} cells.

3.3.2.3 Phagocytosis

To get a broad overview about phagocytosis behavior of all *vacuolin* knock out strains an uptake assay was performed using green fluorescence latex beads. The fluorescent signal of the beads allowed quantification of uptake rates via FACS analysis. Wild type cells that internalized beads reached steady state level after 60 minutes meaning that almost all amoeba cells had phagocytized beads (fig. 3-15: B). In contrast, the slope, which represented uptake ability of *D. discoideum* vacuolin knock out strains, revealed a delay of internalizing particles for all three mutant strains compared to wild type. Most similar to wild type uptake was the phagocytosis behaviour of vacA^{KO}, reaching equilibrium at 60 minutes. A small delay of 20 minutes was measured for vacB^{KO} before equilibrium state was reached.

Interestingly, the lack of *vacuolinC* led to the most constant deceleration of uptake rate. Steady state level was achieved with a delay of 30 minutes compared to the wild type cells. Since this state reflects an equilibrium of endo- and exocytosis it could be

concluded that the loss of *vacuolinC* resulted in a phagocytic delay or a speed up in exocytosis. FACS analysis was methodically limited to solely measure beads uptake via fluorescence signal. Thus, no conclusions could be drawn about possible defects in regard to subsequent intracellular phagosomal maturation.

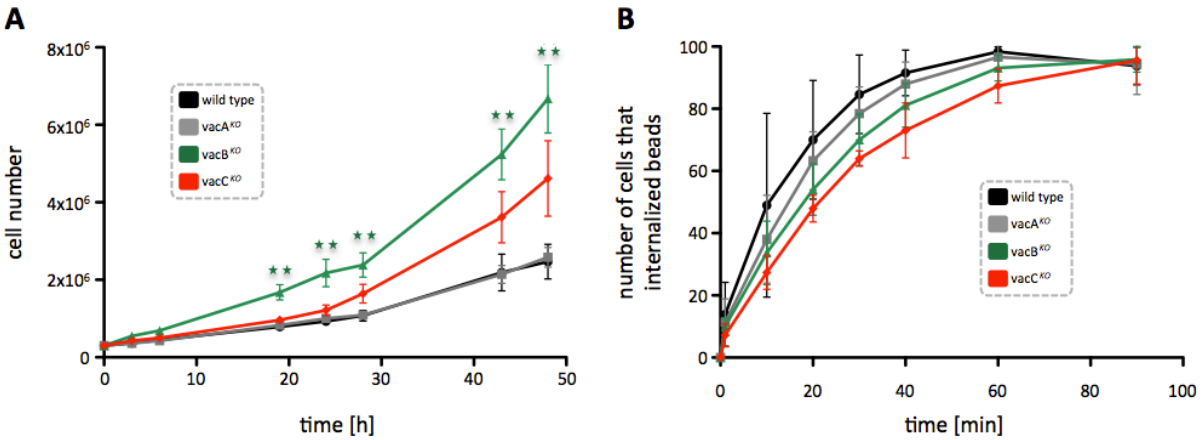

Figure 3-15: Escalated cell division in *vacB^{KO}* compared to *D. discoideum* wild type. (**A**) Proliferation of wild type, *vacA^{KO}*, *vacB^{KO}* and *vacC^{KO}* was followed for 48 hours. Samples of axenic growing strains were counted in regular intervals and are figuratively represented on a time scale (x-axis; h = hour; mean value ± standard deviation). Statistics were performed using the unpaired two-tailed t-test with a confidence interval of 95% in reference to the wild type control, n = 5-8, **p ≤ 0.01. (**B**) *VacA^{KO}*, *vacB^{KO}* and *vacC^{KO}* show a decrease in speed of ingestion of green fluorescent latex beads. VacC^{KO} reached steady state level with a delay of 30 minutes compared to the wild type. Samples were FACS analyzed and cells that internalized beads were depicted on a time scale in minutes. Data was normalized using: X = X/K; K = X, n=3-6.

In nature, *D. discoideum* survives by feeding on microbes. To monitor if the lack of any single vacuolin isoform had an impact on growth and phagocytosis in *D. discoideum*, vacuolin knock out mutants were placed on a lawn of heat-killed *Klebsiella* bacteria. With bacteria as the sole nutrient source *D. discoideum* vacuolin knock out mutants were challenged in both phagocytosis and growth at the same time. *Klebsiella bacteria* were successfully killed and digested by the amoeba, as visualized by clear plaques corresponding to zones where actively feeding and replicating amoebae have phagocytized bacteria (fig. 3-16). Plaques started appearing approximately two days after plating the diameter of growing *D. discoideum* plaques were measured daily (Figure 3-16: A). The lack of *vacuolinA* resulted in an indistinguishable growth and phagocytosis of these cells from the wild type strain. In accordance with the previously determined growth rate, the lack of vauolinB resulted in a faster proliferation and phagocytosis of vacB^{KO} on *Klebsiella* at each time point analyzed. This trend became obvious in the beginning of the experiment and was observable throughout its duration. A very small inhibition emerged in the plaque sizes of vacuolinC deficient cells, however the difference was not significant.

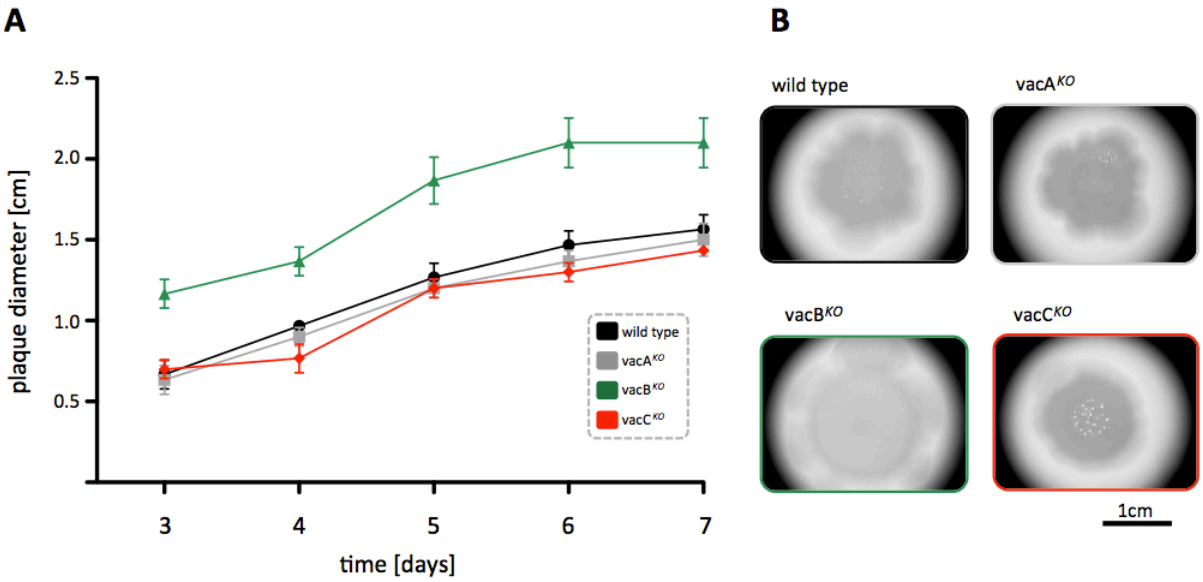

Figure 3-16: Increased plaque formation of *vacB*^{KO} on *Klebsiella* lawn. Plaques of wild type, *vacA*^{KO}, vacB^{KO} and vacC^{KO} on *Klebsiella* were surveyed from day 3 to day 7. (**A**) Feeding on Klebsiella, vacB^{KO} divided at a higher rate than wild type cells. The lead was maintained over several days. (**B**) Plaque diameter of wild type, *vacA*^{KO}, vacB^{KO} and vacC^{KO} were imaged after 7 days. Plaque and feeding zone were enlarged compared to the other cell lines.

In summary, vacB^{KO} and vacC^{KO} showed the strongest phenotype in respect to phagocytosis and growth while vacA^{KO} was rather not distinguishable from wild type. In contrast, an increased growth rate of vacB^{KO} could be observed in axenic culture and on *Klebsiella* lawn although the cells were slightly impaired in phagocytosis. In reference to the measured phagocytosis of latex beads, a phagocytic delay in the vacC^{KO} was detected, which could play a role in the slightly impaired growth on *Klebsiella*.

3.3.2.4 Development: vacB^{KO} impaired in aggregation

Having established the conditions for a simultaneous development, the development of all vacuolin single knock out strains was compared to the *D. discoideum* wild type.

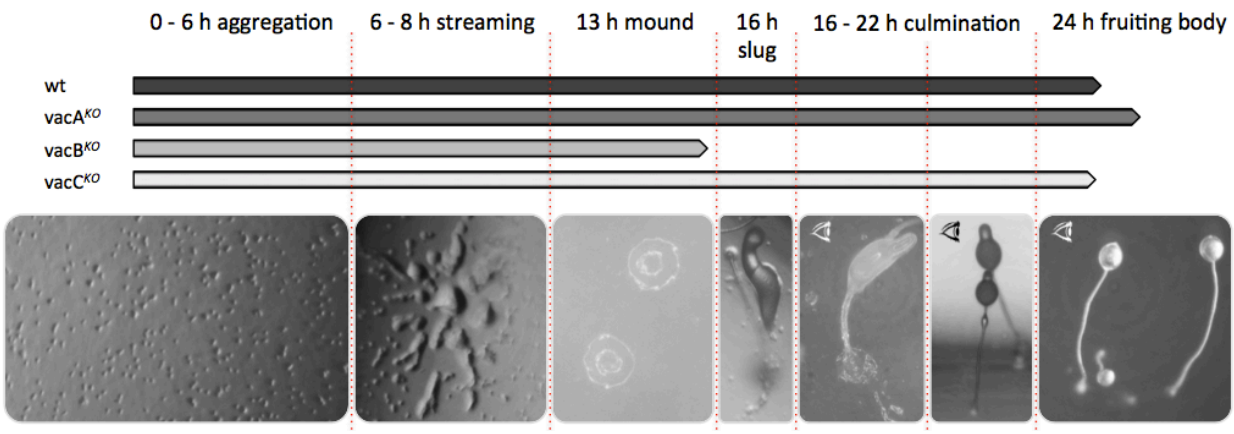

Figure 3-17: **Impaired development of *vacB*^{KO} challenged with an abrupt stop of nutrient supply.** The development process induced by withdrawal of nutrient source was not affected in vacA^{KO} and vacC^{KO}. Such as the wild type, vacA^{KO} and vacC^{KO} went through all developmental stages following the expected time frame. In contrast, vacB^{KO} only reached mound stage at 24 hours.

First, cell lines were analyzed in terms of their ability to develop and second time frames of different development stages were compared. All three *D. discoideum*, vacuolin knock out strains were able to complete the development cycle and to produce fertile spores (data not shown). In terms of stages and timing no differences to the wild type were observed for vacA^{KO} and vacC^{KO}. The lack of *vacuolinB* led to an impaired development (fig. 3-17).
Already during the first stage of development the vacB^{KO} mutant was affected in its ability to stream. With a delay of twelve hours cells managed to assemble and started to form a slug, which exhibited reduced motility. When *vacuolinB* deficient cells assembled to the slug a point of no return was reached and the multicellular organism was able to finish development without further disturbances. Thus, with a twelve-hour delay the rest of the program followed all the way through development until spores were produced. Taken together, vacB^{KO} mutants finished the developmental cycle almost in twice the time compared to wild type cells (fig. 3-17).

3.3.3 Characterizing *vacuolin* knock out mutants in the *M. marinum – D. discoideum* infection model

3.3.3.1 Vacuolins potential for functional compensation of other isoforms

Having analyzed *D. discoideum* vacuolin knock cell lines under the aspects of growth, phagocytosis and development, the mutants were analyzed challenged with *M. marinum* exposure. Firstly, *D. discoideum* vacuolin knock out mutants and a wild type control were infected and *vacuolin* mRNA expression was measured via multiplex TaqMan qPCR at two hpi. Since mRNA expression of respective *vacuolin* isoforms underwent rather small-scale changes when comparing the wild type control and the knock out mutants the samples were diagrammed in one graph to emphasize compensation tendencies (fig. 3-18). In vacA^{KO}, *vacuolinB* mRNA was increased under non-infection conditions in comparison to wild type levels as ΔCt mean value changed from 68 to 104 (fig. 3-18: A). In addition to that, a further increase was measured in response to *M. marinum* leading to the highest ΔCt mean value of 243. At the same time approximately half of the *vacuolinC* mRNA amount was in the mock control and the infection samples compared to *D. discoideum* wild type cells (fig. 3-18: A).
In vacB^{KO} the remaining *vacuolin* isoforms showed an unexpected expression pattern upon infection. As previously determined (fig. 3-14), the *vacuolinA* mRNA abundance in general appeared to be higher in this mutant cells, but in contrast to *M. marinum* infected wild type cells, the bacterial exposure did not lead to a further increase of *vacuolinA* mRNA production. To repeat, no *vacuolinC* expression was detected in *M. marinum* infected as well as mock treated vacB^{KO} (fig. 3-18: B).
In vacC^{KO} cells the mRNA analysis showed an increase of *vacuolinA* already in the mock control confirming data of the axenic cultured sample with a ΔCt mean value of 263 (fig. 3-14: A). On top, an additional increase to a ΔCt mean value of 500 was monitored under infection conditions (fig. 3-18: C). The mRNA level of *vacuolinB* increased in response to

the mycobacterial infection, here the amount reached higher levels in vacC^{KO} (ΔCt mean value = 325) compared to *D. discoideum* wild type (ΔCt mean value = 201).

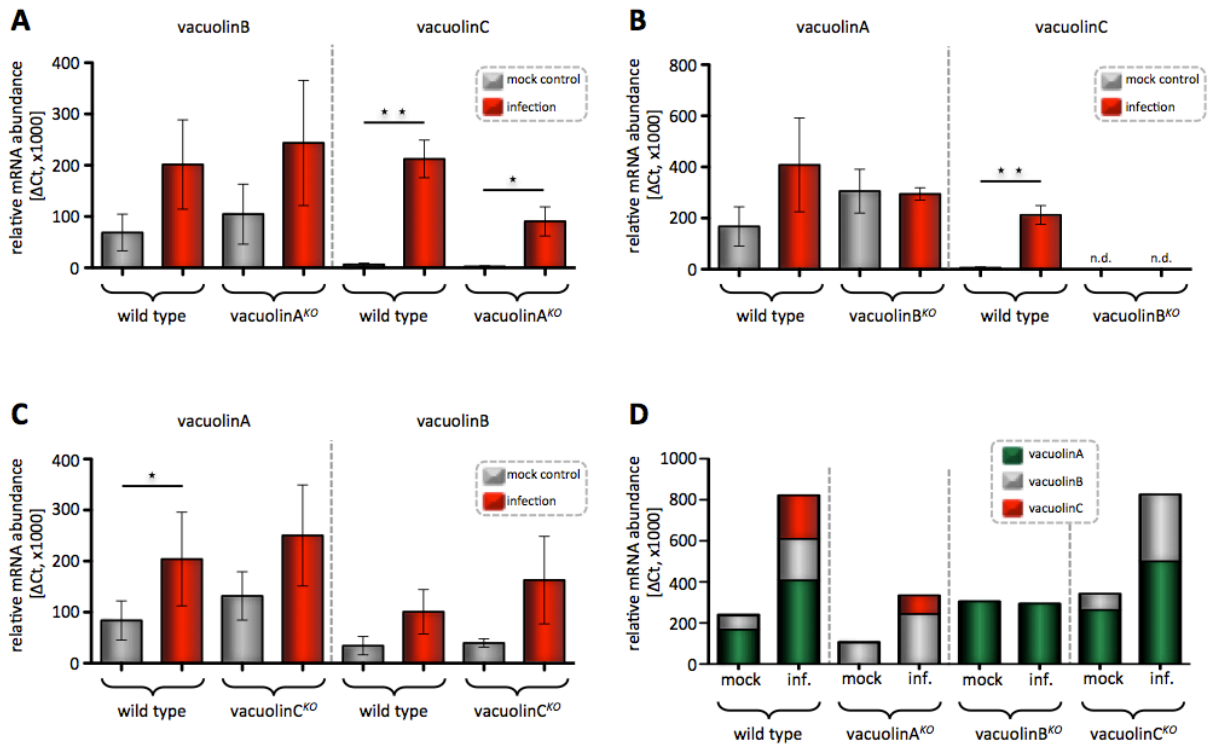

Figure 3-18: Loss of *vacuolinC* led to elevated mRNA levels of residual isoforms *vacuolinA* and B in *vacC^{KO}*. Multiplex TaqMan qPCR analysis of residual *vacuolin* transcription of *M. marinum* infected (red) and mock treated (grey) *D. discoideum* wild type, *vacA^{KO}*, vacB^{KO} and vacC^{KO} mutants two hours post infection (hpi). ΔCt values of vacuolin isoforms were calculated in reference to the housekeeping gene *gapdh* and mean values ± standard deviation were depicted. To simplify comparison to wild type, results of wild type analysis and vacuolin^{KO} were portrayed next to each other. (**A**) Analysis of *vacA^{KO}* revealed elevated *vacuolinB* mRNA abundance in both, mock treated and infected samples in comparison to mRNA level measured in wild type samples. The increase of *vacuolinC* mRNA expression answering the *M. marinum* infection was not as high as seen in infected wild type samples but was still statistically significant compared to mock control. No significant change was calculated comparing infected wild type and infected vacA^{KO} (**B**) Residual *vacuolinA* mRNA abundance in *vacB^{KO}* was already boosted in non-infected cells. Infection with *M. marinum* did not lead to an additional elevation of mRNA. *VacuolinC* mRNA was beneath detection limit in mock treated and infected *vacB^{KO}* samples (not detectable). (**C**) *VacuolinA* and *B* mRNA abundance in both mock treated and infected samples in comparison to mRNA level measured in wild type were elevated in *vacC^{KO}*. Statistics were performed using the unpaired two-tailed t-test with a confidence interval of 95% in reference to the wild type control, n = 3-4, **p = 0.0011, *p = 0.0361. (**D**) Total vacuolin abundance and isoform composition based on ΔCt values. *VacuolinA* mRNA is depicted in green, *vacuolinB* mRNA in grey and *vacuolinC* mRNA in red.

It seems that compensation by vacuolinA via elevated transcription rates already took place in axenic culture while the regulation of *vacuolinB* was initiated by *M. marinum* infection. Wild type multiplex TaqMan qPCR analysis revealed that in response to *M. marinum* infection on the one hand total vacuolin mRNA level increased by the factor of 3.4 and on the other the vacuolin composition was altered (fig. 3-18: D). Especially concerning *vacuolinC*, that made 1.5% of total vacuolin in mock treated samples comprised 25% of total vacuolin abundance in infected wild type. No major changes of total vacuolin abundance were detected in vacA^{KO} and vacB^{KO} while a similar increase occurred in vacC^{KO}.

3.3.3.2 Association of the markers vatA and p80 with the mycobacterial compartment in *vacuolin* knock out cell lines

Most likely, membrane composition at the mycobacterial compartment influences the course of infection. So far, data imply that vacuolin composition at the bacterial compartment appeared very dynamic during early phase of infection in which the phagosome was remodeled and a bacterial niche was established. In order to determine if the loss of particular vacuolin isoforms might influence compositional changes of the compartment localization profiles of two vacuole markers, vatA and p80, were created. *M. marinum* infected *D. discoideum* wild type and vacuolin knock out cells were fixed and immunolabeled. For each time point a minimum of one hundred bacterial compartments were monitored by fluorescence microscopy and percentage of association with the respective marker was calculated. Association of vatA with the bacterial compartment was clearly visible by a coat of vatA surrounding the mycobacterial compartment (fig. 3-19: A). No association could easily be distinguished as shown in figure 3-19: B.

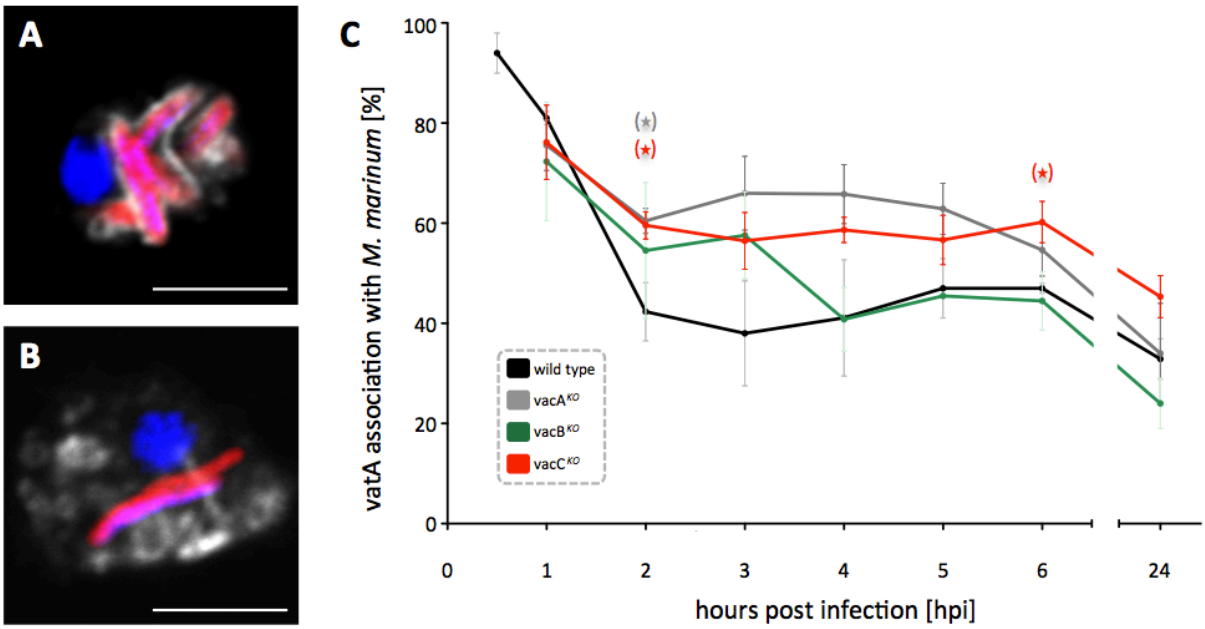

Figure 3-19: Moderate increase of vatA localization at *M. marinum* compartment in *vac*^{KO} mutants. Wild type, *vacA*^{KO}, vacB^{KO} and vacC^{KO} were infected with *M. marinum::*msp12^{mCherry}. (**A**) Example of mycobacterial compartment that was classified positive for vatA association. (**B**) Example of mycobacterial compartment that was classified negative for vatA association. (**C**) The association with one hundred *M. marinum* containing vacuoles was then evaluated by microscopy for each time point and depicted with regard to time (hours post infection; hpi). Hourly samples (one to six and 24 hours) were fixed, permeabilized and incubated with monoclonal α-vatA (mouse) antibody. Green fluorescent α-mouse Alexa Fluor^{488} secondary antibody was used to visualize vatA, a subunit of the H^+-ATPase type V. Double stranded DNA was visualized with DAPI. Bars = 5 µm

In *M. marinum* infected wild type *D. discoideum*, association profiles of vatA could be divided into three stages: The first stage, lasting from beginning of infection until two hpi, was characterized by a constant drop of vatA association with the bacterial compartment. Immediately after phagocytosis of *M. marinum* 95% of bacterial compartments were associated with vatA (fig. 3-19: C). Within two hours association rates dropped down to 40% marking the beginning of the second stage, the plateau-stage. During this stage a balance between association and de-association was maintained and association of vatA and the bacterial compartment was stable at a rate

of 42%. The plateau-stage lasted from two to six hpi. The third stage (24 hpi) was characterized by an association rate of vatA with the bacterial compartment below 40% vatA (fig. 3-19: C).

Examination of *M. marium* infected vacuolin knock out mutants showed similar patterns. However, especially from two to six hpi, small differences of the association level were observed. Due to rather large distribution of determined values no statistical analysis could be applied. If, in spite a t-test was performed, a siginifanct increase of vatA associaction was measured a few cases, marked in brackets in figure 3-19: C. In case of vacA^{KO} the course of infection was characterized by a higher association rate of the bacterial compartment with vatA. For example vatA association rate of 58% during plateau stage was 16% higher than in infected wild type. In contrast, vatA association course of infected vacB^{KO} revealed similarities to the results obtained with wild type cells. The only differences were noticed at 2 and 3 hpi when more vatA association was calculated, approximately 10 to 15%. Although no strong phenotype was observed in infected vacC^{KO} the difference to the wild type control was the highest in all *D. discoideum* vacuolin knock out mutants. Association of vatA with the bacterial compartment was constantly at a rate above 60% in the first five hours of infection. In summary, the loss of any vacuolin isoform in *D. discoideum* led to a deceleration of vatA removal at the mycobacterial compartment (fig. 3-19: C).

The transmembrane protein p80 is described to be part of the mycobacterial compartment membrane composition [82].

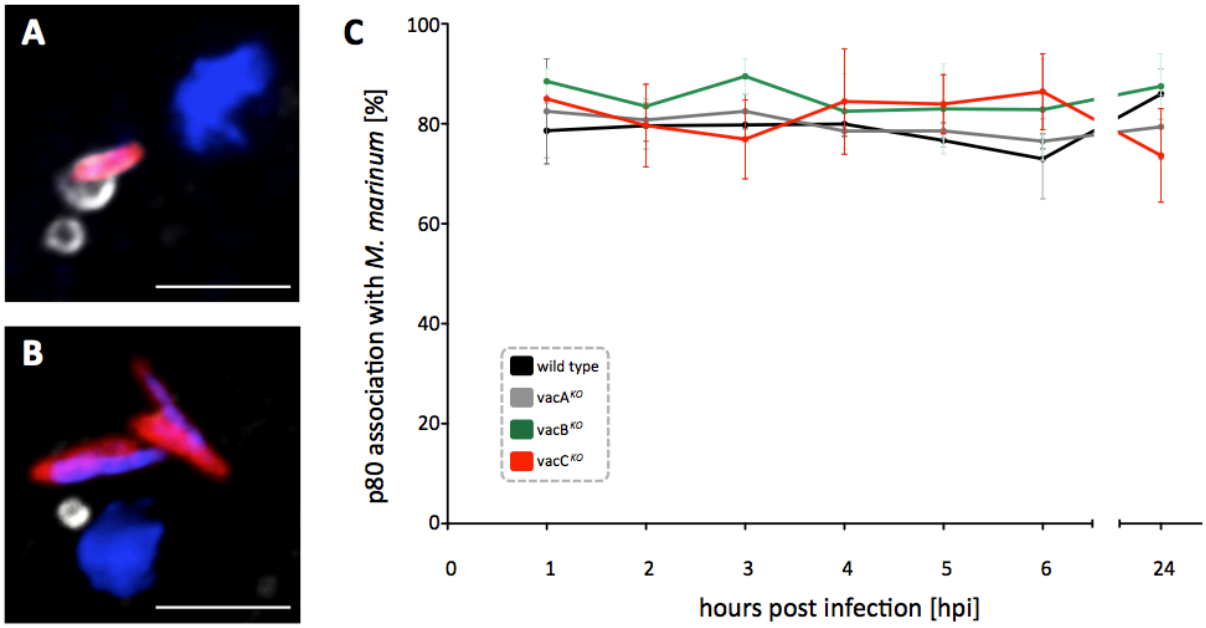

Figure 3-20: Single knock out of vacuolin isoforms had no influence on p80s presence at the *M. marinum* compartment. Wild type, *vacA*^{KO}, vacB^{KO} and vacC^{KO} cell lines were infected with *M. marinum*::msp12^{mCherry}. (**A**) Representative example of mycobacterial compartment that was classified positive for p80 association. (**B**) Representative example of mycobacterial compartment that was classified negative for p80 association. (**C**) The association with one hundred *M. marinum* containing vacuoles was then evaluated by microscopy for each time point and depicted with regard to time (hours post infection; hpi). Hourly samples (one to six and 24 hours) were fixed, permeabilized and incubated with monoclonal α-p80 (mouse) antibody. Green fluorescent α-mouse Alexa Fluor^{488} secondary antibody was used to visualize p80, a putative copper transporter. Bars = 5.5 µm

Based on amino acid homology the host factor p80 is predicted to transport copper out of the mycobacterial compartment. Similar to vatA the association of the mycobacterial compartment with p80 was easy to detect by a strong signal surrounding the bacteria. Examples for p80 associated with *M. marinum* or not are shown in figure 3-20: A&B.
Examination of *D. discoideum* wild type control revealed a strong presence of p80 at the mycobacterial compartment, which was maintained during all analyzed stages (fig. 3-20: C). The marker protein was permanently associated with the mycobacterial compartment at a rate around 80%. The same patterns were observed for all analyzed *D. discoideum* vacuolin^{KO} mutants (fig. 3-20: C). This data set implied that lacking vacuolin genes did not affect the presence of p80 at the bacterial compartment throughout the *M. marinum* infection.

3.3.3.3 Role of vacuolin in regard to *M. marinum* proliferation in *D. discoideum*

So far, questions remained about the function of vacuolin isoforms during *M. marinum* infection. For example, it is still unknown if vacuolin isoforms attached closely to the bacterial compartment were part of the host defense machinery. Alternatively, invaded bacteria could be responsible for vacuolin recruitment and accumulation at the membrane of the replication compartment. One option to gain information about the role of vacuolins was to measure the proliferation of bacteria in respective *D. discoideum* vacuolin knock out mutants. This was done via a cfu (colony forming unit) assay in which mycobacteria were isolated from infected cells at regularly time points, plated on agar and originated colonies were counted. In contrast to microscopic analysis, which cannot distinguish between live and dead cells, the cfu approach estimated viable cells only by quantifying colonies derived from a single progenitor. However, because *Mycobacteria* tend to form aggregates, which were hard to separate, the method was accompanied by a tendency to underestimate bacterial numbers. Nevertheless, this approach was assumed to provide insight into successful bacterial proliferation during the course of infection.
In wild type *D. discoideum,* intracellular *M. marinum* seem to proliferate very slowly, or rather, the majority of *M. marinum* bacteria seemed to persist (fig. 3-21). If, figuratively, the infection started with one bacterium in the first instance (bacterial load of 1 at three hpi), until 24 hpi the host seemed to be able reduce the bacterial load by 20%. At later time points, from 24 hpi to 32 hpi infection recovered reaching a final bacterial load of 1.2, which seemed to present a balance between bacterial proliferation and host defense mechanisms, because this value was kept till the end of the experiment at 48 hours. Interestingly, in all *D. discoideum* vacuolin knock out mutants a small increase of the bacterial load from 1 at three hpi to 1.25 six hpi was monitored. However, this observation was not significant and mycobacterial proliferation in vacA^{KO} and vacC^{KO} cell lines did not show a difference to *D. discoideum* wild type during the whole time course of the experiment (fig. 3-21). In contrast, vacB^{KO} host cells showed an advanced *M. marinum* proliferation. Already during the first phase of infection the infection of the bacteria were more successful in terms of resistance to host defense mechanisms or establishing a replication niche. This was shown by the bacteria load value, which only dropped from 1.25 to 1.1. Subsequent bacterial division was highly increased compared

to wild type cells and finally reached an increase by the factor of 2.2 at 48 hpi. Accordingly, conditions for bacterial survival and proliferation appeared to be changed in favor of the invaded pathogen. The number of experimental replications allowed a statistical analysis, which resulted in a significant difference comparing vacB^{KO} with *D. discoideum* wild type cells at 48 hpi.

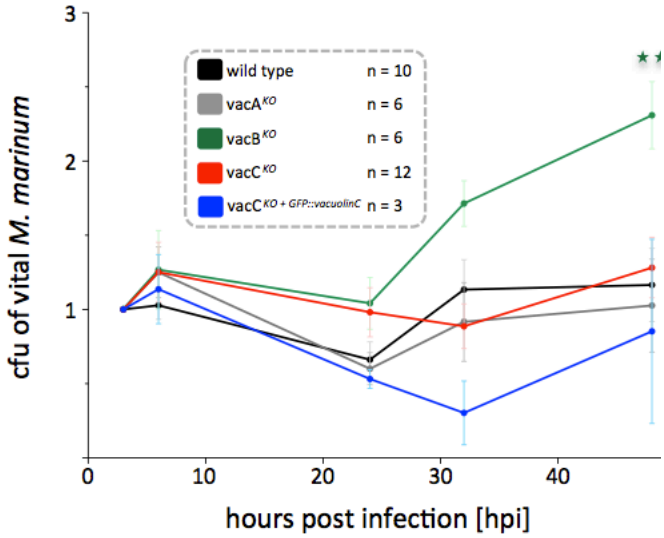

Figure 3-21: Impaired *vacB*^{KO} defense against *M. marinum* infection. Monitoring long-term infections enabled an insight of mycobacterial proliferation in *D. discoideum* host cells. *M. marinum* recovered from infected wild type, *vacA*^{KO}, vacB^{KO}, vacC^{KO} and vacC$^{KO+GFP::vacuolinC}$ were plated in four-log dilution to evaluate the number of intracellular bacteria via counting colony forming units (cfu). To simplify comparison between *D. discoideum* strains, differences of initial infection rates were compensated by normalizing all values using: X = X/K; K = X (three hours post infection; hpi). Statistical analysis using the unpaired two-tailed t-test with a confidence interval of 95% in reference to the wild type control, n = 3 - 12, **p = 0.0074

Although, knock out of *vacuolinC* in the *D. discoideum* host did not lead to a strong impact on the course of *M. marinum* infection, complementation of the vacC^{KO} cell line by overexpression of GFP::vacuolinC seemed to elongate the initial defense success of the host. This was shown by suppressed bacterial proliferation for 32 hours, which was eight hours longer than in vacB^{KO}. Nevertheless, subsequent bacterial proliferation recovered ending in a bacterial load of 1 at 48 hpi, which in total equals persistence.

3.4 Identification of interaction partners

3.4.1 Vacuolin isoforms form heterogenic oligomers

In silico analysis of the vacuolin family members predicted a coiled-coiled region (CC-domain) at the C-terminus that facilitates protein assembly. It was further predicted that several vacuolins form a protein complex that is tightly attached at the cytosolic side of vacuole membranes [207]. Moreover, these complexes could provide a platform for interaction with other proteins by forming membrane micro domains, which could regulate fusion events and signaling pathways. To investigate if vacuolins facilitate protein-protein interactions, an immunoprecipitation was performed. For this assay *D. discoideum* vacuolin knock out mutants were transfected with GFP::vacuolin fusion proteins of respective isoforms. Two samples, axenic growing cells and *M. marinum* infected cells at two hpi, were comparatively analyzed for each vacuolin knock out cell line. From cell lysates GFP::vacuolin fusion proteins were pulled out together with their attached proteins. Subsequently, the protein complexes were separated by SDS PAGE, and an immunoblot analysis was performed using an anti-vacuolin antibody (fig. 3-22).

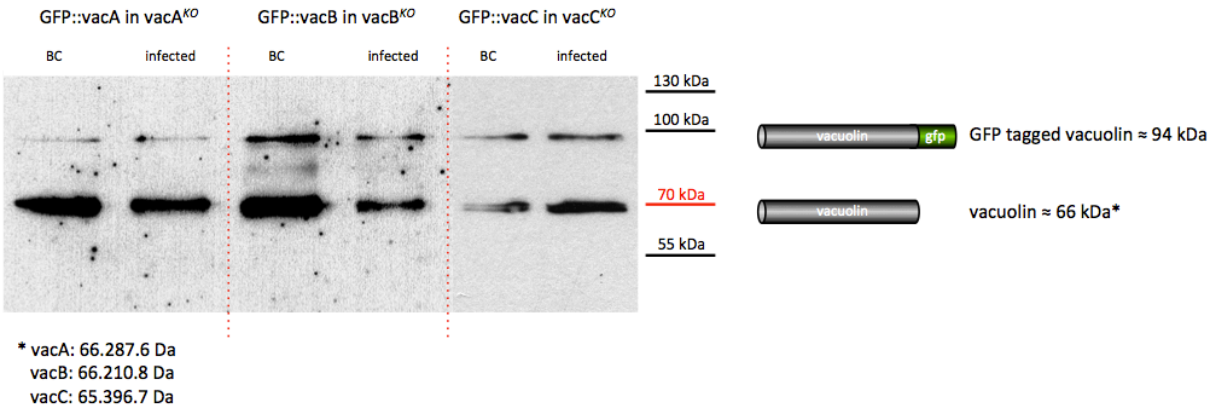

Figure 3-22: VacuolinA, B and C assembled to heterogenic oligomers. Proteins bound to GFP::vacuolin fusion proteins were separated by SDS page and analyzed by immunoblot analysis using α-vacuolin primary antibody. Since pulled out GFP-tagged fusion proteins (approx. 94 kDa) were expressed extra-chromosomal in respective *vacuolin* knock out cells, signals detected from proteins underneath the 70 kDa marker most likely originated from residual vacuolin isoforms.

For each sample two signals were detected. The weaker signal had the size of GFP::vacuolin fusion proteins, the other one seemed to result from the two remaining endogenous vacuolin isoforms. Accordingly, since GFP::vacuolin fusion proteins were expressed in the respective *D. discoideum* vacuolin mutant, this indicated that vacuolin isoforms assembled to heteromeric oligomers under axenic culture condition as well as during *M. marinum* infection. Without further mass spectrometry analysis no assumption could be made about the ratio or composition of vacuolin complexes or post-translational modifications. However, this tool is now ready to use and provides the possibility to find out about vacuolin interaction partners in general and upon *M. marinum* infection.

4 Discussion

In order to identify molecules involved in host defense mechanisms, a broad hypothesis driven screening approach for transcriptional changes was applied to *M. marinum* infected *D. discoideum*. Accordingly, the most strongly up-regulated *vacuolin* gene-family was chosen for a detailed analysis in the *D. discoideum – M. marinum* model system. Genetic, cell biological, biochemical and microscopic methods were applied to dissect the role of vacuolin in several life cycle stages, uptake of various bacteria as well as during infection of *D. discoideum* with pathogens, in particular *M. marinum*, a close relative of *M. tuberculosis* [184].

4.1 Transcriptional changes of putative *D. discoideum* innate immunity genes in response to the *M. marinum* infection

Two quantitative real time PCR systems, based either on SYBR Green accumulation in double-strand DNA or on sequence-specific binding of fluorescent TaqMan probes, were established and used to detect *D. discoideum* transcription changes in response to *M. marinum* infection. The SYBR Green system was chosen to screen 34 potential candidate-genes for quantitative mRNA changes induced in the *D. discoideum – M. marinum model*, due to its reduced assay setup and running costs. The relative expression analysis of qPCR data requires at least one reference gene with a stable expression during experimental setups. Thus, five housekeeping genes often used in *D. discoideum* qPCR analysis were validated for the *D. discoideum – M. marinum* infection model, but only *glyceraldehyde 3-phosphate dehydrogenase* (*gapdh*) fulfilled the criteria of an unchanged mRNA amount during infection of *D. discoideum*. The combination of *gapdh* cDNA amplification with amplification of cDNA of the different target genes allowed qPCR assays to monitor transcriptional changes upon *D. discoideum* infection. Since increasing numbers of extracellular bacteria and thus successive reuptake can result in an asynchronous course of infection at three to five hours post infection (hpi), early time points were chosen for qPCR analysis. Several genes that were transcriptionally altered and thus possibly involved in the innate immune response were identified via qPCR screening. Due to the time frame of this study, not all findings could be pursued. However, to emphasize possibilities now available with the new qPCR system the most promising hits are briefly discussed in the following section.

The *natural resistance-associated macrophage protein 1* (*nramp1*) mRNA level was down-regulated in *M. marinum* infected *Dictyostelium* cells. Nramp1, a proton-driven metal ion transporter and its mammalian orthologue, conferred susceptibility to infection of invasive bacteria such as *M. bovis, M. avium, S. thyphimurium* and *L. pneumophila* as well as the protozoan *Leishmania donovani* [14, 75, 77, 141, 198, 219]. Although the exact mechanism of resistance is currently unknown nramp1 localizes exclusively to

phagosomes or macropinosomes in *Dictyostelium* and macrophages. *D. discoideum nramp1* mRNA was up-regulated upon incubation with pathogenic bacteria and down-regulated upon [75, 140, 141]. Appelberg *et al.* suggested that nramp1 could kill *M. avium* by inducing the production of toxic reactive oxygen species [75]. However, more recently Bozzaro *et al.* proposed that iron was possibly gained for the host cell by degradation of ingested bacteria and efflux via nramp1 from phagosomes to the cytosol [21]. Interestingly, the inactivation of *nramp1* in *Dictyostelium* increased sensitivity to *L. pneumophila* and *M. avium* infection, followed by increased pathogen proliferation rates [141]. Availability of iron is essential for all cells, including *Mycobacteria* [168]. Potentially, reduced levels of nramp1 in infected host cells could favor bacterial proliferation and, moreover, might be induced by the pathogen. In contrast, depletion of iron from the phagosome by nramp1 could also be a host defense strategy to restrict the pathogens iron supply. Iron can be passaged through phagosomal membranes via nramp1. Potential changing directions of the transport and its manipulation due to two-sided function of nramp1 remain to be investigated. Fritsche *et al.* showed in murine macrophages that nramp1 stimulated the expression of the peptide lipocalin2 [66]. Functionally, the cascade started with an increased production of reactive oxygen species, which was mediated via nramp1. That stimulated NF-κB activity and subsequently enhanced *lipocalin2* transcription. Indeed, another gene whose mRNA production was strongly affected by down regulation during *M. marinum* infection of *D. discoideum* was *lipocalin2*. Holmes *et al.* showed that lipocalin2 contributed to antimicrobial activity by scavenging soluble siderophores produced by *Mycobacteria* resulting in inhibition of *M. tuberculosis* growth [88]. In addition increased lipocalin2 levels led to a significant suppression of *Salmonella* growth [66]. However, if down regulation of both, *lipocalin2* and *nramp1* were coincidental or due to *M. marinum* manipulation of solely *nramp1*, was not further addressed in this study.

A broad feedback to the *M. marinum* infection was found in elevated mRNA levels of various investigated candidate-genes. For example, two *D. discoideum* genes, *tirA* and *tirC*, both coding for genes that contain toll/interleukin receptor (TIR) domains were enhanced by the factor of three. *TirA* up-regulation attracted attention before, because Chen *et al.* [29] found an enrichment of *tirA* mRNA (by a factor of eight) in sentinel cells (S-cells). These S-cells are a special cell type in *D. discoideum* multicellular slugs that patrol the organism in search for bacteria and xenobiotics. Furthermore, studies with *tirA* knock out mutants portend to a role of tirA in antimicrobial response in *D. discoideum* as well as the animal kingdom [18, 29]. Remarkably, solely the expression of *tirA* was enhanced upon *Legionella* infection, in contrast to *M. marinum*, which triggered up-regulation of both *tirA* and *tirC*. These pathogen-unique patterns could lead to a general debate of a differential response to different bacteria in *Dictyostelium*. Evidence for that currently emerges also from genome wide microarrays that show distinct transcriptomic patterns caused by *Legionella*, *Salmonella* or *Pseudomonas* infections, respectively [29, 134, 199]. Another aspect, underlining the complexity of immune response, is the ability of toll-like receptors (TLR) to induce autophagy. Indeed, another set of mRNAs found to be elevated by *M. marinum* infection belonged to the autophagy

complex in *D. discoideum*. Importantly, an up-regulation of this particular gene subset was not observed in response to the phagocytosis of the non-pathogenic *M. smegmatis* [own unpublished data]. In general, the role of autophagy in *M. marinum* infected *D. discoideum* is subject of intense current investigations. Studies with extrachromosomal overexpression of *atg8* described transient patches of the fusion protein, which were targeted to ruptures of *M. marinum* containing vacuoles [25]. The ubiquitin-like protein atg8 known as LC3 in mammals was recruited to early phagophores and involved in vesicle expansion and completion [93, 109]. Therefore, these observations might suggest a causal link between vacuole disruption, the bacterial exposure to the cytosol and xenophagy [25]. Moreover, surface proteins of cytosolic *M. marinum* were ubiquitinated [38], which in turn is a signal for autophagosome induction. Important for this process is p62, a ubiquitin binding protein, for which increased mRNA levels were detected in *M. marinum* infected *D. discoideum*. In *Legionella* infections autophagy is a controversial issue. A milestone was set when Farbrother *et al.* discovered a strong regulation of three autophagy genes (*atg8, atg9* and *atg16*) induced by *Legionella* and with a genome wide microarray inquiry [59]. On the one hand it was then shown that autophagy limited *Legionella* infection [188] and one the other hand that *Legionella* suppressed polyubiquitination of its host by molecular mimicry [146]. As seen for *M. marinum*, invading *Salmonella* were surrounded by GFP::Atg8-positive membranes about two hpi. And while killed in *D. discoideum* wild type cells *Salmonella* replication took place in *D. discoideum*$^{atg1;\ atg6}$ and *atg7* knock out mutants [98]. In principal, autophagy can defend against intracellular pathogens (by digestion in autophagosomes) or it is exploited by pathogens, which use its components to build up their replication compartment. Autophagy as a defense strategy against *Mycobacteria* was shown in *M. bovis BCG* infected macrophages: The mycobacterial induced phagosomal maturation arrest could be overpowered by induced autophagy, subsequently leading to resumed fusion with lysosomes and killing of the invaded bacteria [79].

Another candidate-gene that showed up-regulated mRNA amounts in *M. marinum* infected *D. discoideum* by a factor of almost five was *wfdc*. *Wfdc* encodes a protein that embodies the WAP four-disulfide core domain protein (wfdc) and contains a putative N-terminal signal sequence. According to the gene description on dictybase, the protein is predicted to be secreted [204]. In mammalian cells the WAP domain is characterized by highly conserved four-disulfide core that is thought to have protease inhibitor and/or antibacterial properties [13, 215]. A recently described macrophage protein that contains a WAP domain is the whey acid protein domain protein AMWAP. It acted as a counter-regulator of proinflammatory response against *E. coli*, *P. aeruginosa* and *Bacillus subtilus* [103]. The gene *wfdc* is the only gene that contains a WAP domain in *D. discoideum* and its up-regulation in response to *M. marinum* raised a new aspect to the mycobacterial host-pathogen crosstalk. A knock out construct targeting the *wfdc* coding sequence was designed but owing to the timeframe the project was not followed further on. Nevertheless, the general up-regulation of proteins that contain the WAP domain in

response to pathogenic bacteria supports the hypothesis of an ancient defense pattern omnipresent in all professional phagocytes.
The mRNA level of the *D. discoideum* orthologue of the conserved lipopolysaccharide induced tumor necrosis factor alpha (*litaf, simple* or *pig7*) was also monitored to be elevated in the qPCR screening approach. Corresponding findings were made in monocytes exposed to *M. bovis BCG* or its cell wall complex where the mRNA level of *litaf* was enhanced as well [129]. This observation suggests that litaf participates in the immune response against mycobacteria in general.

However, the most outstanding result of the screening was that in response to *M. marinum*, the entire *vacuolin* isoforms were up-regulated, a unity in relative transcriptional changes that was not monitored for any other gene subset analyzed. Accordingly, the vacuolin family was selected for comprehensive examinations as a major part of the study in hand.

4.2 The role of the vacuolin family in the *D. discoideum – M. marinum* model system

Dictyostelium vacuolins are the homologues of eukaryotic flotillins [207]. Flotillins have been implied to be involved in numerous cellular processes, including endocytosis, signal transduction and regulation of the cortical cytoskeleton. However, the precise underlying molecular mechanisms of flotillin function in these processes are yet poorly understood and remain to be investigated [138]. To further address the question of a putative role of flotillin in respect to mycobacterial infections, the expression and localization of vacuolin family was characterized in the *D. discoideum – M. marinum* infection model.

4.2.1 The vacuolin isoforms are differentially regultated in *M. marinum* infected *D. discoideum*

Via TaqMan qPCR the individual *vacuolin* mRNA abundances were profiled in different experimental setups. In vegetative cells *vacuolinA* mRNA comprised the majority of the total *vacuolin* mRNA amount with 70%, while *vacuolinB* mRNA proportion made 28.5% and *vacuolinC* mRNA quantities were the lowest with 1.5% (fig. 3-18: D). These datasets confirmed observations reported by Jenne *et al.* who estimated higher *vacuolinA* mRNA levels than *vacuolinB* mRNA levels in *D. discoideum* via northern blotting [97]. A simple explanation for the high expression of *vacuolinA* in general could be its gene localization downstream of six *actin* genes and two *actin* pseudogenes. Even though these *actin* genes do not belong to the act8 group that comprises 95% of the actinome in *Dictyostelium* [100], it is likely that these genes are nevertheless highly transcribed. Thus DNA in that area might be uncoiled and transcription factors as well as polymerases in topological closeness; conditions that might facilitate *vacuolinA* transcription. Detection

of *vacuolinC* mRNA highlights the sensitivity of the developed qPCR system since *vacuolinC* was not predicted to be expressed in axenic cultured cells [190]. Even though existence of vacuolinC in the macropinocytic proteome supported the presence of *vacuolinC* transcripts [101].
As shown in this work (fig. 3-9) by immunofluorescence in axenic growing *D. discoideum* cells vacuolinA and vacuolinB localize to mature endosomes. This correlates with findings of Rauchenberg *et al.* [148]. Corresponding observations were made in eukaryotic systems where flotillins localized to endosomal compartments and exosomes [47, 48, 115]. In contrast, episomal overexpressed vacuolinC was additionally found at endosomal organelles colocalizing with vatA, a marker for lysosomes and late endosomal structures. This suggested a localization at lysosomes.
In response to *M. marinum* infection not only the general *vacuolin* mRNA level was elevated by the factor of 3.4, additionally, the ratio of vacuolin isoforms was altered. The most obvious increase of mRNA level was detected for *vacuolinC*, which was significantly enhanced by the factor of over 100, comprising 25% of total *vacuolin* abundance under infection conditions. In contrast to minor transcriptional changes that indicate housekeeping activity, the drastic possibly *M. marinum* induced up-regulation of *vacuolinC* points to a functional role of vacuolinC in the infection. Adding the aspect of time, mRNA profiles of all vacuolin isoforms during the innate phase of *M. marinum* infection, uncovered that infected *Dictyostelium* cells exhibited a pathogen-specific transcriptional regulation with isoform-specific kinetics, whereas the strongest relative change of mRNA abundance occurred for *vacuolinC*.
In order to evaluate if *vacuolinC* was subjected to a pathogen-specific regulation, *D. discoideum* was challenged with other pathogenic and non-pathogenic bacteria. The systematic analysis of *D. discoideum* when exposed to different bacteria revealed transcriptional responses of *vacuolinA* and *C* explicitly triggered by *M. marinum*. In contrast, elevated *vacuolinB* mRNA levels were further induced by pathogenic *Legionella*. Our data suggests that vacuolinA and C may play a role specific to *M. marinum* infection while vacuolinB might be part of a broader response directed against internalized pathogens. Taken together, the *vacuolin* transcriptional response in *Dictyostelium* to phagocytized pathogens seems to be more complex and differential than previously assumed. This hypothesis, as suggested above, was supported by the results of several much broader non-hypothesis driven microarray analysis investigating the response of *D. discoideum* to different infections by different pathogens that presumably use different virulence strategies [29, 134, 199].

In the present study it was shown that the recruitment of vacuolin isoforms to the *M. marinum* compartment occurred in an isoform specific manner. These analysis were performed using overexpressed GFP::fusion proteins. Despite being constantly present in excessive amounts, all three vacuolin isoforms targeted the *M. marinum* phagosome at distinct times. Immediately after infection the majority of vacuolin at the mycobacterial compartment was comprised of vacuolinA and C. In the progression of infection, vacuolinA was removed from the *M. marinum* compartment while association of

vacuolinC constantly increased. Maximum association rates were reached at two hpi and maintained. At 24 hpi, rising vacuolinB recruitment revealed the third composition adjustment at the *M. marinum* containing vacuole. Characteristic for that time point are the highest association scores of vacuolin abundance, composed of equal vacuolinB and C amounts. Thus, throughout the course of infection, vacuolinC provided the main vacuolin component at mycobacterial compartments. Time points of isoform recruitment on protein level were compatible with increased *vacuolin* mRNA production. Importantly, this observation could be confirmed on protein level using the *D. discoideum* wild type$^{KI\ vacC:gfp}$ strain enabling for the first time insight into endogenous vacuolin expression. In concordance with the enhanced mRNA level, this cell line clearly showed an elevated vacuolinC protein level in *M. marinum* infected *D. discoideum* as judged by immunoblot analysis (fig. 3-8: C). This chronologically compatible data set suggested that *vacuolinC* mRNA is immediately translated to a functional protein.

Vacuolin accumulation at the *M. marinum* replication niche throughout the innate phase of infection (0.5-6hpi; fig. 3-13) observed in this study is contrary to previous observations [82], where vacuolins were found at the *M. marinum* containing vacuole much later (from 12 to 43 hpi). These differences could be due to different culture conditions, shaking versus adherent, which might have a strong impact on *D. discoideum* cells not only during infection. Comparing both culture conditions in our laboratory revealed that cells growing in shaking tend to be impaired in their cell division, marked by multinuclear cells. Multinuclearity was reported as a phenotype and considered to have a cytokinesis defect as described for *Dictyostelium abiA* knock out mutants [45]. The majority of infected cells described in the previous study did contain multiple nuclei and were cultured in shaking [82]. Another phenotype exhibited by cells cultured under shaking conditions was an elevated irregular protrusion formation in comparison to adherent cultured cells [data not shown]. The regulation of pseudopods, lamellipods and their relatives in *Dictyostelium* is a fine tuned organization that should not emerge randomly [94]. Laboratories that focus on investigation of motility particularly culture *D. discoideum* under adherent conditions [45, 203, 212]. Consequently, it is possible that differences observed in the course of the *M. marinum* infection emerge from differential culture conditions. Comparing infection rates, *D. discoideum* cultivated in shaking seems to be more susceptible to the *M. marinum* infection as Hagedorn *et al.* obtained a high proportion of infected cells that was maintained up to 37 hpi [82]. From that it might be concluded that cells cultured under shaking conditions are more stressed and therefore more susceptible to infections. It is further possible that under shaking conditions host defense machinery might have been delayed, which would correlate with the delay of vacuolin abundance at the *M. marinum* compartment. Interestingly, under shaking conditions, vacuolins were immediately found at the phagosome of non-pathogenic *M. smegmatis* and non-virulent *M. marinum L1D* mutant showing that the vacuolin recruitment in general was still functional [82]. However, these observations were made by immune fluorescence analysis using an α-vacuolin antibody that does not distinguish between the individual vacuolin isoforms. Hypothetically, according to its availability

vacuolinA could be immediately recruited to phagosomes in general while especially vacuolinC is produced and recruited to *M. marinum* wild type containing phagosomes. Investigations using extrachromosomal overexpressing GFP::vacuolin cell lines did not enable the visualization of bacterial escape to the cytosol typically taking place at the last phase of infection [82]. These observations were made under conditions with unnaturally high vacuolin abundance. However, from this it may be concluded that vacuolins are able to stabilize the enclosed vacuoles by assisting to imprison invaded bacteria and make it difficult for them to escape the phagosome.

VacuolinB was shown to be involved in the exocytosis of mature endosomes [148]. Accumulation of vacuolinB at the *M. marinum* containing vacuole, which increased at 24 hpi, suggested that vacuolinB might escort *M. marinum* containing phagosomes out of infected cells, with increasing efficiency towards the late phase of infection. Hence, this could explain constantly decreasing infection rates seen under adherent culture conditions. Besides vacuolin an additional marker is known to localize at *M. marinum* phagosomes: p80, a putative copper transporter [82]. Its distribution was analyzed in this study under adherent culture conditions. Immune fluorescence analysis disclosed a continuous accumulation of p80 at the *M. marinum* containing compartments. These findings were in concordance with experiments from Kolonko *et al.* where p80 was also rapidly found at the *M. marinum* containing compartment [111]. Both results stand in contrast to previously described *M. marinum* infections, where p80 was recruited gradually during the first 12 hours, while phagosomes of non-pathogenic bacteria were rapidly marked [82]. In axenic *Dictyostelium* cells, p80 has been found to be present on endosomes and to accumulate to high amounts in membranes of late endosomes and patches at the cell surface due to fusion of the late endosome with the plasma membrane [28]. Based on homology with other channel transporters, p80 is expected to transport copper outside of vacuoles [21]. Nevertheless, functional studies are not available at the moment and it is unknown whether disruption or overexpression of p80 had an impact on host-pathogen interactions. Since p80 was reported as a late phagosomal marker [28, 82], its early recruitment to the *M. marinum* containing vacuole, which otherwise was solely seen for non-pathogenic bacteria, strengthen the assumption of a stronger and more efficient prevention of *M. marinum* trying to bypass phagosomal maturation pathway of *Dictyostelium* cells are capable to if cultured adherently. These findings revealed that the procedure of culturing *D. discoideum* itself had a strong impact on *D. discoideum* cells and their ability to cope with the *M. marinum* infection. However, collective data of *M. marinum* infected *D. discoideum* suggests that vacuolin proteins targeted to the *M. marinum* phagosome play a role during infection.

The challenge of the *D. discoideum – M. marinum* model system was the translation of information to a mammalian system. The existence of the human homologue flotillin1 on phagosomes was first verified in 2001 by proteomic analysis [72]. Dermine *et al.* were able to show that flotillin accumulation at the phagosomes chronologically took place after lamp1 accumulation [48]. The gradual accumulation of vacuolin and homologue flotillin

suggests that the proteins do not originate from the plasma membrane. It was hypothesized that flotillin was recruited from endosomal organelles [48]. This is a possibility for vacuolins in *D. discoideum* as well. That means that *M. marinum* containing phagosomes would stay connected with the endosomal pathway. That, in turn would lead to the speculation that simultaneously internal *M. marinum* bacteria would actively counter by permanently removing hostile compounds away from the compartment. Furthermore, flotillin1 was found to accumulate at *M. marinum* containing compartments in human macrophages [82] suggesting the existence of ancient defense strategies against ancient pathogens.

4.2.2 Protective function of vacuolins in the *D. discoideum – M. marinum* model system

Transcription, expression and localization of flotillin-like vacuolins in the *D. discoideum – M. marinum* model system suggested that vacuolin isoforms participate in pathogen host interaction. The question remained about their function. To address that question *D. discoideum* mutants lacking single vacuolin isoforms were analyzed. VacA^{KO} and vacB^{KO} cells were generously provided from the laboratory of Prof. Markus Maniak. Unexpectedly, targeted PCR analysis of gDNA as well as qPCR analysis of mRNA both isolated from vacB^{KO} mutants suggested that in vacB^{KO} not only *vacuolinB* was depleted but also that the *vacuolinC* gene locus was not functional.

Verification of the two knock out cell lines was originally performed via southern blotting using probes of vacuolinA and B to confirm that one gene was depleted while the other one was intact [96, 97]. Both knock out mutants were created at a time where the *D. discoideum* genome was not yet sequenced and the existence of *vacuolinC* not yet known. Since 2005 the genome of *D. discoideum* is fully annotated which revealed the presence of the third isoform, *vacuolinC*, which is localized upstream of *vacuolinB* separated by an 800 base pair interval of non-coding sequence [57]. Due to spatially closeness and high similarities of both coding sequences (86.3%) it is imaginable that not only *vacuolinB* but also *vacuolinC* was targeted by the knock out construct of Jenne *et al.* in 1998 [97]. Therefore, to fully understand the genomic features of that region in the vacB^{KO} mutant cells used in this study, further investigations are necessary: For example, PCR analysis of vacB^{KO} gDNA with primer combinations that include the vector sequence of the knock out construct and the region up- and down-stream of the target sequence. This could uncover a possible insertion of the whole knock out vector. In addition sequencing of the whole region may shed light on the genetic composition of the respective region.

It might be possible that genetic alterations occurred over time by culturing the strain in different laboratories. Growing experience also improved *D. discoideum* cell culture handling and it is now known that random mutagenesis occurs if cells are cultured for longer than two to four weeks [60]. To gain clarification in this issue it would be recommended to either newly generate the cell line or to get original stocks of the mutant (from Prof. M. Maniak).

In order to complete the assumed set of single vacuolin knock out mutants a vacC^{KO} cell line was newly created, in which major parts of the *vacuolinC* coding sequence were substituted by a blasticidin resistance cassette by homologous recombination. The verification of vacC^{KO} was first performed on gDNA level. In addition, mRNA production of both remaining *vacuolin* isoforms was analyzed. Transcipts of both, *vacuolinA* and *B* were detected indicating functionality of *vaculinA* and *B* genes in vacC^{KO} cells.
The first analysis of vacuolin knock out strains revealed enhanced cell division rates of vacB^{KO} and a tendency of elevated cell division of vacC^{KO} under adherent culture conditions. The considerable enhanced diversion of *D. discoideum* vacB^{KO} mutant was not expected. Experiments from Jenne *et al.* who generated the mutant did not show proliferation differences in comparison to wild type cells [97]. However, handling of cell culture was very different in the laboratory of Prof. Markus Maniak. In the study of Jenne *et al.* cells were grown under shaking conditions at a density of 10^7 cells/ml while in this study cells were kept in adherent axenic culture at a density of approximately 10^7 cells/10 cm dish containing 10 ml medium. We therefore conclude, that exclusively under the described conditions the lack of either *vacuolinB* and *C* or solely *vacuolinC* had a notable impact on division of vegetative *D. discoideum* cells.
In addition to rapid growth at adherent conditions, vacB^{KO} exhibited a severe delay in development. The delay emerged during the early phase of differentiation, due to impaired aggregation. The driving force of aggregation is chemotaxis towards extracellular cyclic adenosine 3', 5'- monophosphate (cAMP). cAMP is produced by starving cells and serves as a signal for neighboring cells to aggregate [30, 50, 54]. In combination with the impaired agility of vacB^{KO} slugs this suggests a chemotaxis disorder in vacB^{KO} mutants. In further investigations it could be analyzed if this defect could be rescued by the application of exogenous cAMP pulses. Studies with mice lacking flotillin1 led to the conclusion that flotillin microdomains have important functions during neutrophil migration and in uropod formation, similar to the impaired function observed in vacB^{KO} [121].
In regard to vacuolin isoform-specific expression patterns, vacuolinA expression was enhanced during early starvation and therefore predicted to be involved in the development process [97]. However, the existence of only vacuolinA could not accomplish wild type like differentiation of the putative *vacB/C* double knock out. For further investigations it would be of interest to determine the expression of typical developmental genes such as *dscA* (*discoidinI*) and *car1* (*carA*; cAMP receptor) in vacB^{KO} mutant cells [33, 128, 147]. Complementation assays via episomal expression of vaculinB, vacuolinC or even the human homologue flotillin would shed light about hypothetical redundant functions.
Analysis of *vacuolin* knock out mutants throughout the course of the *M. marinum* infection in respect to association with two phagosomal markers (p80 and vatA) showed no influence of p80 accumulation at the compartment. Small differences in vatA accumulation in comparison to infected wild type were determined for all analyzed mutant strains. Depletion of either *vacuolinA* or *C* led to elevated vatA accumulation at the *M. marinum* containing compartment. Nevertheless, no long term influence was

monitored on bacterial proliferation in both knock out mutants. This could be due to the mycobacterial resistance to acidic environment. *Mycobacteria* carry multiple genes dedicated to survive low pH, either by resistance to acid [155, 192] or by interference with phagosomal maturation [23, 142, 177]. *M. tuberculosis* for example is able to deal with acidic pH for several days of exposure [192]. Another hint that initial acidification did not play a major role in mycobacterial survival is the observation that stronger vatA accumulation at phagosomes of vacB^{KO} mutants was only detected until three hpi and afterwards resumed the same pattern observed for *D. discoideum* wild type. Independent from vatA accumulation *M. marinum* exhibited significantly augmented intracellular proliferation in this mutant than in wild type *Dictyostelium*. The lysosomal physiology in terms of pH and respective enzymes was shown to have a limited impact on intracellular killing of *K. pneumoniae* in *D. discoideum* [114]. The increased proliferation of *M. marinum* in vacB^{KO} stands in contrast to observations from Hagedorn *et al.* where vacB^{KO} cells were more immune against the *M. marinum* infection [82].

Unexpectedly, in *D. discoideum* wild type M. *marinum* rather persisted in the infected host instead of the expected proliferation. As discussed above *D. discoideum* culture conditions seem to have a large share on the course of the infection.

In this study *M. marinum* proliferation in *Dictyostelium* was estimated by counting colony forming units (cfu) at different time points of infection. The cfu approach estimated viable cells by quantifying the number of colonies derived from a single progenitor. Cfu analysis was methodically limited to a status quo by estimation of total bacterial numbers. A dynamic picture with insight to the state or origin of the pathogen is not given. Hence, it is possible that the host cell killed some of the invaded bacteria and others survived and proliferated in infected host cells. On the other hand, original bacteria numbers could persist in the host cells.

Since *Mycobacteria* tend to aggregate and form clusters, which are hard to separate, this method was accompanied by a tendency to underestimate bacterial numbers. To gain reliable information with the assay rather high experiment repetition numbers were performed in this study.

Laboratories working with *Mycobacteria* currently try to find solutions to determine intracellular proliferation of *Mycobacteria* with other approaches. For example following mycobacterial growth by qPCR or firefly luciferase based assays [2, 3]. Concomitant with both approaches is waxy coat of the mycobacterial cell wall that makes it difficult to get chemical substrates in or genomic DNA out of the bacteria. However, it can be concluded that functional depletion of *vacuolinB* and *C* led to an increased *M. marinum* proliferation. Conclusively, both proteins, maybe even in combination, seem to play an immuno-protective role in the host defense machinery.

In contrast, the extrachromosomal overexpression of GFP::vacuolinC led to a suppression of bacterial growth in the early steps of infection. The protective delay was then overcome over time, after 32 to 48 hpi. In further studies, it would be interesting to monitor *M. marinum* proliferation in *D. discoideum* host cells that overexpress vacuolinB and C, since it would be expected that bacterial growth would be impaired putatively due to quick exocytosis of invaded pathogens and suppression of bacterial escape into

the cytosol. In addition, in further studies infection of *vacuolin* knock out mutants with other pathogens would improve our knowledge about pathogen specific roles of vacuolin isoforms, especially vacuolinC.

4.2.3 Partial complementation of vacuolin isoforms

Shown in this study, depletion of single vacuolin isoforms or rather absence of either *vacuolinA* or *vacuolinC* did not result in severe phenotypes. This might be due to a partial redundancy of the remaining vacuolin isoforms.

In fact, in vacA^{KO} cells *vacuolinB* mRNA was up-regulated in axenic cells if compared to wild type. In the course of *M. marinum* infection an additive increase of *vacuolinB* mRNA was detected. In comparison to infected wild type cells the increase of *vacuolinC* mRNA was approximately half as much, nevertheless still significantly increased. Total vacuolin level in infected vacA^{KO} cells was reduced to more than half of the amount measured in wild type cells under the same infection conditions. However, after 48 hours no increase of *M. marinum* proliferation was detected, suggesting that vacuolinB and C efficiently participate in the defense against invasive *M. marinum*.

In vacC^{KO} cells, *vacuolinA* mRNA level was already elevated under axenic conditions by approximately one third and reached even higher levels in response to *M. marinum* infection in comparison to wild type cells. Total *vacuolin* levels in infected vacC^{KO} cells were as high as in infected wild type cells. For 24 hours of *M. marinum* infection cfu analysis were indistinguishable from vacB^{KO}, the putative *vacB/C* double knock out mutant. However, concurrently with the course of infection, instead of the hypothesized lack of defense, after 48 hours only a slight increase of total bacterial proliferation was measured, similar to the *D. discoideum* wild type.

In contrast, mRNA analysis of vacB^{KO} cells revealed that loss of *vacuolinB* and *C* led to an increased *vacuolinA* abundance in vegetative cells. Unexpectedly, this did not result in a further increase of *vacuolinA* mRNA in response to the *M. marinum* infection.

Conclusively, if detected mRNA would be directly translated to protein, either a reduced vacuolin level composed out of vacuolinB and C or a high abundance of vacuolinA and B would be sufficient to cope with a *M. marinum* infection with the same efficiency as wild type cells. The lack of both, vacuolinB and C could not be completely compensated by remaining vacuolinA and led to increased intracellular *M. marinum* proliferation.

Because *vacuolinA* levels did not further increase during *M. marinum* infection it might be concluded that vacuolin isoforms might facilitate each other's transcription. Such a regulative bias is known from the human vacuolin homologues, where flotillin1 and 2 regulated each other's expression [7]. The data implied that each single vacuolin isoform itself could at least partially complement other vacuolin isoforms, but at least two vacuolin isoforms seemed to be necessary for an efficient defense against *M. marinum.*

In silico analysis revealed high amino acid similarities between vacuolin isoforms. The highest similarity score of 81.06% was shared between vacuolinB and C. The lowest score was the alignment of vacuolinA and C with 72.53%. Since *D. discoideum* bears a remarkably compact genome with 65% composed of genes, a certain redundancy might protect survival to some extent if a gene is randomly disrupted for example by retrotransposons [210]. Other cases of functional substitution are known for *D. discoideum*,

for example was RasC capable to substitute for RasG in chemotaxis [16]. In addition, Phg1B plays a redundant role with Phg1A in controlling cellular amounts of Kil1. Kil1 is a sulfotransferase necessary for efficient intracellular killing of *K. pneumoniae* [114].

4.2.4 Potential vacuolin organization in membrane microdomains

Distribution of endogenous vacuolinC in clusters of different shapes and sizes at the *M. marinum* containing compartment implied that vacuolins in *D. discoideum* (like flotillins in mammalian cells) might be organized in membrane microdomains (fig. 3-11: B) [7]. These structures have been postulated as a key platform involved in the killing and degradation of intracellular pathogens [126]. The human homologues flotillins are known as markers for membrane microdomains. Existence of lipid subdomains on phagosomes and historically the first suggestion of flotillin1 present on them was in 2001 [72]. Flotillin1 contains a palmitoylation site, Cys34 that was essential to direct its localization to plasma membrane in kidney cells [131]. Post-translational palmitoylation is a reversible modification important for localization, trafficking, stability and activity [67, 91, 119, 151]. All three vacuolin isoforms in *Dictyostelium* contain a codon for cysteine and thus provide putative palmitoylation sites. VacuolinA contains two and vacuolinB and C both, contain three. Their localization in the amino acid sequence shares little homology to each other. The localization of the first cysteine of vacuolinC is at position 19, which is unique compared to the others. These differences may lead to different membrane association and curvature capacities characteristic for each isoform. Flotillin2 is palmitoylated by DHHC5, a protein palmitoyltransferase belonging to the DHHC family [117]. Encoded in the D. discoideum genome are two putative palmitoyltransferase (DDB_G0275149, DDB_G0293930), which contain a zinc finger DHHC domain and six and four putative transmembrane domains [213]. It is therefore possible that vacuolin isoforms are palmitoylated in *D. discoideum* and thus are anchored in endosomal membranes.

Additionally, if an association with the palmitoytransferase remains its putative transmembrane domains could tighten the proteins' attachment to the membrane. All vacuolin isoforms contain a coiled-coil domain at the N-terminus a protein motif leading to alpha-helical secondary structure. Via the coiled-coil domain oligomerisation is facilitated. It was shown in this study that all vacuolin isoforms assembled to heteromeric oligomers (fig. 3-22). The immunoprecipitation experiments were performed in respective knock out backgrounds, thus it can be concluded that all vacuolin isoforms are able to assemble to a complex with the others. These findings confirmed results of Wienke *et al.* who analyzed vacuolinB protein domains [208]. The hetero oligomerization of flotillin1 was required to translocate flotillin2 to membranes of endocytic vesicles, which did not take place in the absence of flotllin1 [7].

Flotillin based membrane microdomains are discussed as scaffolding proteins [216]. With the ability of these subdomains to gather certain proteins while excluding others regulations of signal transduction pathways could be coordinated [48, 104, 120, 179]. In the progression of the *M. marinum* infection the mycobacterial vacuole became fully caged by vacuolin presumably composed of disparate homo and hetero oligomeric subdomains. These subdomains may tether distinct complexes by interaction and

promote binding of different proteins. Most likely, the compartment membrane composition and its modification play an important role in the host pathogen interaction and the course of infection. The acquisition of their functional properties depends on subsets of interactions partners.

In order to dissect the putative role of vacuolin complexes as signaling platforms and to identify proteins, which might be selectively recruited to participate in the *M. marinum* induced modulation of the phagosome mass spectrometry analysis of vacuolin interaction partners were planned. This approach would provide additional insight to the vacuolin stoichiometry and post-translational modifications in *D. discoideum*.

In silico analysis of the vacuolin isoforms also revealed putative myristoylation sites. These may be uniquely modified in response to the infection, which could be revealed by mass spectrometry. Unfortunately, all attempts made to analyze vacuolin interaction partners by mass spectrometry failed. Nevertheless, a small hint that infection specific interaction partners bind to vacuolin complexes was made with silver stained SDS-PAGE gels of proteins that bound to GFP::vacuolin fusion proteins. Comparison of vacuolin-bound samples of non-infected and infected samples revealed additional protein bands that appeared only in the infection samples. This might indicate that, due to the infection, protein compositions at vacuolin subdomains were possibly altered by the host and / or the invaded *M. marinum* [data not shown].

It is known that the arrest of macrophage phagosome maturation is dependent on the *M. marinum* ESX-1 secretion system required to export proteins across their complex cell walls. It involves the secretion of early secreting antigenic 6 kDa (ESAT-6) and culture filtrate protein-10 (CFP-10) [185, 214]. In M. tuberculosis, in addition to the ESX1-secretion system, the accessory SecA2 system is a specialized protein export system that is required for phagosome maturation arrest [182]. . Independent of mass spectrometry, in future experiments the existence of mycobacterial factors bound to immunoprecipitated GFP::vacuolin could be analyzed via immunoblotting. At least those factors for which commercial antibodies are available could be tested.

It has been shown that flotillins were a target of diverse pathogens. The parasite Plasmodium falciparum exported its own orthologue of human band 7 stomatin, a protein that is related to flotillin into the infected erythrocyte [87]. A different strategy was pursued by the protozoan *Leishmania donovani*. *L. donovani* actively inhibited flotillin accumulation at the phagosome and thus its maturation [48]. Another strategy, although the same target, was developed by the animal pathogen *Brucella* and the plant pathogen *Sinorhizobium meliloti*, that induced flotillin recruitment an the up regulation of flotillin, respectively [4, 84, 200].

4.3 The value of the *D. discoideum – M. marinum* model system

This study confirmed the potential of the *D. discoideum – M. marinum* model system to advance *Mycobacteria* research. The established SYBR Green qPCR system uncovered a large number of candidate-genes with a relative change of mRNA abundance in response to the *M. marinum* infection. Since the system is ready to use, it will now be used to

complement the results of the deep sequencing approach mentioned in the result section.

One major contribution of *D. discoideum* as a host is the identification of host cell factors that are involved in the infection. Investigations of these factors is facilitated by a large number of *D. discoideum* knock out mutants which can be freely obtained via Dictyostelium stock center [90]. Among them are knock out mutants of promising candidate-genes from the qPCR screening such as *nramp*, *tirA* or *atg8*. As shown in this study, additional genes of interest can be easily tagged or depleted.

The basic mechanisms of host pathogen interactions are evolutionary conserved between higher and lower eukaryotes [20, 53, 99], which allows safe and fast research using this model since it comes along with a broad variety of molecular tools.

With this study the model system was further established and can contribute to deepen the understanding of the mycobacterial – host interaction, which in turn is an important factor on the way to find targets in the treatment of tuberculosis infections. Utilization of *D. discoideum* as a host to study infections diseases already led to the discovery of several new host factors, which are important for *L. pneumophila* infection [118]. The pathogen-specific regulation of vacuolinC and its localization at the *M. marinum* containing phagosome suggested a functional role in the infection. Further this study showed that vacuolinB and C played a protective role to limit intracellular replication of *M. marinum*. Parts of these observations were already translated into more complex mammalian systems: The accumulation of flotillin1 at the *M. marinum* containing vacuole in human blood derived monocytes provided positive evidence of the D. *discoideum* – *M. marinum* model systems potential to find unknown factors involved in tuberculosis infection [82]. Future experiments will be performed to address the role of flotillins in *Mycobacteria* infected macrophages.

5 References

1 P. Andersen, and T. M. Doherty, 'The Success and Failure of Bcg - Implications for a Novel Tuberculosis Vaccine', *Nat Rev Microbiol,* 3 (2005), 656-62.

2 N. Andreu, A. Zelmer, T. Fletcher, P. T. Elkington, T. H. Ward, J. Ripoll, T. Parish, G. J. Bancroft, U. Schaible, B. D. Robertson, and S. Wiles, 'Optimisation of Bioluminescent Reporters for Use with Mycobacteria', *PLoS One,* 5 (2010), e10777.

3 N. Andreu, A. Zelmer, S. L. Sampson, M. Ikeh, G. J. Bancroft, U. E. Schaible, S. Wiles, and B. D. Robertson, 'Rapid in Vivo Assessment of Drug Efficacy against Mycobacterium Tuberculosis Using an Improved Firefly Luciferase', *J Antimicrob Chemother,* 68 (2013), 2118-27.

4 B. Arellano-Reynoso, N. Lapaque, S. Salcedo, G. Briones, A. E. Ciocchini, R. Ugalde, E. Moreno, I. Moriyon, and J. P. Gorvel, 'Cyclic Beta-1,2-Glucan Is a Brucella Virulence Factor Required for Intracellular Survival', *Nat Immunol,* 6 (2005), 618-25.

5 J. A. Armstrong, and P. D. Hart, 'Response of Cultured Macrophages to Mycobacterium Tuberculosis, with Observations on Fusion of Lysosomes with Phagosomes', *J Exp Med,* 134 (1971), 713-40.

6 J. M. Ashworth, and D. J. Watts, 'Metabolism of the Cellular Slime Mould Dictyostelium Discoideum Grown in Axenic Culture', *Biochem J,* 119 (1970), 175-82.

7 T. Babuke, M. Ruonala, M. Meister, M. Amaddii, C. Genzler, A. Esposito, and R. Tikkanen, 'Hetero-Oligomerization of Reggie-1/Flotillin-2 and Reggie-2/Flotillin-1 Is Required for Their Endocytosis', *Cell Signal,* 21 (2009), 1287-97.

8 T. Babuke, and R. Tikkanen, 'Dissecting the Molecular Function of Reggie/Flotillin Proteins', *Eur J Cell Biol,* 86 (2007), 525-32.

9 H. Bach, K. G. Papavinasasundaram, D. Wong, Z. Hmama, and Y. Av-Gay, 'Mycobacterium Tuberculosis Virulence Is Mediated by Ptpa Dephosphorylation of Human Vacuolar Protein Sorting 33b', *Cell Host Microbe,* 3 (2008), 316-22.

10 H. Bach, D. Wong, and Y. Av-Gay, 'Mycobacterium Tuberculosis Ptka Is a Novel Protein Tyrosine Kinase Whose Substrate Is Ptpa', *Biochem J,* 420 (2009), 155-60.

11 C. E. Barry, 3rd, H. I. Boshoff, V. Dartois, T. Dick, S. Ehrt, J. Flynn, D. Schnappinger, R. J. Wilkinson, and D. Young, 'The Spectrum of Latent Tuberculosis: Rethinking the Biology and Intervention Strategies', *Nat Rev Microbiol,* 7 (2009), 845-55.

12 R. D. Berg, and L. Ramakrishnan, 'Insights into Tuberculosis from the Zebrafish Model', *Trends in Molecular Medicine,* 18 (2012), 689-90.

13 C. D. Bingle, and A. Vyakarnam, 'Novel Innate Immune Functions of the Whey Acidic Protein Family', *Trends Immunol,* 29 (2008), 444-53.

14 J. M. Blackwell, T. Goswami, C. A. Evans, D. Sibthorpe, N. Papo, J. K. White, S. Searle, E. N. Miller, C. S. Peacock, H. Mohammed, and M. Ibrahim, 'Slc11a1 (Formerly Nramp1) and Disease Resistance', *Cell Microbiol,* 3 (2001), 773-84.

15 C. C. Boehme, P. Nabeta, D. Hillemann, M. P. Nicol, S. Shenai, F. Krapp, J. Allen, R. Tahirli, R. Blakemore, R. Rustomjee, A. Milovic, M. Jones, S. M. O'Brien, D. H. Persing, S. Ruesch-Gerdes, E. Gotuzzo, C. Rodrigues, D. Alland, and M. D. Perkins,

'Rapid Molecular Detection of Tuberculosis and Rifampin Resistance', *N Engl J Med,* 363 (2010), 1005-15.

16 P. Bolourani, G. Spiegelman, and G. Weeks, 'Ras Proteins Have Multiple Functions in Vegetative Cells of Dictyostelium', *Eukaryot Cell,* 9 (2010), 1728-33.

17 S. Borrell, and S. Gagneux, 'Infectiousness, Reproductive Fitness and Evolution of Drug-Resistant Mycobacterium Tuberculosis', *Int J Tuberc Lung Dis,* 13 (2009), 1456-66.

18 I. Botos, D. M. Segal, and D. R. Davies, 'The Structural Biology of Toll-Like Receptors', *Structure,* 19 (2011), 447-59.

19 J. Boulais, M. Trost, C. R. Landry, R. Dieckmann, E. D. Levy, T. Soldati, S. W. Michnick, P. Thibault, and M. Desjardins, 'Molecular Characterization of the Evolution of Phagosomes', *Molecular systems biology,* 6 (2010), 423.

20 S. Bozzaro, C. Bucci, and M. Steinert, 'Phagocytosis and Host-Pathogen Interactions in Dictyostelium with a Look at Macrophages', *Int Rev Cell Mol Biol,* 271 (2008), 253-300.

21 S. Bozzaro, S. Buracco, and B. Peracino, 'Iron Metabolism and Resistance to Infection by Invasive Bacteria in the Social Amoeba Dictyostelium Discoideum', *Front Cell Infect Microbiol,* 3 (2013), 50.

22 S. Bozzaro, and L. Eichinger, 'The Professional Phagocyte Dictyostelium Discoideum as a Model Host for Bacterial Pathogens', *Current Drug Targets,* 12 (2011), 942-54.

23 P. Brodin, Y. Poquet, F. Levillain, I. Peguillet, G. Larrouy-Maumus, M. Gilleron, F. Ewann, T. Christophe, D. Fenistein, J. Jang, M. S. Jang, S. J. Park, J. Rauzier, J. P. Carralot, R. Shrimpton, A. Genovesio, J. A. Gonzalo-Asensio, G. Puzo, C. Martin, R. Brosch, G. R. Stewart, B. Gicquel, and O. Neyrolles, 'High Content Phenotypic Cell-Based Visual Screen Identifies Mycobacterium Tuberculosis Acyltrehalose-Containing Glycolipids Involved in Phagosome Remodeling', *PLoS Pathog,* 6 (2010), e1001100.

24 D. T. Browman, M. B. Hoegg, and S. M. Robbins, 'The Spfh Domain-Containing Proteins: More Than Lipid Raft Markers', *Trends Cell Biol,* 17 (2007), 394-402.

25 J. Calvo-Garrido, S. Carilla-Latorre, Y. Kubohara, N. Santos-Rodrigo, A. Mesquita, T. Soldati, P. Golstein, and R. Escalante, 'Autophagy in Dictyostelium: Genes and Pathways, Cell Death and Infection', *Autophagy,* 6 (2010), 686-701.

26 S. V. Capuano, 3rd, D. A. Croix, S. Pawar, A. Zinovik, A. Myers, P. L. Lin, S. Bissel, C. Fuhrman, E. Klein, and J. L. Flynn, 'Experimental Mycobacterium Tuberculosis Infection of Cynomolgus Macaques Closely Resembles the Various Manifestations of Human M. Tuberculosis Infection', *Infect Immun,* 71 (2003), 5831-44.

27 M. Carnell, T. Zech, S. D. Calaminus, S. Ura, M. Hagedorn, S. A. Johnston, R. C. May, T. Soldati, L. M. Machesky, and R. H. Insall, 'Actin Polymerization Driven by Wash Causes V-Atpase Retrieval and Vesicle Neutralization before Exocytosis', *The Journal of cell biology,* 193 (2011), 831-9.

28 S. J. Charette, and P. Cosson, 'Exocytosis of Late Endosomes Does Not Directly Contribute Membrane to the Formation of Phagocytic Cups or Pseudopods in Dictyostelium', *FEBS Lett,* 580 (2006), 4923-8.

29 G. Chen, O. Zhuchenko, and A. Kuspa, 'Immune-Like Phagocyte Activity in the Social Amoeba', *Science,* 317 (2007), 678-81.

30 R. L. Chisholm, and R. A. Firtel, 'Insights into Morphogenesis from a Simple Developmental System', *Nat Rev Mol Cell Biol,* 5 (2004), 531-41.

31 J. Chua, I. Vergne, S. Master, and V. Deretic, 'A Tale of Two Lipids: Mycobacterium Tuberculosis Phagosome Maturation Arrest', *Curr Opin Microbiol,* 7 (2004), 71-7.

32 J. R. Chubb, T. Trcek, S. M. Shenoy, and R. H. Singer, 'Transcriptional Pulsing of a Developmental Gene', *Curr Biol,* 16 (2006), 1018-25.

33 M. Clarke, S. C. Kayman, and K. Riley, 'Density-Dependent Induction of Discoidin-I Synthesis in Exponentially Growing Cells of Dictyostelium Discoideum', *Differentiation,* 34 (1987), 79-87.

34 M. Clarke, J. Kohler, Q. Arana, T. Liu, J. Heuser, and G. Gerisch, 'Dynamics of the Vacuolar H(+)-Atpase in the Contractile Vacuole Complex and the Endosomal Pathway of Dictyostelium Cells', *J Cell Sci,* 115 (2002), 2893-905.

35 M. Clarke, and L. Maddera, 'Phagocyte Meets Prey: Uptake, Internalization, and Killing of Bacteria by Dictyostelium Amoebae', *Eur J Cell Biol* (2006).

36 M. Clarke, L. Maddera, U. Engel, and G. Gerisch, 'Retrieval of the Vacuolar H-Atpase from Phagosomes Revealed by Live Cell Imaging', *PLoS One,* 5 (2010), e8585.

37 D. L. Clemens, and M. A. Horwitz, 'Characterization of the Mycobacterium Tuberculosis Phagosome and Evidence That Phagosomal Maturation Is Inhibited', *J Exp Med,* 181 (1995), 257-70.

38 C. A. Collins, A. De Maziere, S. van Dijk, F. Carlsson, J. Klumperman, and E. J. Brown, 'Atg5-Independent Sequestration of Ubiquitinated Mycobacteria', *PLoS Pathog,* 5 (2009), e1000430.

39 F. M. Collins, V. Montalbine, and N. E. Morrison, 'Growth and Immunogenicity of Photochromogenic Strains of Mycobacteria in the Footpads of Normal Mice', *Infect Immun,* 11 (1975), 1079-87.

40 A. M. Cooper, 'Cell-Mediated Immune Responses in Tuberculosis', *Annu Rev Immunol,* 27 (2009), 393-422.

41 C. L. Cosma, D. R. Sherman, and L. Ramakrishnan, 'The Secret Lives of the Pathogenic Mycobacteria', *Annu Rev Microbiol,* 57 (2003), 641-76.

42 C. L. Cosma, L. E. Swaim, H. Volkman, L. Ramakrishnan, and J. M. Davis, 'Zebrafish and Frog Models of Mycobacterium Marinum Infection', *Curr Protoc Microbiol,* Chapter 10 (2006), Unit 10B 2.

43 P. Cosson, and T. Soldati, 'Eat, Kill or Die: When Amoeba Meets Bacteria', *Curr Opin Microbiol,* 11 (2008), 271-6.

44 P. Cosson, L. Zulianello, O. Join-Lambert, F. Faurisson, L. Gebbie, M. Benghezal, C. Van Delden, L. K. Curty, and T. Kohler, 'Pseudomonas Aeruginosa Virulence Analyzed in a Dictyostelium Discoideum Host System', *J Bacteriol,* 184 (2002), 3027-33.

45 A. J. Davidson, S. Ura, P. A. Thomason, G. Kalna, and R. H. Insall, 'Abi Is Required for Modulation and Stability but Not Localization or Activation of the Scar/Wave Complex', *Eukaryot Cell,* 12 (2013), 1509-16.

46 P. D. Davies, and M. Pai, 'The Diagnosis and Misdiagnosis of Tuberculosis', *Int J Tuberc Lung Dis,* 12 (2008), 1226-34.

47 A. de Gassart, C. Geminard, B. Fevrier, G. Raposo, and M. Vidal, 'Lipid Raft-Associated Protein Sorting in Exosomes', *Blood,* 102 (2003), 4336-44.

48 J. F. Dermine, S. Duclos, J. Garin, F. St-Louis, S. Rea, R. G. Parton, and M. Desjardins, 'Flotillin-1-Enriched Lipid Raft Domains Accumulate on Maturing Phagosomes', *J Biol Chem,* 276 (2001), 18507-12.

49 J. F. Dermine, G. Goyette, M. Houde, S. J. Turco, and M. Desjardins, 'Leishmania Donovani Lipophosphoglycan Disrupts Phagosome Microdomains in J774 Macrophages', *Cell Microbiol,* 7 (2005), 1263-70.

50 M. C. Dinauer, S. A. MacKay, and P. N. Devreotes, 'Cyclic 3',5'-Amp Relay in Dictyostelium Discoideum Iii. The Relationship of Camp Synthesis and Secretion During the Camp Signaling Response', *J Cell Biol,* 86 (1980), 537-44.

51 M. S. Dionne, N. Ghori, and D. S. Schneider, 'Drosophila Melanogaster Is a Genetically Tractable Model Host for Mycobacterium Marinum', *Infect Immun,* 71 (2003), 3540-50.

52 H. D. Donoghue, M. Spigelman, C. L. Greenblatt, G. Lev-Maor, G. K. Bar-Gal, C. Matheson, K. Vernon, A. G. Nerlich, and A. R. Zink, 'Tuberculosis: From Prehistory to Robert Koch, as Revealed by Ancient DNA', *Lancet Infect Dis,* 4 (2004), 584-92.

53 M. S. Dorer, and R. R. Isberg, 'Non-Vertebrate Hosts in the Analysis of Host-Pathogen Interactions', *Microbes Infect,* 8 (2006), 1637-46.

54 D. Dormann, B. Vasiev, and C. J. Weijer, 'Propagating Waves Control Dictyostelium Discoideum Morphogenesis', *Biophys Chem,* 72 (1998), 21-35.

55 C. Dye, and B. G. Williams, 'The Population Dynamics and Control of Tuberculosis', *Science,* 328 (2010), 856-61.

56 P. Q. Edwards, and L. B. Edwads, 'Story of the Tuberculin Test from an Epidemiologic Viewpoint', *Am Rev Respir Dis,* 81(1)Pt 2 (1960), 1-47.

57 L. Eichinger, J. A. Pachebat, G. Glockner, M. A. Rajandream, R. Sucgang, M. Berriman, J. Song, R. Olsen, K. Szafranski, Q. Xu, B. Tunggal, S. Kummerfeld, M. Madera, B. A. Konfortov, F. Rivero, A. T. Bankier, R. Lehmann, N. Hamlin, R. Davies, P. Gaudet, P. Fey, K. Pilcher, G. Chen, D. Saunders, E. Sodergren, P. Davis, A. Kerhornou, X. Nie, N. Hall, C. Anjard, L. Hemphill, N. Bason, P. Farbrother, B. Desany, E. Just, T. Morio, R. Rost, C. Churcher, J. Cooper, S. Haydock, N. van Driessche, A. Cronin, I. Goodhead, D. Muzny, T. Mourier, A. Pain, M. Lu, D. Harper, R. Lindsay, H. Hauser, K. James, M. Quiles, M. Madan Babu, T. Saito, C. Buchrieser, A. Wardroper, M. Felder, M. Thangavelu, D. Johnson, A. Knights, H. Loulseged, K. Mungall, K. Oliver, C. Price, M. A. Quail, H. Urushihara, J. Hernandez, E. Rabbinowitsch, D. Steffen, M. Sanders, J. Ma, Y. Kohara, S. Sharp, M. Simmonds, S. Spiegler, A. Tivey, S. Sugano, B. White, D. Walker, J. Woodward, T. Winckler, Y. Tanaka, G. Shaulsky, M. Schleicher, G. Weinstock, A. Rosenthal, E. C. Cox, R. L. Chisholm, R. Gibbs, W. F. Loomis, M. Platzer, R. R. Kay, J. Williams, P. H. Dear, A. A. Noegel, B. Barrell, and A. Kuspa, 'The Genome of the Social Amoeba Dictyostelium Discoideum', *Nature,* 435 (2005), 43-57.

58 P. T. Elkington, 'Tuberculosis: Time for a New Perspective?', *J Infect,* 66 (2013), 299-302.

59 P. Farbrother, C. Wagner, J. Na, B. Tunggal, T. Morio, H. Urushihara, Y. Tanaka, M. Schleicher, M. Steinert, and L. Eichinger, 'Dictyostelium Transcriptional Host Cell Response Upon Infection with Legionella', *Cell Microbiol,* 8 (2006), 438-56.

60 P. Fey, A. S. Kowal, P. Gaudet, K. E. Pilcher, and R. L. Chisholm, 'Protocols for Growth and Development of Dictyostelium Discoideum', *Nat Protoc,* 2 (2007), 1307-16.

61 R. S. Flannagan, V. Jaumouille, and S. Grinstein, 'The Cell Biology of Phagocytosis', *Annu Rev Pathol,* 7 (2012), 61-98.

62 Michael Worboys Flurin Condrau, *Tuberculosis Then and Now: Perspectives on the History of an Infectious Disease* (McGill-Queen's University Press 2010, 2010).

63 J. L. Flynn, and J. Chan, 'What's Good for the Host Is Good for the Bug', *Trends Microbiol,* 13 (2005), 98-102.

64 M. Frick, N. A. Bright, K. Riento, A. Bray, C. Merrified, and B. J. Nichols, 'Coassembly of Flotillins Induces Formation of Membrane Microdomains, Membrane Curvature, and Vesicle Budding', *Curr Biol,* 17 (2007), 1151-6.

65 T. R. Frieden, T. R. Sterling, S. S. Munsiff, C. J. Watt, and C. Dye, 'Tuberculosis', *Lancet,* 362 (2003), 887-99.

66 G. Fritsche, M. Nairz, S. J. Libby, F. C. Fang, and G. Weiss, 'Slc11a1 (Nramp1) Impairs Growth of Salmonella Enterica Serovar Typhimurium in Macrophages Via Stimulation of Lipocalin-2 Expression', *J Leukoc Biol,* 92 (2012), 353-9.

67 Y. Fukata, and M. Fukata, 'Protein Palmitoylation in Neuronal Development and Synaptic Plasticity', *Nat Rev Neurosci,* 11 (2010), 161-75.

68 S. Gagneux, 'Host-Pathogen Coevolution in Human Tuberculosis', *Philos Trans R Soc Lond B Biol Sci,* 367 (2012), 850-9.

69 N. R. Gandhi, A. Moll, A. W. Sturm, R. Pawinski, T. Govender, U. Lalloo, K. Zeller, J. Andrews, and G. Friedland, 'Extensively Drug-Resistant Tuberculosis as a Cause of Death in Patients Co-Infected with Tuberculosis and Hiv in a Rural Area of South Africa', *Lancet,* 368 (2006), 1575-80.

70 L. Y. Gao, S. Guo, B. McLaughlin, H. Morisaki, J. N. Engel, and E. J. Brown, 'A Mycobacterial Virulence Gene Cluster Extending Rd1 Is Required for Cytolysis, Bacterial Spreading and Esat-6 Secretion', *Mol Microbiol,* 53 (2004), 1677-93.

71 L. Y. Gao, F. Laval, E. H. Lawson, R. K. Groger, A. Woodruff, J. H. Morisaki, J. S. Cox, M. Daffe, and E. J. Brown, 'Requirement for Kasb in Mycobacterium Mycolic Acid Biosynthesis, Cell Wall Impermeability and Intracellular Survival: Implications for Therapy', *Mol Microbiol,* 49 (2003), 1547-63.

72 J. Garin, R. Diez, S. Kieffer, J. F. Dermine, S. Duclos, E. Gagnon, R. Sadoul, C. Rondeau, and M. Desjardins, 'The Phagosome Proteome: Insight into Phagosome Functions', *J Cell Biol,* 152 (2001), 165-80.

73 M. S. Glickman, J. S. Cox, and W. R. Jacobs, Jr., 'A Novel Mycolic Acid Cyclopropane Synthetase Is Required for Cording, Persistence, and Virulence of Mycobacterium Tuberculosis', *Mol Cell,* 5 (2000), 717-27.

74 S. J. Gluckman, 'Mycobacterium Marinum', *Clin Dermatol,* 13 (1995), 273-6.

75 M. S. Gomes, and R. Appelberg, 'Nramp1- or Cytokine-Induced Bacteriostasis of Mycobacterium Avium by Mouse Macrophages Is Independent of the Respiratory Burst', *Microbiology,* 148 (2002), 3155-60.

76 G. Greub, and D. Raoult, 'Microorganisms Resistant to Free-Living Amoebae', *Clinical Microbiology Reviews,* 17 (2004), 413-33.

77 S. Gruenheid, E. Pinner, M. Desjardins, and P. Gros, 'Natural Resistance to Infection with Intracellular Pathogens: The Nramp1 Protein Is Recruited to the Membrane of the Phagosome', *J Exp Med,* 185 (1997), 717-30.

78 C. Grundner, H. L. Ng, and T. Alber, 'Mycobacterium Tuberculosis Protein Tyrosine Phosphatase Ptpb Structure Reveals a Diverged Fold and a Buried Active Site', *Structure,* 13 (2005), 1625-34.

79 M. G. Gutierrez, S. S. Master, S. B. Singh, G. A. Taylor, M. I. Colombo, and V. Deretic, 'Autophagy Is a Defense Mechanism Inhibiting Bcg and Mycobacterium Tuberculosis Survival in Infected Macrophages', *Cell,* 119 (2004), 753-66.

80 D. J. Hackam, O. D. Rotstein, W. J. Zhang, N. Demaurex, M. Woodside, O. Tsai, and S. Grinstein, 'Regulation of Phagosomal Acidification. Differential Targeting of Na+/H+ Exchangers, Na+/K+-Atpases, and Vacuolar-Type H+-Atpases', *J Biol Chem,* 272 (1997), 29810-20.

81 M. Hagedorn, K. H. Rohde, D. G. Russell, and T. Soldati, 'Infection by Tubercular Mycobacteria Is Spread by Nonlytic Ejection from Their Amoeba Hosts', *Science,* 323 (2009), 1729-33.

82 M. Hagedorn, and T. Soldati, 'Flotillin and Rach Modulate the Intracellular Immunity of Dictyostelium to Mycobacterium Marinum Infection', *Cell Microbiol,* 9 (2007), 2716-33.

83 S. Hagele, R. Kohler, H. Merkert, M. Schleicher, J. Hacker, and M. Steinert, 'Dictyostelium Discoideum: A New Host Model System for Intracellular Pathogens of the Genus Legionella', *Cell Microbiol,* 2 (2000), 165-71.

84 C. H. Haney, and S. R. Long, 'Plant Flotillins Are Required for Infection by Nitrogen-Fixing Bacteria', *Proc Natl Acad Sci U S A,* 107 (2010), 478-83.

85 C. V. Harding, and W. H. Boom, 'Regulation of Antigen Presentation by Mycobacterium Tuberculosis: A Role for Toll-Like Receptors', *Nat Rev Microbiol,* 8 (2010), 296-307.

86 Y. He, W. Li, G. Liao, and J. Xie, 'Mycobacterium Tuberculosis-Specific Phagosome Proteome and Underlying Signaling Pathways', *J Proteome Res,* 11 (2012), 2635-43.

87 N. L. Hiller, T. Akompong, J. S. Morrow, A. A. Holder, and K. Haldar, 'Identification of a Stomatin Orthologue in Vacuoles Induced in Human Erythrocytes by Malaria Parasites. A Role for Microbial Raft Proteins in Apicomplexan Vacuole Biogenesis', *J Biol Chem,* 278 (2003), 48413-21.

88 M. A. Holmes, W. Paulsene, X. Jide, C. Ratledge, and R. K. Strong, 'Siderocalin (Lcn 2) Also Binds Carboxymycobactins, Potentially Defending against Mycobacterial Infections through Iron Sequestration', *Structure,* 13 (2005), 29-41.

89 E. N. Houben, L. Nguyen, and J. Pieters, 'Interaction of Pathogenic Mycobacteria with the Host Immune System', *Curr Opin Microbiol,* 9 (2006), 76-85.

90 http://dictybase.org/StockCenter/StockCenter.html.

91 K. Huang, and A. El-Husseini, 'Modulation of Neuronal Protein Trafficking and Function by Palmitoylation', *Curr Opin Neurobiol,* 15 (2005), 527-35.

92 J. Huotari, and A. Helenius, 'Endosome Maturation', *EMBO J,* 30 (2011), 3481-500.

93 Y. Ichimura, T. Kirisako, T. Takao, Y. Satomi, Y. Shimonishi, N. Ishihara, N. Mizushima, I. Tanida, E. Kominami, M. Ohsumi, T. Noda, and Y. Ohsumi, 'A Ubiquitin-Like System Mediates Protein Lipidation', *Nature,* 408 (2000), 488-92.

94 R. Insall, 'The Interaction between Pseudopods and Extracellular Signalling During Chemotaxis and Directed Migration', *Curr Opin Cell Biol,* 25 (2013), 526-31.

95 E. Ishikawa, T. Ishikawa, Y. S. Morita, K. Toyonaga, H. Yamada, O. Takeuchi, T. Kinoshita, S. Akira, Y. Yoshikai, and S. Yamasaki, 'Direct Recognition of the Mycobacterial Glycolipid, Trehalose Dimycolate, by C-Type Lectin Mincle', *J Exp Med,* 206 (2009), 2879-88.

96 N Jenne, R Rauchenberger, U Hacker, T Kast, and M Maniak, 'Targeted Gene Disruption Reveals a Role for Vacuolin B in the Late Endocytic Pathway and Exocytosis.', *J. Cell Sci.,* 111 (1998), 61-70.

97 N. Jenne, R. Rauchenberger, U. Hacker, T. Kast, and M. Maniak, 'Targeted Gene Disruption Reveals a Role for Vacuolin B in the Late Endocytic Pathway and Exocytosis', *J Cell Sci,* 111 (Pt 1) (1998), 61-70.

98 K. Jia, C. Thomas, M. Akbar, Q. Sun, B. Adams-Huet, C. Gilpin, and B. Levine, 'Autophagy Genes Protect against Salmonella Typhimurium Infection and Mediate Insulin Signaling-Regulated Pathogen Resistance', *Proc Natl Acad Sci U S A,* 106 (2009), 14564-9.

99 T. Jin, X. Xu, J. Fang, N. Isik, J. Yan, J. A. Brzostowski, and D. Hereld, 'How Human Leukocytes Track Down and Destroy Pathogens: Lessons Learned from the Model Organism Dictyostelium Discoideum', *Immunol Res,* 43 (2009), 118-27.

100 J. M. Joseph, P. Fey, N. Ramalingam, X. I. Liu, M. Rohlfs, A. A. Noegel, A. Muller-Taubenberger, G. Glockner, and M. Schleicher, 'The Actinome of Dictyostelium Discoideum in Comparison to Actins and Actin-Related Proteins from Other Organisms', *PLoS One,* 3 (2008), e2654.

101 A. Journet, G. Klein, S. Brugiere, Y. Vandenbrouck, A. Chapel, S. Kieffer, C. Bruley, C. Masselon, and L. Aubry, 'Investigating the Macropinocytic Proteome of Dictyostelium Amoebae by High-Resolution Mass Spectrometry', *Proteomics,* 12 (2012), 241-5.

102 F. N. Judson, and R. A. Feldman, 'Mycobacterial Skin Tests in Humans 12 Years after Infection with Mycobacterium Marinum', *Am Rev Respir Dis,* 109 (1974), 544-7.

103 M. Karlstetter, Y. Walczak, K. Weigelt, S. Ebert, J. Van den Brulle, H. Schwer, R. Fuchshofer, and T. Langmann, 'The Novel Activated Microglia/Macrophage Wap Domain Protein, Amwap, Acts as a Counter-Regulator of Proinflammatory Response', *J Immunol,* 185 (2010), 3379-90.

104 V. L. Katanaev, G. P. Solis, G. Hausmann, S. Buestorf, N. Katanayeva, Y. Schrock, C. A. Stuermer, and K. Basler, 'Reggie-1/Flotillin-2 Promotes Secretion of the Long-Range Signalling Forms of Wingless and Hedgehog in Drosophila', *EMBO J,* 27 (2008), 509-21.

105 Edited by Dieter Kabelitz and Stefan H.E. Kaufmann, *Immunology of Infection*. Vol. Volume 37, 2010), pp. 1-527.

106 S. H. Kaufmann, 'Immunity to Intracellular Bacteria', *Annu Rev Immunol,* 11 (1993), 129-63.

107 S. H. Kaufmann, G. Hussey, and P. H. Lambert, 'New Vaccines for Tuberculosis', *Lancet,* 375 (2010), 2110-9.

108 R. H. Kessin, *Dictyostelium - Evolution, Cell Biology, and the Development of Multicellularity*, *Cambridge Univ. Press* (Cambridge, UK, 2001).

109 T. Kirisako, M. Baba, N. Ishihara, K. Miyazawa, M. Ohsumi, T. Yoshimori, T. Noda, and Y. Ohsumi, 'Formation Process of Autophagosome Is Traced with Apg8/Aut7p in Yeast', *J Cell Biol,* 147 (1999), 435-46.

110 Robert Koch, 'Aetiologie Der Tuberculose', (Berliner Klinische Wochenschrift, 1882), pp. 221-30.

111 M. Kolonko, A. C. Geffken, T. Blumer, K. Hagens, U. E. Schaible, and M. Hagedorn, 'Wash-Driven Actin Polymerization Is Required for Efficient Mycobacterial Phagosome Maturation Arrest', *Cell Microbiol* (2013).

112 C. K. Kwan, and J. D. Ernst, 'Hiv and Tuberculosis: A Deadly Human Syndemic', *Clin Microbiol Rev,* 24 (2011), 351-76.

113 R. Lang, 'Recognition of the Mycobacterial Cord Factor by Mincle: Relevance for Granuloma Formation and Resistance to Tuberculosis', *Front Immunol,* 4 (2013), 5.

114 M. Le Coadic, R. Froquet, W. C. Lima, M. Dias, A. Marchetti, and P. Cosson, 'Phg1/Tm9 Proteins Control Intracellular Killing of Bacteria by Determining Cellular Levels of the Kil1 Sulfotransferase in Dictyostelium', *PLoS One,* 8 (2013), e53259.

115 B. Y. Lee, D. Jethwaney, B. Schilling, D. L. Clemens, B. W. Gibson, and M. A. Horwitz, 'The Mycobacterium Bovis Bacille Calmette-Guerin Phagosome Proteome', *Mol Cell Proteomics,* 9 (2010), 32-53.

116 E. Lee, and D. A. Knecht, 'Visualization of Actin Dynamics During Macropinocytosis and Exocytosis', *Traffic,* 3 (2002), 186-92.

117 Y. Li, B. R. Martin, B. F. Cravatt, and S. L. Hofmann, 'Dhhc5 Protein Palmitoylates Flotillin-2 and Is Rapidly Degraded on Induction of Neuronal Differentiation in Cultured Cells', *J Biol Chem,* 287 (2012), 523-30.
118 Z. Li, A. S. Dugan, G. Bloomfield, J. Skelton, A. Ivens, V. Losick, and R. R. Isberg, 'The Amoebal Map Kinase Response to Legionella Pneumophila Is Regulated by Dupa', *Cell Host Microbe,* 6 (2009), 253-67.
119 M. E. Linder, and R. J. Deschenes, 'Palmitoylation: Policing Protein Stability and Traffic', *Nat Rev Mol Cell Biol,* 8 (2007), 74-84.
120 J. Liu, S. M. Deyoung, M. Zhang, L. H. Dold, and A. R. Saltiel, 'The Stomatin/Prohibitin/Flotillin/Hflk/C Domain of Flotillin-1 Contains Distinct Sequences That Direct Plasma Membrane Localization and Protein Interactions in 3t3-L1 Adipocytes', *J Biol Chem,* 280 (2005), 16125-34.
121 A. Ludwig, G. P. Otto, K. Riento, E. Hams, P. G. Fallon, and B. J. Nichols, 'Flotillin Microdomains Interact with the Cortical Cytoskeleton to Control Uropod Formation and Neutrophil Recruitment', *J Cell Biol,* 191 (2010), 771-81.
122 H. Makinoshima, and M. S. Glickman, 'Regulation of Mycobacterium Tuberculosis Cell Envelope Composition and Virulence by Intramembrane Proteolysis', *Nature,* 436 (2005), 406-9.
123 M. Maniak, 'Conserved Features of Endocytosis in Dictyostelium', *Int Rev Cytol,* 221 (2002), 257-87.
124 K. A. McDonough, Y. Kress, and B. R. Bloom, 'Pathogenesis of Tuberculosis: Interaction of Mycobacterium Tuberculosis with Macrophages', *Infect Immun,* 61 (1993), 2763-73.
125 P. K. Mehta, A. K. Pandey, S. Subbian, S. H. El-Etr, S. L. Cirillo, M. M. Samrakandi, and J. D. Cirillo, 'Identification of Mycobacterium Marinum Macrophage Infection Mutants', *Microb Pathog,* 40 (2006), 139-51.
126 S. Meresse, O. Steele-Mortimer, E. Moreno, M. Desjardins, B. Finlay, and J. P. Gorvel, 'Controlling the Maturation of Pathogen-Containing Vacuoles: A Matter of Life and Death', *Nat Cell Biol,* 1 (1999), E183-8.
127 Y. Miyake, K. Toyonaga, D. Mori, S. Kakuta, Y. Hoshino, A. Oyamada, H. Yamada, K. Ono, M. Suyama, Y. Iwakura, Y. Yoshikai, and S. Yamasaki, 'C-Type Lectin Mcl Is an Fcrgamma-Coupled Receptor That Mediates the Adjuvanticity of Mycobacterial Cord Factor', *Immunity,* 38 (2013), 1050-62.
128 T. Morita, A. Amagai, and Y. Maeda, 'Translocation of the Dictyostelium Trap1 Homologue to Mitochondria Induces a Novel Prestarvation Response', *J Cell Sci,* 117 (2004), 5759-70.
129 Y. Moriwaki, N. A. Begum, M. Kobayashi, M. Matsumoto, K. Toyoshima, and T. Seya, 'Mycobacterium Bovis Bacillus Calmette-Guerin and Its Cell Wall Complex Induce a Novel Lysosomal Membrane Protein, Simple, That Bridges the Missing Link between Lipopolysaccharide and P53-Inducible Gene, Litaf(Pig7), and Estrogen-Inducible Gene, Eet-1', *J Biol Chem,* 276 (2001), 23065-76.
130 I. C. Morrow, and R. G. Parton, 'Flotillins and the Phb Domain Protein Family: Rafts, Worms and Anaesthetics', *Traffic,* 6 (2005), 725-40.
131 I. C. Morrow, S. Rea, S. Martin, I. A. Prior, R. Prohaska, J. F. Hancock, D. E. James, and R. G. Parton, 'Flotillin-1/Reggie-2 Traffics to Surface Raft Domains Via a Novel Golgi-Independent Pathway. Identification of a Novel Membrane Targeting Domain and a Role for Palmitoylation', *J Biol Chem,* 277 (2002), 48834-41.
132 C. Munderloh, G. P. Solis, V. Bodrikov, F. A. Jaeger, M. Wiechers, E. Malaga-Trillo, and C. A. Stuermer, 'Reggies/Flotillins Regulate Retinal Axon Regeneration in the

Zebrafish Optic Nerve and Differentiation of Hippocampal and N2a Neurons', *J Neurosci,* 29 (2009), 6607-15.

133 T. Muramoto, D. Cannon, M. Gierlinski, A. Corrigan, G. J. Barton, and J. R. Chubb, 'Live Imaging of Nascent Rna Dynamics Reveals Distinct Types of Transcriptional Pulse Regulation', *Proc Natl Acad Sci U S A,* 109 (2012), 7350-5.

134 W. Nasser, B. Santhanam, E. R. Miranda, A. Parikh, K. Juneja, G. Rot, C. Dinh, R. Chen, B. Zupan, G. Shaulsky, and A. Kuspa, 'Bacterial Discrimination by Dictyostelid Amoebae Reveals the Complexity of Ancient Interspecies Interactions', *Curr Biol,* 23 (2013), 862-72.

135 C. Neumann-Giesen, B. Falkenbach, P. Beicht, S. Claasen, G. Luers, C. A. Stuermer, V. Herzog, and R. Tikkanen, 'Membrane and Raft Association of Reggie-1/Flotillin-2: Role of Myristoylation, Palmitoylation and Oligomerization and Induction of Filopodia by Overexpression', *Biochem J,* 378 (2004), 509-18.

136 E. J. North, M. Jackson, and R. E. Lee, 'New Approaches to Target the Mycolic Acid Biosynthesis Pathway for the Development of Tuberculosis Therapeutics', *Curr Pharm Des* (2013).

137 World Health Organization, 'Global Tuberculosis Report 2013', (WHO Library Cataloguing-in-Publication Data, 2013).

138 G. P. Otto, and B. J. Nichols, 'The Roles of Flotillin Microdomains--Endocytosis and Beyond', *J Cell Sci,* 124 (2011), 3933-40.

139 P. Pancholi, A. Mirza, N. Bhardwaj, and R. M. Steinman, 'Sequestration from Immune Cd4+ T Cells of Mycobacteria Growing in Human Macrophages', *Science,* 260 (1993), 984-6.

140 B. Peracino, S. Buracco, and S. Bozzaro, 'The Nramp (Slc11) Proteins Regulate Development, Resistance to Pathogenic Bacteria and Iron Homeostasis in Dictyostelium Discoideum', *J Cell Sci,* 126 (2013), 301-11.

141 B. Peracino, C. Wagner, A. Balest, A. Balbo, B. Pergolizzi, A. A. Noegel, M. Steinert, and S. Bozzaro, 'Function and Mechanism of Action of Dictyostelium Nramp1 (Slc11a1) in Bacterial Infection', *Traffic,* 7 (2006), 22-38.

142 K. Pethe, D. L. Swenson, S. Alonso, J. Anderson, C. Wang, and D. G. Russell, 'Isolation of Mycobacterium Tuberculosis Mutants Defective in the Arrest of Phagosome Maturation', *Proc Natl Acad Sci U S A,* 101 (2004), 13642-7.

143 S. R. Pfeffer, 'Rab Gtpase Regulation of Membrane Identity', *Curr Opin Cell Biol,* 25 (2013), 414-9.

144 J. Pieters, 'Evasion of Host Cell Defense Mechanisms by Pathogenic Bacteria', *Curr Opin Immunol,* 13 (2001), 37-44.

145 J. Pieters, 'Mycobacterium Tuberculosis and the Macrophage: Maintaining a Balance', *Cell Host Microbe,* 3 (2008), 399-407.

146 C. T. Price, S. Al-Khodor, T. Al-Quadan, M. Santic, F. Habyarimana, A. Kalia, and Y. A. Kwaik, 'Molecular Mimicry by an F-Box Effector of Legionella Pneumophila Hijacks a Conserved Polyubiquitination Machinery within Macrophages and Protozoa', *PLoS Pathog,* 5 (2009), e1000704.

147 A. Rathi, and M. Clarke, 'Expression of Early Developmental Genes in Dictyostelium Discoideum Is Initiated During Exponential Growth by an Autocrine-Dependent Mechanism', *Mech Dev,* 36 (1992), 173-82.

148 R Rauchenberger, U Hacker, J Murphy, J Niewohner, and M Maniak, 'Coronin and Vacuolin Identify Consecutive Stages of a Late, Actin-Coated Endocytic Compartment in Dictyostelium.', *Curr. Biol.,* 7 (1997), 215-18.

149 K. Ravanel, B. de Chassey, S. Cornillon, M. Benghezal, L. Zulianello, L. Gebbie, F. Letourneur, and P. Cosson, 'Membrane Sorting in the Endocytic and Phagocytic Pathway of Dictyostelium Discoideum', *Eur J Cell Biol,* 80 (2001), 754-64.
150 M. C. Raviglione, and I. M. Smith, 'Xdr Tuberculosis--Implications for Global Public Health', *N Engl J Med,* 356 (2007), 656-9.
151 M. D. Resh, 'Palmitoylation of Ligands, Receptors, and Intracellular Signaling Molecules', *Sci STKE,* 2006 (2006), re14.
152 B. L. Rezabek, J. M. Rodriguez-Paris, J. A. Cardelli, and C. P. Chia, 'Phagosomal Proteins of Dictyostelium Discoideum', *J Eukaryot Microbiol,* 44 (1997), 284-92.
153 S. E. Rieder, and S. D. Emr, 'A Novel Ring Finger Protein Complex Essential for a Late Step in Protein Transport to the Yeast Vacuole', *Mol Biol Cell,* 8 (1997), 2307-27.
154 E. Rivera-Milla, C. A. Stuermer, and E. Malaga-Trillo, 'Ancient Origin of Reggie (Flotillin), Reggie-Like, and Other Lipid-Raft Proteins: Convergent Evolution of the Spfh Domain', *Cell Mol Life Sci,* 63 (2006), 343-57.
155 K. Rohde, R. M. Yates, G. E. Purdy, and D. G. Russell, 'Mycobacterium Tuberculosis and the Environment within the Phagosome', *Immunol Rev,* 219 (2007), 37-54.
156 M. G. Roth, 'Phosphoinositides in Constitutive Membrane Traffic', *Physiol Rev,* 84 (2004), 699-730.
157 E. Rothmeier, G. Pfaffinger, C. Hoffmann, C. F. Harrison, H. Grabmayr, U. Repnik, M. Hannemann, S. Wolke, A. Bausch, G. Griffiths, A. Muller-Taubenberger, A. Itzen, and H. Hilbi, 'Activation of Ran Gtpase by a Legionella Effector Promotes Microtubule Polymerization, Pathogen Vacuole Motility and Infection', *PLoS Pathog,* 9 (2013), e1003598.
158 D. G. Russell, 'Who Puts the Tubercle in Tuberculosis?', *Nat Rev Microbiol,* 5 (2007), 39-47.
159 D. G. Russell, C. E. Barry, 3rd, and J. L. Flynn, 'Tuberculosis: What We Don't Know Can, and Does, Hurt Us', *Science,* 328 (2010), 852-6.
160 D. G. Russell, P. J. Cardona, M. J. Kim, S. Allain, and F. Altare, 'Foamy Macrophages and the Progression of the Human Tuberculosis Granuloma', *Nat Immunol,* 10 (2009), 943-8.
161 M. T. Saleh, and J. T. Belisle, 'Secretion of an Acid Phosphatase (Sapm) by Mycobacterium Tuberculosis That Is Similar to Eukaryotic Acid Phosphatases', *J Bacteriol,* 182 (2000), 6850-3.
162 Cecilia Bucci and Michael Steinert Salvatore Bozzaro, 'Phagocytosis and Host–Pathogen Interactions in Dictyostelium with a Look at Macrophages', in *International Review of Cell and Molecular Biology*, ed. by Kwan W. Jeon, 2008).
163 M. U. Shiloh, and P. A. DiGiuseppe Champion, 'To Catch a Killer. What Can Mycobacterial Models Teach Us About Mycobacterium Tuberculosis Pathogenesis?', *Curr Opin Microbiol,* 13 (2010), 86-92.
164 A. Sillo, G. Bloomfield, A. Balest, A. Balbo, B. Pergolizzi, B. Peracino, J. Skelton, A. Ivens, and S. Bozzaro, 'Genome-Wide Transcriptional Changes Induced by Phagocytosis or Growth on Bacteria in Dictyostelium', *BMC Genomics,* 9 (2008), 291.
165 C. Skriwan, M. Fajardo, S. Hagele, M. Horn, M. Wagner, R. Michel, G. Krohne, M. Schleicher, J. Hacker, and M. Steinert, 'Various Bacterial Pathogens and Symbionts Infect the Amoeba Dictyostelium Discoideum', *Int J Med Microbiol,* 291 (2002), 615-24.
166 J. Smith, J. Manoranjan, M. Pan, A. Bohsali, J. Xu, J. Liu, K. L. McDonald, A. Szyk, N. LaRonde-LeBlanc, and L. Y. Gao, 'Evidence for Pore Formation in Host Cell

Membranes by Esx-1-Secreted Esat-6 and Its Role in Mycobacterium Marinum Escape from the Vacuole', *Infect Immun,* 76 (2008), 5478-87.

167 D. E. Snider, Jr., 'Bacille Calmette-Guerin Vaccinations and Tuberculin Skin Tests', *JAMA,* 253 (1985), 3438-9.

168 T. Soldati, and O. Neyrolles, 'Mycobacteria and the Intraphagosomal Environment: Take It with a Pinch of Salt(S)!', *Traffic,* 13 (2012), 1042-52.

169 G. P. Solis, M. Hoegg, C. Munderloh, Y. Schrock, E. Malaga-Trillo, E. Rivera-Milla, and C. A. Stuermer, 'Reggie/Flotillin Proteins Are Organized into Stable Tetramers in Membrane Microdomains', *Biochem J,* 403 (2007), 313-22.

170 J. M. Solomon, G. S. Leung, and R. R. Isberg, 'Intracellular Replication of Mycobacterium Marinum within Dictyostelium Discoideum: Efficient Replication in the Absence of Host Coronin', *Infect Immun,* 71 (2003), 3578-86.

171 J. M. Solomon, A. Rupper, J. A. Cardelli, and R. R. Isberg, 'Intracellular Growth of Legionella Pneumophila in Dictyostelium Discoideum, a System for Genetic Analysis of Host-Pathogen Interactions', *Infect Immun,* 68 (2000), 2939-47.

172 B. P. Somesh, C. Neffgen, M. Iijima, P. Devreotes, and F. Rivero, 'Dictyostelium Rach Regulates Endocytic Vesicular Trafficking and Is Required for Localization of Vacuolin', *Traffic* (2006).

173 L. M. Stamm, and E. J. Brown, 'Mycobacterium Marinum: The Generalization and Specialization of a Pathogenic Mycobacterium', *Microbes Infect,* 6 (2004), 1418-28.

174 L. M. Stamm, J. H. Morisaki, L. Y. Gao, R. L. Jeng, K. L. McDonald, R. Roth, S. Takeshita, J. Heuser, M. D. Welch, and E. J. Brown, 'Mycobacterium Marinum Escapes from Phagosomes and Is Propelled by Actin-Based Motility', *J Exp Med,* 198 (2003), 1361-8.

175 H. Stenmark, 'Rab Gtpases as Coordinators of Vesicle Traffic', *Nat Rev Mol Cell Biol,* 10 (2009), 513-25.

176 M. Stevense, T. Muramoto, I. Muller, and J. R. Chubb, 'Digital Nature of the Immediate-Early Transcriptional Response', *Development,* 137 (2010), 579-84.

177 G. R. Stewart, J. Patel, B. D. Robertson, A. Rae, and D. B. Young, 'Mycobacterial Mutants with Defective Control of Phagosomal Acidification', *PLoS Pathog,* 1 (2005), 269-78.

178 T. P. Stinear, T. Seemann, P. F. Harrison, G. A. Jenkin, J. K. Davies, P. D. Johnson, Z. Abdellah, C. Arrowsmith, T. Chillingworth, C. Churcher, K. Clarke, A. Cronin, P. Davis, I. Goodhead, N. Holroyd, K. Jagels, A. Lord, S. Moule, K. Mungall, H. Norbertczak, M. A. Quail, E. Rabbinowitsch, D. Walker, B. White, S. Whitehead, P. L. Small, R. Brosch, L. Ramakrishnan, M. A. Fischbach, J. Parkhill, and S. T. Cole, 'Insights from the Complete Genome Sequence of Mycobacterium Marinum on the Evolution of Mycobacterium Tuberculosis', *Genome Research,* 18 (2008), 729-41.

179 C. A. Stuermer, D. M. Lang, F. Kirsch, M. Wiechers, S. O. Deininger, and H. Plattner, 'Glycosylphosphatidyl Inositol-Anchored Proteins and Fyn Kinase Assemble in Noncaveolar Plasma Membrane Microdomains Defined by Reggie-1 and -2', *Mol Biol Cell,* 12 (2001), 3031-45.

180 S. Sturgill-Koszycki, U. E. Schaible, and D. G. Russell, 'Mycobacterium-Containing Phagosomes Are Accessible to Early Endosomes and Reflect a Transitional State in Normal Phagosome Biogenesis', *EMBO J,* 15 (1996), 6960-8.

181 S. Sturgill-Koszycki, P. H. Schlesinger, P. Chakraborty, P. L. Haddix, H. L. Collins, A. K. Fok, R. D. Allen, S. L. Gluck, J. Heuser, and D. G. Russell, 'Lack of Acidification in

Mycobacterium Phagosomes Produced by Exclusion of the Vesicular Proton-Atpase', *Science,* 263 (1994), 678-81.
182 J. T. Sullivan, E. F. Young, J. R. McCann, and M. Braunstein, 'The Mycobacterium Tuberculosis Seca2 System Subverts Phagosome Maturation to Promote Growth in Macrophages', *Infect Immun,* 80 (2012), 996-1006.
183 G. H. Sun-Wada, H. Tabata, N. Kawamura, M. Aoyama, and Y. Wada, 'Direct Recruitment of H+-Atpase from Lysosomes for Phagosomal Acidification', *J Cell Sci,* 122 (2009), 2504-13.
184 L. E. Swaim, L. E. Connolly, H. E. Volkman, O. Humbert, D. E. Born, and L. Ramakrishnan, 'Mycobacterium Marinum Infection of Adult Zebrafish Causes Caseating Granulomatous Tuberculosis and Is Moderated by Adaptive Immunity', *Infect Immun,* 74 (2006), 6108-17.
185 T. Tan, W. L. Lee, D. C. Alexander, S. Grinstein, and J. Liu, 'The Esat-6/Cfp-10 Secretion System of Mycobacterium Marinum Modulates Phagosome Maturation', *Cell Microbiol,* 8 (2006), 1417-29.
186 D. M. Tobin, and L. Ramakrishnan, 'Comparative Pathogenesis of Mycobacterium Marinum and Mycobacterium Tuberculosis', *Cell Microbiol,* 10 (2008), 1027-39.
187 T. Tonjum, D. B. Welty, E. Jantzen, and P. L. Small, 'Differentiation of Mycobacterium Ulcerans, M. Marinum, and M. Haemophilum: Mapping of Their Relationships to M. Tuberculosis by Fatty Acid Profile Analysis, DNA-DNA Hybridization, and 16s Rrna Gene Sequence Analysis', *J Clin Microbiol,* 36 (1998), 918-25.
188 S. M. Tung, C. Unal, A. Ley, C. Pena, B. Tunggal, A. A. Noegel, O. Krut, M. Steinert, and L. Eichinger, 'Loss of Dictyostelium Atg9 Results in a Pleiotropic Phenotype Affecting Growth, Development, Phagocytosis and Clearance and Replication of Legionella Pneumophila', *Cell Microbiol,* 12 (2010), 765-80.
189 Z. F. Udwadia, 'Mdr, Xdr, Tdr Tuberculosis: Ominous Progression', *Thorax,* 67 (2012), 286-8.
190 vacuolinC, http://dictybase.org/gene/DDB_G0279307%3E
191 N. van der Wel, D. Hava, D. Houben, D. Fluitsma, M. van Zon, J. Pierson, M. Brenner, and P. J. Peters, 'M. Tuberculosis and M. Leprae Translocate from the Phagolysosome to the Cytosol in Myeloid Cells', *Cell,* 129 (2007), 1287-98.
192 O. H. Vandal, L. M. Pierini, D. Schnappinger, C. F. Nathan, and S. Ehrt, 'A Membrane Protein Preserves Intrabacterial Ph in Intraphagosomal Mycobacterium Tuberculosis', *Nat Med,* 14 (2008), 849-54.
193 D. M. Veltman, G. Akar, L. Bosgraaf, and P. J. Van Haastert, 'A New Set of Small, Extrachromosomal Expression Vectors for Dictyostelium Discoideum', *Plasmid,* 61 (2009), 110-8.
194 I. Vergne, J. Chua, and V. Deretic, 'Tuberculosis Toxin Blocking Phagosome Maturation Inhibits a Novel Ca2+/Calmodulin-Pi3k Hvps34 Cascade', *J Exp Med,* 198 (2003), 653-9.
195 I. Vergne, J. Chua, H. H. Lee, M. Lucas, J. Belisle, and V. Deretic, 'Mechanism of Phagolysosome Biogenesis Block by Viable Mycobacterium Tuberculosis', *Proc Natl Acad Sci U S A,* 102 (2005), 4033-8.
196 I. Vergne, J. Chua, S. B. Singh, and V. Deretic, 'Cell Biology of Mycobacterium Tuberculosis Phagosome', *Annu Rev Cell Dev Biol,* 20 (2004), 367-94.
197 L. E. Via, D. Deretic, R. J. Ulmer, N. S. Hibler, L. A. Huber, and V. Deretic, 'Arrest of Mycobacterial Phagosome Maturation Is Caused by a Block in Vesicle Fusion between Stages Controlled by Rab5 and Rab7', *J Biol Chem,* 272 (1997), 13326-31.

198 S. Vidal, M. L. Tremblay, G. Govoni, S. Gauthier, G. Sebastiani, D. Malo, E. Skamene, M. Olivier, S. Jothy, and P. Gros, 'The Ity/Lsh/Bcg Locus: Natural Resistance to Infection with Intracellular Parasites Is Abrogated by Disruption of the Nramp1 Gene', *J Exp Med,* 182 (1995), 655-66.
199 A. Walk, J. Callahan, P. Srisawangvong, J. Leuschner, D. Samaroo, D. Cassilly, and M. L. Snyder, 'Lipopolysaccharide Enhances Bactericidal Activity in Dictyostelium Discoideum Cells', *Dev Comp Immunol,* 35 (2011), 850-6.
200 M. Watarai, S. Makino, Y. Fujii, K. Okamoto, and T. Shirahata, 'Modulation of Brucella-Induced Macropinocytosis by Lipid Rafts Mediates Intracellular Replication', *Cell Microbiol,* 4 (2002), 341-55.
201 D. J. Watts, and J. M. Ashworth, 'Growth of Myxameobae of the Cellular Slime Mould Dictyostelium Discoideum in Axenic Culture', *Biochem J,* 119 (1970), 171-4.
202 K. Weber, and M. Osborn, 'The Reliability of Molecular Weight Determinations by Dodecyl Sulfate-Polyacrylamide Gel Electrophoresis', *J Biol Chem,* 244 (1969), 4406-12.
203 D. Wessels, D. F. Lusche, S. Kuhl, P. Heid, and D. R. Soll, 'Pten Plays a Role in the Suppression of Lateral Pseudopod Formation During Dictyostelium Motility and Chemotaxis', *J Cell Sci,* 120 (2007), 2517-31.
204 wfdc, http://dictybase.org/gene/DDB_G0274699%3E
205 WHO, 'Who 2010 Global Tuberculosis Control—Surveillance, Planning, Financing. Geneva, Switzerland', (2010).
206 S. Wiegand, J. Kruse, S. Gronemann, and C. Hammann, 'Efficient Generation of Gene Knockout Plasmids for Dictyostelium Discoideum Using One-Step Cloning', *Genomics,* 97 (2011), 321-5.
207 D. Wienke, A. Drengk, C. Schmauch, N. Jenne, and M. Maniak, 'Vacuolin, a Flotillin/Reggie-Related Protein from Dictyostelium Oligomerizes for Endosome Association', *Eur J Cell Biol* (2006).
208 ———, 'Vacuolin, a Flotillin/Reggie-Related Protein from Dictyostelium Oligomerizes for Endosome Association', *Eur J Cell Biol,* 85 (2006), 991-1000.
209 L. G. Wilson, 'The Historical Decline of Tuberculosis in Europe and America: Its Causes and Significance', *J Hist Med Allied Sci,* 45 (1990), 366-96.
210 T. Winckler, J. Schiefner, T. Spaller, and O. Siol, 'Dictyostelium Transfer Rna Gene-Targeting Retrotransposons: Studying Mobile Element-Host Interactions in a Compact Genome', *Mob Genet Elements,* 1 (2011), 145-50.
211 D. Wong, H. Bach, J. Sun, Z. Hmama, and Y. Av-Gay, 'Mycobacterium Tuberculosis Protein Tyrosine Phosphatase (Ptpa) Excludes Host Vacuolar-H+-Atpase to Inhibit Phagosome Acidification', *Proceedings of the National Academy of Sciences of the United States of America,* 108 (2011), 19371-6.
212 C. Wu, S. B. Asokan, M. E. Berginski, E. M. Haynes, N. E. Sharpless, J. D. Griffith, S. M. Gomez, and J. E. Bear, 'Arp2/3 Is Critical for Lamellipodia and Response to Extracellular Matrix Cues but Is Dispensable for Chemotaxis', *Cell,* 148 (2012), 973-87.
213 http://www.dictybase.org.
214 J. Xu, O. Laine, M. Masciocchi, J. Manoranjan, J. Smith, S. J. Du, N. Edwards, X. Zhu, C. Fenselau, and L. Y. Gao, 'A Unique Mycobacterium Esx-1 Protein Co-Secretes with Cfp-10/Esat-6 and Is Necessary for Inhibiting Phagosome Maturation', *Mol Microbiol,* 66 (2007), 787-800.
215 J. Yang, J. Zhu, D. Sun, and A. Ding, 'Suppression of Macrophage Responses to Bacterial Lipopolysaccharide (Lps) by Secretory Leukocyte Protease Inhibitor

(Slpi) Is Independent of Its Anti-Protease Function', *Biochim Biophys Acta,* 1745 (2005), 310-7.

216 F. Zhao, J. Zhang, Y. S. Liu, L. Li, and Y. L. He, 'Research Advances on Flotillins', *Virol J,* 8 (2011), 479.

217 A. Zumla, P. Nahid, and S. T. Cole, 'Advances in the Development of New Tuberculosis Drugs and Treatment Regimens', *Nat Rev Drug Discov,* 12 (2013), 388-404.

218 Gordon C. Cook und Alimuddin Zumla, *Manson's Tropical Diseases*. 22nd Revised edition ednSaunders 2008).

219 B. S. Zwilling, D. E. Kuhn, L. Wikoff, D. Brown, and W. Lafuse, 'Role of Iron in Nramp1-Mediated Inhibition of Mycobacterial Growth', *Infect Immun,* 67 (1999), 1386-92.

6 Acknowledgements

An erster Stelle möchte ich mich herzlich bei Dr. Monica Hagedorn für die Themenstellung, die vielen anregenden Diskussionen und die Betreuung meiner Doktorarbeit bedanken. Monica, vielen Dank für die mir zugetraute Selbständigkeit und für deine immer offene Bürotür.

Bei Prof. Dr. Iris Bruchhaus und Dr. Tobias Spielmann bedanke ich mich für die Mitbetreuung meiner Arbeit.

Weiter danke ich Prof. Dr. Iris Bruchhaus und Prof. Dr. Egbert Tannich für die bereitwillige Übernahme des Referats, bzw. des Koreferats - obwohl die lange Liste der Betreuten dadurch noch länger wurde.

Vielen Dank an meine Arbeitsgruppe, ganz besonders:
Silke, durch die Bereitschaft deine große Erfahrung im Labor und im Leben mit mir zu teilen, konnte ich viel von dir lernen. Durch dich habe ich es geschafft eine unglaubliche Ordnung einzuhalten und das Leben im verregneten Hamburg sowie im sonnigen Portugal zu genießen.
Margie, having you here was an amazing experience in- and outside of work. I guess we both learned a lot from each other. And despite a lot of obstacles, everything turned out so well in the end. We made an unbeatable team and I appreciate it a lot that I got to know you!
Ulrike du Schatz, ohne deine unermüdliche Unterstützung und deine Hilfsbereitschaft wäre vieles nicht so rund gelaufen, wie es nun doch ist-auch außerhalb des Labors!!!

Mein ganz besonderer Dank gilt dem *office*. Vielen Dank für alle Gespräche und Diskussionen, die wir geführt haben. Kaum ein Kaffee ohne *science talk*, es gibt eben auch *coole nerds* ;) Ohne Zweifel gehört auch Anna zu meinem *office*, was macht schon ein Flur aus? Anna, ich kann kaum in Worte fassen, wie sehr du mir geholfen hast: dein Rat, deine Antworten auf alle meine Fragen und letztendlich das Korrigieren der ersten Version dieser Arbeit!

Herzlich bedanken möchte ich mich bei Jürgen Sievers und Heidrun von Thien, ohne eure Hilfe und Erfahrung wäre die *customized multiplex qPCR* nicht so schnell funktionsfähig geworden!

I would also like to express my gratitude to Dr. Tim Lawrence and Dr. Erin Boyle who proofread this thesis and made sure it complied with the rules of the English language. Even though you both are very busy with your own work. Thank you so much!

Und Volker, mein Dank aus tiefen Herzen geht an dich und daran, dass du an mich geglaubt hast. Danke, dass du immer ein offenes Ohr für meine Angelegenheiten hattest. Deine Meinung ist mir sehr wichtig und ich habe den größten Respekt davor. Überdies bin ich sehr dankbar und glücklich darüber, dass du immer schnell reagiert hast. - ganz besonders bei dem Korrekturlesen dieser Arbeit.

An dieser Stelle möchte ich mich bei meinen Freunden bedanken. Ihr habt euch mit mir gefreut, mir beigestanden, wenn ich die Übersicht zu verlieren drohte und mich von allen Zweifeln befreit. „*With a little help of my friends*“ wird der Alltag zu einer unvergesslichen Zeit. Ihr seid super!!!

Last but not least, möchte ich noch herzlich meiner Familie danken: Danke, Mama und Papa, für eure große Unterstützung von der ersten Klasse bis zur Doktorarbeit! Ihr habt für Inga und mich einen der wunderbarsten Rückzugsorte erschaffen, den ich mir vorstellen kann und uns gleichzeitig die Tore der Welt geöffnet und uns ermutigt sie zu erkunden. Inga, tausend Dank für deine, nicht nur moralische Unterstützung! Wie schön ist es zu wissen, dass du immer da bist, wenn ich dich brauche?! Auch wenn hin und wieder ein Ozean zwischen uns lag - *muchas gracias*!

Eidesstattliche Versicherung

Hiermit versichere ich, an Eides Statt, dass ich diese Arbeit selbstständig verfasst und keine anderen als die angegebenen Quellen und Hilfsmittel verwendet habe. Wörtlich oder sinngemäß übernommenes Gedankengut habe ich als solches kenntlich gemacht.

Diese Arbeit ist darüber hinaus keiner anderen Prüfungsbehörde vorgelegt worden.

28. Januar 2014

Declaration on oath

I hereby declare, on oath, that I have written the present dissertation by my own and have not used other than the acknowledged resources and aids.

I also declare that the dissertation has neither been accepted nor graded 'failed' in a previous doctoral procedure.

28. Januar 2014